UNIVERSITÀ DEGLI STUDI DELL'AQUILA
DIPARTIMENTO DI INGEGNERIA INDUSTRIALE E DELL'INFORMAZIONE E DI ECONOMIA

DOTTORATO DI RICERCA IN INGEGNERIA INDUSTRIALE E DELL'INFORMAZIONE E DI ECONOMIA

CURRICULUM INGEGNERIA CHIMICA E DEI MATERIALI

XXXVIII CICLO

TESI DI DOTTORATO IN

Development of advanced technologies for the recovery of ethanol from wastewater deriving from human plasma production processes

SSD: ICHI 02/A

Coordinatore del Corso
Prof.ssa Katia Gallucci

Dottorando
Federico Cecchini

Tutor
Prof.ssa Marina Prisciandaro
Prof.ssa Valentina Innocenzi

Anno Accademico 2024/2025

ABSTRACT

The fractionation of human plasma relies extensively on cold ethanol precipitation, generating large volumes of hydroalcoholic waste streams that contain significant amounts of recoverable ethanol. Efficient ethanol recovery is therefore a key factor for both the economic and environmental sustainability of plasma fractionation processes. However, the reuse of recovered ethanol is often limited by the presence of volatile and semi-volatile contaminants, as well as by the high energy demand associated with conventional distillation systems.

This work investigates the recovery of ethanol from hydroalcoholic effluents generated during plasma fractionation, with a specific focus on the industrial process operated at the Takeda Manufacturing Italia plant in Cittaducale (Italy). The work adopts an integrated approach combining experimental analysis, process simulation, and techno-economic and environmental evaluation. Attention is devoted to the chemical quality of the recovered ethanol, addressing the formation of contaminants such as acetaldehyde and related compounds, which are subject to strict regulatory limits for reuse in pharmaceutical applications.

A detailed characterization of the waste streams was performed to assess their compositional variability and to identify potential precursors of volatile contaminants. Laboratory-scale experiments were conducted to investigate the influence of operating conditions, such as temperature, residence time,

and redox environment, on contaminant formation, enabling the identification of key kinetic trends and critical process parameters. These insights were used to support strategies aimed at mitigating contaminant generation at the source and reducing fouling phenomena in distillation equipment.

In parallel, the existing ethanol recovery system was analysed and optimized through process simulation. Innovative distillation configurations assisted by heat pump technologies were evaluated as alternatives to conventional steam-based systems, demonstrating significant potential for reducing energy consumption and operating costs while maintaining the required solvent quality. Economic and energy performance indicators were used to compare different scenarios and to identify optimal configurations aligned with industrial feasibility and sustainability goals.

Finally, the thesis explores a complementary valorisation strategy for pharmaceutical wastewater, proposing the integration of hydrodynamic cavitation into the existing wastewater treatment plant to enhance effluent quality and enable water reuse for irrigation in compliance with stringent European regulations.

Overall, this work provides a comprehensive, case-specific framework for ethanol recovery from complex pharmaceutical effluents, combining chemical insight with process and energy optimization. The results contribute practical guidelines for improving solvent quality, reducing environmental impact, and supporting circular economy strategies in plasma fractionation and related industrial contexts.

CONTENTS

LIST OF FIGURES

LIST OF TABLES

LIST OF ABBREVIATIONS

ADH	Alcohol Dehydrogenase
AE	Average cost of electricity
ALDH	Aldehyde Dehydrogenase
AOP	Advanced Oxidation Process
APAT–CNR IRSA	Italian National Agency for Environmental Protection – National Research Council, Institute for Water Research
AS	Average cost of Steam
BK	Centrifuge unit
BOD_5	Biochemical Oxygen Demand (5-day)
Bi–Bi	Sequential enzymatic reaction mechanism
CAPEX	Capital Expenditure
C310	First distillation column (alcohol depletion column)
C320	Second distillation column (ethanol concentration column)
COD	Chemical Oxygen Demand
COP	Coefficient Of Performance
CS	Cooling Skid
DF	Diafiltration

D01	Distillation unit D01
D201	Distillation unit D201 (being phased out)
D301	Main industrial distillation unit studied
D310	Condensate drum downstream of column C310
D320	Reflux accumulator of column C320
D401	New distillation unit under construction
DOE	Design of Experiments
DomWaste	Generic biodegradable organic substrate used in the kinetic model
EtOH	Ethanol
EU	European Union
FP	Filter Press
FT	Flow Transmitter
GC	Gas Chromatography
GC–FID	Gas Chromatography with Flame Ionization Detector
GC–MS	Gas Chromatography–Mass Spectrometry
GC-MS	Gas Chromatography – Mass Spectrometry
GMP	Good Manufacturing Practice
HC	Hydrodynamic Cavitation
HE	High cost of electricity
HP	Heat Pump (Case Study)
HP + VR	Heat Pump + Vapor Recompression (Case Study)
HS	High cost of Steam
HS–GC	Headspace Gas Chromatography
HS-GC-MS	Headspace Gas Chromatography – Mass Spectrometry

HYHT	High Yield High Throughput process
Kjeldahl (Nx6.25)	Method for total protein determination
LCA	Life Cycle Assessment
LE	Low cost of electricity
LLE	Liquid–Liquid Extraction
LS	Low cost of Steam
LSG	Liquid Specific Gravity
MBR	Membrane Bioreactor
NAD^+	Nicotinamide Adenine Dinucleotide (oxidized form)
NADH	Nicotinamide Adenine Dinucleotide (reduced form)
NG	Next Generation fractionation process
NG1	Next Generation 1 fractionation workflow
NIST	National Institute of Standards and Technology (mass spectral library)
OPEX	Operating Expenditure (Operating Costs)
PLC	Programmable Logic Controller
PP	Payback Period
PSG	Particle Specific Gravity
PSD	Particle Size Distribution
PT	Pressure Transmitter
PW / PW1	Pathway 1 fractionation process
SCADA	Supervisory Control and Data Acquisition
SVOC	Semi-Volatile Organic Compounds
TAC	Total Annual Costs
TCD	Total Costs Distribution

TDS	Total Dissolved Solids
TKN	Total Kjeldahl Nitrogen
TK	Tank
TOC	Total Organic Carbon
TP	Total Protein
TSS	Total Suspended Solids
TT	Temperature Transmitter
UF	Ultrafiltration
VOC	Volatile Organic Compounds
VR	Vapour Recompression (Case Study)
WWTP	Wastewater Treatment Plant
YADH	Yeast Alcohol Dehydrogenase

NOMENCLATURE

LATIN

C_i	organic specie with number of carbons equal to "i"
i	Interest Rate
k	Reaction rate constant (h^{-1})
K_s	Half-saturation (Monod) constant (mg/l)
kPaA	Absolute pressure in kPa
Lift	Temperature difference between the hot sink and cold sink of a heat pump
n	Number of years
pH	Measure of acidity/basicity ($-\log_{10}[H^+]$)
ppm	Parts per million
R^2	Coefficient of regression
t_{inc}	Incubation time
T_{eb}	Boiling temperature
T_{inc}	Incubation temperature

v/v	Volume per volume
w/v	Weight per volume
w/w	Weight per weight
$X_{vss}h$	Heterotrophic volatile suspended solids biomass
$X_{vss}i$	Inert volatile suspended solids fraction
$X_{vss}n$	Nitrifying volatile suspended solids biomass
Y	Response variable

GREEK

Δp	Pressure drop across the cavitation device
μm	Micrometer

DECLARATION OF GENERATIVE AI AND AI-ASSISTED TECHNOLOGIES

During the preparation of this work, the author utilized ChatGPT to assist with the writing and editing. After using this tool, the author reviewed and edited the content as needed and takes full responsibility for the content of this work. These tools were not used for data analysis, data processing, result interpretation, or drawing scientific conclusions. All scientific content, analyses, and interpretations were developed entirely by the authors.

BACKGROUND AND MOTIVATION

The separation and purification of plasma proteins have been central to the development of modern biotherapeutics, with the Cohn fractionation process representing a pivotal advance in this field. Developed in the 1940s by Edwin J. Cohn and colleagues, the method relies on cold ethanol precipitation under carefully controlled conditions of pH, ionic strength, temperature, and protein concentration. This approach enabled the selective enrichment of major plasma proteins such as albumin, immunoglobulins, and fibrinogen, each with specific therapeutic applications [1,2]. Initially designed to meet urgent clinical needs during World War II, particularly the demand for plasma-derived albumin, the process has since been adapted for large-scale production of multiple plasma-derived medicines, including immunoglobulins and coagulation factors [1,3]. Its ability to efficiently utilize each plasma donation for multiple therapeutic products has made it a cornerstone of the plasma fractionation industry, supporting treatments for millions of patients worldwide [1].

Despite its robustness and long-standing relevance, the Cohn method presents several drawbacks. It is labor-intensive and requires precise control of multiple parameters, which makes it complex and costly to operate on an industrial scale. Product quality is also affected, as certain proteins such as albumin may be recovered with relatively low yield and purity compared to modern alternatives [4]. The harsh conditions of ethanol precipitation can lead to protein denaturation and loss of activity [5], while viral contaminants such as hepatitis-associated antigens or HCV RNA have been shown to persist in some fractions [6,7]. Furthermore, the underutilization of plasma components, such as those contained in Fraction IV, represents an

inefficient use of valuable biological resources [5,8]. Collectively, these issues highlight the need for improved strategies that increase yield and safety, reduce costs, and maximize plasma utilization.

Another important aspect concerns the management of ethanol, employed as the primary solvent in the Cohn process. Large volumes of ethanol-rich wastewater are generated, traditionally treated through incineration or purification, practices associated with high economic and environmental costs. Since ethanol is both a costly raw material and a recoverable resource, its reuse represents a significant opportunity. Ethanol recovery and purification can lower the demand for fresh solvent—generating direct cost savings—while also reducing the volume of wastewater requiring treatment and disposal, thereby improving the environmental performance of plasma fractionation [5]. In this perspective, ethanol recovery is not merely a waste minimization practice but a key element for the sustainability of the entire process. The implementation of innovative recovery technologies, capable of reducing energy consumption while improving solvent quality, is therefore of great interest to both the biopharmaceutical industry and academic research, in line with the broader principles of circular economy and resource valorisation.

OBJECTIVE AND SCOPE

This thesis is devoted to the analysis and optimization of the ethanol recovery process carried out at the Takeda Italia plant in Cittaducale (RI). The overarching objective is to critically evaluate the performance of the current recovery system and to address the technical, chemical, economic, and environmental issues that limit its efficiency and sustainability. By combining process analysis, chemical investigations, energy optimization, and environmental assessment, the work aims to provide a comprehensive perspective on the challenges and opportunities associated with ethanol recovery in plasma fractionation.

The first part of the research focused on a detailed study of the ethanol concentration unit currently in use at the plant. This analysis aimed to identify the primary bottlenecks of the system, including efficiency losses, operating constraints, and reliability issues. Given that ethanol is continuously reused in large quantities, understanding the critical aspects of the recovery system is essential for ensuring both process robustness and economic competitiveness.

A central component of the study was the investigation of the chemical quality of the recovered ethanol. Over time, different contaminants have been detected in the recovered streams, raising concerns about solvent purity and its suitability for reuse in plasma fractionation. These contaminants were systematically analysed, and possible formation pathways were explored to clarify their origin. Special emphasis was placed on acetaldehyde, a compound of particular concern due to its potential toxicity, volatility, and frequent occurrence as a degradation product of ethanol.

In addition to chemical aspects, attention was also given to operational issues, particularly the frequent fouling of the distillation equipment. This phenomenon not only reduces the efficiency of the recovery process but also increases maintenance needs and downtime. The study therefore examined potential causes of fouling, with a focus on the role of contaminant precursors, and explored possible strategies to mitigate both equipment fouling and contaminant generation at their source.

Beyond process reliability and chemical purity, the work also addressed the energy performance of the ethanol recovery system. An optimization study was carried out on the existing distillation process, with the aim of reducing energy consumption and operating costs while maintaining the required solvent quality. Improving energy efficiency is a crucial step toward enhancing the overall sustainability of the recovery process and reducing its environmental footprint.

Finally, part of this study focused on the company's wastewater treatment plant. In this context, an additional treatment to the current wastewater treatment plant was proposed, aimed at improving the quality of the effluent. The goal of this treatment is to ensure that the quality of the effluent complies with the latest and most stringent European standards for water reuse in irrigation.

Taken together, these activities define the scope of the present thesis: to analyse the ethanol recovery process from multiple perspectives—technical, chemical, energetic, and environmental—to identify its current limitations and outline possible improvements aimed at increasing the sustainability and competitiveness of the entire plasma fractionation process.

1. LITERATURE REVIEW

1.1 INTRODUCTION

The increased emphasis on environmental sustainability and energy efficiency in industrial operations has accelerated the development of innovative wastewater treatment and resource recovery systems. Among these, recovering ethanol from pharmaceutical industry effluent provides a particularly major difficulty, both in terms of the solvent's economic importance and the complexity of the matrix from which it must be extracted. Ethanol is commonly utilized in human plasma fractionation procedures, and its efficient recovery can assist lower production costs and the overall environmental impact of the operation.

The purpose of this literature review is to assess the current level of ethanol recovery from pharmaceutical wastewater, with a particular emphasis on relevant distillation technologies, the production of pollutants in distillates, and the process's energy and environmental implications. To that goal, the review has been organized using a thematic approach.

It will begin by discussing the usual properties of pharmaceutical wastewater and the primary treatment procedures used. This will be followed by an overview of distillation methods, ranging from traditional to more novel approaches, such as heat pump-assisted systems or vacuum distillation. The subject of contaminant production in distillates will next be

examined in depth, with an emphasis on the generation methods and primary antecedents. Finally, energy and environmental aspects of ethanol recovery will be studied, considering current Life Cycle Assessment (LCA) research.

The review will conclude with an identification of the significant gaps in the current literature, as well as the scientific rationale for the research presented in this thesis, which aims to propose innovative solutions for ethanol recovery from complex waste streams using low-impact technologies.

1.2 PHARMACEUTICAL INDUSTRY WASTEWATER: CHARACTERISTICS AND TREATMENT

1.2.1 OVERVIEW OF THE INDUSTRIAL SECTOR

The pharmaceutical sector is widely recognized as a high-impact industry, both economically and socially, due to its central role in public health and its strong orientation toward innovation [9]. It is also among the most resource- and solvent-intensive sectors, characterized by complex manufacturing processes that generate diverse liquid waste streams [10].

Globally, the industry is experiencing steady growth and increasing geographical diversification of production. In this context, Italy plays a leading role, ranking as the second-largest pharmaceutical producer in the EU by value [11]. The sector is marked by a high degree of technological sophistication, a strong presence of multinational corporations—controlling approximately 80% of the domestic market—and a dynamic network of specialized SMEs [12].

The industrial processes adopted—especially in sectors such as plasma fractionation—require large volumes of organic solvents, like ethanol, which is used in both formulation and purification steps [10]. As a result,

the pharmaceutical industry generates liquid effluents with variable and often complex compositions, including residues of solvents, process intermediates, and other organic and inorganic substances [9].

This complexity poses significant challenges in terms of waste management and environmental impact. At the same time, the presence of high-value solvents in these streams has encouraged the development of recovery and valorisation strategies, aimed at both economic savings and improved sustainability [10].

Among the various contributors to pharmaceutical waste streams, solvents play a particularly central role—both in terms of volume and environmental relevance. Their use is therefore a key factor in assessing the sustainability of pharmaceutical production.

Solvents are fundamental to pharmaceutical manufacturing, comprising 80–90% of the total mass used in the production of active pharmaceutical ingredients (APIs) and representing the largest source of process waste and environmental impact in the sector [13].

The environmental burden of solvent use is captured by the E factor, which measures the mass of waste generated per mass of product. In pharmaceutical processes, E factors are typically very high—often exceeding 100, and in some cases reaching values above 2000 for complex syntheses. For example, the E factor for atropine synthesis was reduced from 2245 to 24, and for diazepam from 36 to 9, through the adoption of continuous-flow processes and solvent minimization strategies [14].

Solvent-related waste can account for up to 80% of total waste in API production, as reported by major pharmaceutical companies [15]. Life cycle assessments consistently identify solvent use and waste management as the dominant contributors to the environmental footprint of pharmaceutical products, with solvent replacement often proving more effective than energy optimization in reducing impacts [16].

To address these challenges, the industry is increasingly adopting green chemistry principles, such as the use of deep eutectic solvents (DESs), ethanol, and advanced recycling technologies like nanofiltration, which can reduce the E factor and carbon footprint by over 90% [17]. These innovations, along with solvent selection guides and process intensification, are driving significant progress toward more sustainable pharmaceutical manufacturing [18].

The pharmaceutical industry produces substantial amounts of liquid waste containing both organic and inorganic compounds, primarily because of manufacturing, extraction, and formulation processes.

These liquid wastes are complex mixtures, often rich in organic substances such as API, solvents, and phenolic compounds like dihydroferulic acid, as well as inorganic components including salts and heavy metals [19].

Such wastes are frequently classified as hazardous due to their toxicity and persistence in the environment, posing significant challenges for conventional wastewater treatment systems [20]. The environmental impact is considerable, as untreated or partially treated effluents can contaminate water sources and harm aquatic life [21].

To address these issues, advanced treatment methods—such as chemical coagulation, wet oxidation, and biological processes—are employed to reduce toxicity and recover valuable materials, supporting circular economy initiatives. Effective management and valorisation of these liquid wastes are essential for minimizing environmental risks and promoting sustainability in pharmaceutical production [19].

1.2.2 Characteristics of Pharmaceutical Wastewaters

Pharmaceutical wastewater is recognized for its complex and highly variable composition, which is largely influenced by the diversity of products and processes within the pharmaceutical industry. It typically contains high concentrations of organic matter, significant levels of nitrogen

and phosphorus, elevated salinity, and strong colour, with pH values that can fluctuate widely depending on the specific production process [22].

A summary of the typical physicochemical properties of pharmaceutical wastewater is provided in Table 1.1.

The presence of refractory and toxic organic compounds, such as antibiotics (e.g., cephalexin, cefradine), analgesics, esters, acids, heterocycles, and organosilicon compounds, is common, and many of these are resistant to conventional biological degradation [23]. Acute toxicity is a critical concern, as these effluents can be highly toxic to aquatic organisms and may promote the spread of antibiotic resistance genes in the environment [24].

Table 1.1: Typical Physicochemical Properties of Pharmaceutical Wastewater [22].

Parameter	**Typical Range**
COD (mg/l)	1000-10000
BOD_5 (mg/l)	500-2500
TN (mg/l)	500-1500
TP (mg/l)	50-250
SS (mg/l)	200-500
Chromaticity	500-1000
T (°C)	25-80
pH	1-8

Treatment of pharmaceutical wastewater presents several critical challenges. The poor biodegradability and high toxicity of many constituents inhibit the effectiveness of standard biological processes, often resulting in incomplete removal of pollutants and the persistence of trace pharmaceuticals and toxic organics in treated effluent [25].

High salinity further complicates biological treatment and can damage treatment infrastructure [26]. Advanced treatment methods, such as advanced oxidation processes (AOPs), ozonation, activated carbon adsorption, and membrane technologies, have been explored to address these issues. While AOPs and ozonation can effectively degrade many persistent pharmaceuticals, they may also generate toxic by-products if not carefully managed [27]. Adsorption and membrane processes can remove a broad spectrum of contaminants but often transfer pollutants to another

phase, requiring additional handling and disposal. Consequently, integrated or hybrid treatment systems that combine biological, chemical, and physical processes are increasingly recommended to maximize removal efficiency and minimize environmental risks [28].

Overall, the complex and hazardous nature of pharmaceutical wastewater necessitates advanced, multi-stage treatment strategies to ensure effective pollutant removal and to mitigate the associated environmental and public health risks [22].

1.2.3 CONVENTIONAL TREATMENTS

Conventional treatment methods for pharmaceutical wastewaters, such as activated sludge and oxidation ditches, are widely used to reduce organic load and remove some pharmaceutically active compounds. However, these methods often show only moderate removal efficiencies, particularly for persistent and recalcitrant pharmaceuticals like carbamazepine, which can remain in the effluent at detectable concentrations. While compounds such as ibuprofen, naproxen, and caffeine are efficiently removed (up to 99%), others are much less affected, highlighting the limitations of conventional biological and physical-chemical treatments [29].

A significant challenge in treating pharmaceutical wastewaters is the presence of organic solvents, which are commonly used in drug manufacturing. These solvents, including methanol, propanol, and acetone, can be partially degraded by biological processes, but at higher concentrations they may inhibit microbial activity, reducing the overall efficiency of conventional treatments [30]. Physical-chemical methods, such as coagulation and flocculation, are generally less effective for solvent removal, often transferring these compounds to the sludge phase, which then requires further management. Membrane filtration can physically separate some solvents, but this approach is costly, prone to fouling, and generates concentrated waste streams that need additional treatment.[31]

The complex mixture of pharmaceuticals and solvents in these wastewaters means that conventional treatments alone are insufficient for comprehensive

removal. As a result, there is a growing consensus that advanced or hybrid treatment technologies—such as advanced oxidation processes, adsorption, and membrane-based systems—are necessary to achieve higher removal efficiencies and address the toxicity and persistence of both pharmaceuticals and solvents in wastewater effluents [32].

1.2.4 Solvent Recovery and Reuse

Solvent recovery and reuse have become central to the pharmaceutical industry's efforts to reduce costs, environmental impact, and reliance on virgin materials, as previously mentioned solvents can account for up to 90% of the mass used in active pharmaceutical ingredient production. Economic analyses consistently demonstrate that solvent recovery systems can yield substantial benefits, including operating cost reductions exceeding 80%, significant emission cuts, and payback periods as short as 2–4.5 years, with internal rates of return up to 28% [33].

Ethanol, a widely used solvent, exemplifies both the promise and challenges of recovery: while traditional distillation remains common, its high energy demand and inefficiency with azeotropic mixtures have spurred the adoption of hybrid processes such as distillation combined with pervaporation or nanofiltration, which can achieve higher purity and lower energy consumption [34]. Membrane-based technologies, including organic solvent nanofiltration and forward osmosis, offer further advantages in terms of modularity, scalability, and reduced energy use, but may face limitations related to membrane fouling, solvent compatibility, and the need for additional dehydration steps to meet pharmaceutical-grade purity requirements [35].

Despite these advances, the complexity of waste stream compositions, stringent purity specifications, and integration challenges within existing facilities continue to limit the widespread adoption of solvent recovery, particularly for low-volume or highly contaminated streams [36]. Recent studies have also highlighted the potential of innovative approaches such as solar distillation for acetone recovery, which, while achieving up to 85%

efficiency, still falls short of the purity required for pharmaceutical reuse, thus restricting its application to less demanding uses [37]. Systems-level analyses emphasize that the design of recovery processes must account for the diverse nature of waste streams, techno-economic constraints, and environmental impacts, with flexible, multi-campaign recovery systems showing promise for improving the feasibility of recovering solvents from both high- and low-volume streams [33,36]. Furthermore, the adoption of advanced hybrid processes—such as extractive distillation with ionic liquids, heat pump integration, and adsorptive membrane scaffolds—has demonstrated significant reductions in energy consumption, emissions, and total annual costs, but these solutions often require complex optimization and may not be universally applicable across all solvent types or process scales [38,39]. Thus, while the economic and environmental incentives for solvent recovery—especially for ethanol—are clear, ongoing research is focused on overcoming technical, regulatory, and process integration barriers to enable broader and more efficient implementation across the pharmaceutical sector.

1.3 Ethanol Recovery: Traditional and Innovative Technologies

1.3.1 Distillation for Ethanol Recovery

Distillation is a fundamental separation technique that operates on the principles of mass transfer and phase equilibrium, enabling the separation of components in a liquid mixture based on differences in their volatilities. The process involves heating the mixture to vaporize the more volatile component, which is then condensed and collected as a purified product. Various forms of distillation—including fractional, azeotropic, extractive, steam, vacuum, and membrane distillation—are employed to address specific challenges such as azeotrope formation or the need to process heat-sensitive compounds. These methods are particularly relevant in the chemical and pharmaceutical industries, where high purity and efficient recovery of solvents and active ingredients are essential [40]. Distillation is

especially suitable for ethanol recovery because ethanol and water have sufficiently different boiling points, allowing for effective separation. Advanced techniques, such as membrane distillation and hybrid processes that combine distillation with pervaporation or heat integration, further enhance the efficiency and sustainability of ethanol recovery, even in the presence of azeotropes or dilute solutions [41]. In the chemical and pharmaceutical fields, distillation is indispensable for solvent recovery, purification of active pharmaceutical ingredients (APIs), and the treatment of process wastewaters, supporting both economic and environmental sustainability. Recent advancements in distillation technology focus on process intensification, energy efficiency, and integration with other separation methods, such as pervaporation and heat pump-assisted systems, which further reduce energy consumption and environmental impact. These innovations ensure that distillation remains a versatile and indispensable method for the purification and recovery of valuable compounds, meeting the evolving demands for sustainability, regulatory compliance, and process optimization in modern chemical and pharmaceutical manufacturing [40].

1.3.2 CONVENTIONAL DISTILLATION

Conventional distillation continues to be a mainstay in industrial separation processes due to its reliability and ability to achieve high product purity, but the literature highlights both its strengths and persistent limitations. Batch steam distillation, while widely used for essential oil extraction and solvent recovery, is often hampered by high energy consumption, long processing times, and significant steam requirements, which can negatively impact operational costs and environmental sustainability [42]. Continuous steam distillation systems, especially those utilizing packed columns, have been developed to address these issues, offering reductions in steam consumption by 32–60% and process times by up to 50%, while maintaining oil recovery efficiencies above 90% and enabling the production of differentiated product fractions with unique compositions [43]. In the recovery of solvents and alcohols, direct steam distillation (DSD) and extractive distillation are commonly employed, with DSD providing advantages such as operation at

atmospheric pressure, use of low-pressure steam, and lower energy requirements for preheating, all contributing to reduced total annualized costs [44].

Despite these improvements, conventional distillation processes still face notable challenges. High energy consumption remains a significant limitation, particularly for multi-stage or azeotropic separations, though process innovations such as heat integration, hybrid designs, and advanced heating methods (e.g., ohmic and microwave-assisted distillation) can reduce energy use by 16–54% [45]. For example, microwave-assisted distillation has been shown to increase oil yield by up to 10% and reduce energy consumption by 25–33% compared to conventional methods, while ohmic-accelerated steam distillation can cut energy use by more than half and significantly shorten extraction times, all without compromising product quality [42]. The environmental impact of distillation is also influenced by the choice of steam source, with biomass-based steam generation offering lower environmental burdens than fossil fuels [46].

Fouling and scaling in columns and heat exchangers are persistent operational issues, leading to reduced efficiency and increased maintenance requirements [42]. The thermal instability of certain compounds is another concern, as prolonged exposure to high temperatures—especially in batch processes—can result in degradation or loss of valuable components. Additionally, the formation of contaminants through side reactions or degradation is a risk, particularly in batch operations with long residence times [43]. Process complexity further increases when dealing with azeotropic or multi-component mixtures, necessitating sophisticated control strategies to maintain product purity and process stability; advanced control schemes and process optimization are therefore critical for robust operation [45].

Recent studies also emphasize the importance of process intensification and integration. For instance, the use of decanters in batch distillation can improve recovery and energy efficiency by up to 8% over conventional units [47], while extractive and azeotropic distillation methods—sometimes

employing inorganic salts or specialized entrainers—can achieve product purities of 99% or higher for chemicals like ethanol [48]. Furthermore, heat-integrated and hybrid distillation configurations have demonstrated substantial reductions in energy consumption and total annual costs, with some advanced designs achieving over 50% energy savings compared to conventional systems [45].

In summary, while conventional distillation remains a robust and effective method for industrial separations, ongoing research and technological advancements are essential to address its inherent energy and operational limitations. The integration of continuous systems, process intensification, advanced heating methods, and environmentally friendly steam sources are key trends that promise to enhance the sustainability and efficiency of distillation in modern industry [42].

1.3.3 Heat Pump Systems in Distillation Plants

Heat pumps are versatile thermal devices that transfer heat from a low-temperature source to a higher-temperature sink, playing a crucial role in energy-efficient heating, cooling, and industrial waste heat recovery. The most common technology, the vapor compression heat pump, uses a mechanical compressor to circulate a refrigerant through evaporation and condensation cycles, achieving high coefficients of performance (COP) but often relying on environmentally problematic fluorocarbon refrigerants [49]. In contrast, absorption and adsorption heat pumps are thermally driven, using either a liquid absorbent-refrigerant pair (such as ammonia-water) or a solid adsorbent (such as silica gel or zeolite) with a refrigerant, respectively. These systems can utilize low-grade or waste heat, avoid harmful refrigerants, and are particularly suited for industrial applications, though they typically exhibit lower COPs and larger system sizes compared to vapor compression systems. Adsorption heat pumps rely on the reversible bonding of refrigerant molecules to a solid adsorbent, with heat input driving desorption and subsequent heat transfer cycles, and ongoing research focuses on improving their efficiency through advanced materials and cycle designs [50,51]. Supercritical heat pump cycles, often employing

CO_2 as the working fluid, operate above the critical temperature and pressure, enabling higher temperature lifts and improved thermodynamic efficiency due to enhanced heat transfer properties and better temperature matching between the heat source and working fluid [52,53]. Hybrid systems, such as combined compression-adsorption or absorption-compression cycles, integrate the strengths of multiple technologies to achieve higher temperature lifts, improved efficiency, and greater operational flexibility, making them promising for high-temperature industrial applications and waste heat recovery [49,54]. The ongoing development of these advanced cycles—including the use of novel adsorbents, optimized hybrid configurations, and supercritical working fluids—continues to expand the applicability and environmental benefits of heat pump technologies across residential, commercial, and industrial sectors [49,50].

The integration of heat pumps into industrial applications presents significant economic and energy advantages, positioning them as a key technology for decarbonizing industrial heat supply. Heat pumps, particularly when used in combined heating and cooling systems (CCHSs), can achieve energy savings ranging from 12% to 34% compared to conventional separate systems, with optimal performance dependent on the specific heating-to-cooling demand ratio and careful system design [55]. High-temperature heat pumps (HTHPs) further enhance process efficiency, as demonstrated in ammonia plants and pulp mills, where their integration can reduce energy consumption and associated CO_2 emissions by up to 45% relative to traditional gas boilers, while also increasing exergy efficiency by 9% [56]. Economic analyses reveal that heat pumps can be cost-competitive, especially when waste heat at temperatures above 80°C is available, leading to levelized cost of heat (LCOH) reductions exceeding 15% compared to electric boiler alternatives, primarily due to substantial electricity savings [57]. In industrial parks, the deployment of heat pump-based waste heat recovery systems has been shown to decrease annual total costs and steam power consumption by 33% and 39%, respectively, with

payback periods as short as six years [58]. However, the economic viability of heat pumps is sensitive to the electricity-to-gas price ratio and the temperature of available heat sources, with higher efficiencies and lower costs achieved when waste heat is utilized at elevated temperatures [59].

The integration of heat pump technology into industrial distillation plants has emerged as a highly effective strategy for improving energy efficiency, reducing operational costs, and minimizing environmental impact. In various sectors such as chemical, petrochemical, and wastewater treatment, heat pumps are employed to recover and upgrade waste heat, thereby significantly lowering the demand for external utilities. For example, the application of heat pumps in pressure-swing distillation and extractive distillation processes has demonstrated total annual cost reductions of up to 51% and energy savings exceeding 60%, with payback periods as short as three years [60,61]. Mechanical heat pumps, including vapor recompression and bottom flashing systems, are particularly effective in processes with moderate temperature lifts, while absorption heat pumps are suitable for larger temperature differences [62,63]. In addition, advanced configurations such as triple-column distillation and hybrid systems that combine heat pumps with heat integration networks have achieved energy and emission reductions of over 60% compared to conventional designs [61,64]. The adoption of heat pump-assisted distillation is also supported by environmental benefits, including substantial decreases in CO_2 and other greenhouse gas emissions [61,65]. Furthermore, the electrification of distillation processes through heat pump integration aligns with the broader industrial goal of transitioning to low-carbon operations, as it enables the use of renewable electricity and further reduces fossil fuel consumption [65,66]. Overall, the deployment of heat pumps in distillation plants represents a mature and economically viable approach to process intensification, offering significant advantages in terms of sustainability, cost-effectiveness, and operational flexibility across a range of industrial applications.

1.3.4 VACUUM DISTILLATION SYSTEMS

Vacuum distillation has emerged as a critical technique in both industrial and research settings due to its ability to lower the boiling points of substances by reducing system pressure, thereby enabling the separation of high-boiling or thermally sensitive compounds at significantly reduced temperatures. This reduction in boiling temperature is particularly advantageous for preventing thermal degradation of valuable or heat-sensitive molecules, as demonstrated in the purification of complex mixtures such as post-consumer plastic pyrolysis oils, where vacuum distillation effectively removes contaminants and preserves product quality [67]. In the context of large-scale applications like oil refining, vacuum distillation units (VDUs) are optimized to enhance yield and operational efficiency by carefully adjusting parameters such as temperature, pressure, and steam flow rate, which not only improve product recovery but also contribute to economic and environmental sustainability [68]. Furthermore, the integration of vacuum distillation with advanced systems, such as vacuum membrane distillation (VMD) and mechanical vapor recompression, has shown substantial energy benefits. These hybrid systems can achieve significant reductions in specific energy consumption, sometimes by as much as 77%, through the recovery of latent heat and improved thermal efficiency [69]. However, the adoption of vacuum distillation is not without limitations. The requirement for larger equipment to accommodate lower pressures, the need for enhanced inert-removal facilities, and the potential for operational challenges such as temperature polarization and scaling can offset some of the energy and cost advantages [67,70]. Additionally, the trade-off between production rate and energy consumption must be carefully managed, as increasing the number of effects or membrane area in multi-effect systems can reduce energy use but may lower specific permeate flux and increase capital costs [71]. Despite these challenges, vacuum distillation remains a versatile and essential process, particularly when the preservation of product integrity and energy efficiency are paramount.

Vacuum distillation has found extensive application across a range of industrial sectors due to its ability to separate and purify compounds at reduced temperatures, thereby minimizing thermal degradation and improving product quality. In the petrochemical industry, vacuum distillation units are integral to oil refineries, where they facilitate the separation of heavy crude oil fractions into valuable products such as vacuum gas oils and feedstocks for further processing [72]. The recycling and purification of post-consumer plastic pyrolysis oils also rely on vacuum distillation to remove contaminants and produce fractions suitable for use as chemical feedstocks in steam crackers, supporting the circular economy in plastics [73]. In the field of metal refining, vacuum distillation is employed to recover and purify high-value metals from industrial wastes and alloys, such as the extraction of selenium, tellurium, silver, and copper from flotation tailings and secondary resources, achieving high recovery efficiencies and meeting the demands for cleaner metallurgical processes [74]. The technology is further utilized in the treatment and recycling of waste oil-based drilling fluids, where it enables the recovery of base oils and solids for reuse, thus contributing to resource efficiency and pollution control in the petrochemical sector [75]. Additionally, vacuum distillation is applied in the pharmaceutical and food industries, particularly in the purification of bioactive compounds, essential oils, and the refinement of vegetable oils, where molecular distillation—a form of vacuum distillation—preserves sensitive components and enhances product purity [76]. The versatility and effectiveness of vacuum distillation in these diverse applications underscore its importance as a sustainable and efficient separation technology in modern industry [77].

1.4 Contaminants in the Distilled Ethanol

Despite its widespread application for ethanol recovery, distillation may also contribute to the presence of unwanted contaminants in the distillate. These substances can originate from co-evaporation, degradation of residual

compounds, or chemical reactions occurring under specific process conditions. Understanding the mechanisms behind their formation—as well as their potential impact on solvent quality and reuse—is essential when dealing with complex effluents such as those generated by plasma fractionation.

1.4.1 CONTAMINANTS OBSERVED IN ETHANOL

Ethanol produced by fermentation or recovered from industrial effluents, particularly those generated in pharmaceutical production, may contain a variety of volatile and semi-volatile impurities that can compromise its quality and limit its potential for reuse. In pharmaceutical applications, ethanol must meet strict purity requirements defined by official standards. These standards are generally compiled in the International Pharmacopoeia. In Europe, as in other continents, the text has been adapted in the European Pharmacopoeia (Ph. Eur.) [78].

According to the Ph. Eur. monograph for Ethanol (96% by volume), the permitted limits for volatile impurities are defined by gas chromatography analysis. Methanol is allowed up to a concentration corresponding to no more than half the area of the methanol peak in the reference chromatogram, equivalent to 200 ppm V/V. Acetaldehyde and acetal are regulated as a combined group, with a maximum allowable concentration of 10 ppm V/V, expressed as acetaldehyde. Benzene, due to its toxicity, is strictly limited to 2 ppm V/V, while the residue on evaporation must not exceed 25 ppm V/V, corresponding to a dry residue of up to 2.5 mg per 100 mL of ethanol evaporated at 100–105 °C for 1 hour.

In addition to these regulated compounds, the Pharmacopeia identifies a series of known impurities that may be present in trace amounts. These include aldehydes (acetaldehyde, furfural), ketones (acetone, 2-butanone, 4-methylpentan-2-one), alcohols (methanol, propan-2-ol, butanols, hexanols), ethers and acetals, as well as aromatic and aliphatic hydrocarbons such as benzene and cyclohexane.

While some of these compounds may be introduced as residual solvents from upstream processes, others can result from thermal degradation, co-distillation, or chemical transformations occurring during ethanol recovery. Their presence in the final product, even at concentrations below regulatory limits, can lead to sensory alterations (e.g., odor, color), reduced stability during storage, or non-compliance with internal quality specifications used in pharmaceutical settings.

In practice, ethanol recovered from complex effluents—such as those originating from plasma fractionation—may fail to meet these pharmacopeial specifications, particularly when operated under suboptimal distillation conditions. Reports of yellow coloration, persistent odors, or high TOC values in the distillate are indicative of contamination by low-molecular-weight organic compounds that are not completely removed during phase separation.

Given the regulatory and technical importance of ethanol purity, the identification and control of such contaminants are essential not only for process optimization but also for ensuring that the recovered solvent is suitable for reuse in a pharmaceutical context.

1.4.2 Formation Pathways

During the distillation of ethanol, the behavior and distribution of volatile and semi-volatile compounds are governed by their physicochemical properties—primarily their relative volatility, solubility in water and ethanol, and their interactions with the evolving ethanol concentration in the distillation column. Volatile compounds such as methanol, acetaldehyde, and various esters typically exhibit higher volatility than ethanol and are therefore concentrated in the early distillation fractions, often referred to as the "heads." The release and separation of these compounds are not dictated solely by their boiling points, but also by their solubility and the ethanol content of the boiling liquid, which modulates their partitioning between vapor and liquid phases [79]. As distillation progresses and the ethanol concentration in the boiler decreases, the relative volatility of semi-volatile

compounds—such as higher alcohols (e.g., isoamyl alcohol, 2-phenylethanol), certain esters, and volatile acids—increases, resulting in their appearance in later fractions, commonly known as the "tails" [80]. The design and operational parameters of the distillation apparatus, including the number of trays in a column, reflux ratio, and the ethanol profile maintained in the column, play a critical role in optimizing the separation of these compounds. For instance, maintaining a higher ethanol concentration in the column can delay the release of higher alcohols and semi-volatiles, thereby sharpening their separation and enhancing the sensory quality of the distillate [81]. Furthermore, the initial alcohol content of the feed significantly influences the evaporation dynamics of both methanol and higher alcohols, with lower initial ethanol concentrations favouring the early separation of higher alcohols and the later appearance of methanol in the distillate [82]. The fractionation strategy, including the precise cut points between heads, hearts, and tails, is thus essential for minimizing undesirable volatiles while retaining or enriching desirable aroma compounds, ultimately determining both the safety and organoleptic profile of the final ethanol product [83].

Understanding these mechanisms is essential to designing effective strategies for minimizing contaminant formation, whether by optimizing process parameters (temperature, pressure, residence time), implementing pre-treatment steps, or modifying the configuration of the distillation unit.

1.4.3 PRECURSORS

The biosynthesis of volatile and semi-volatile compounds during alcoholic fermentation and subsequent distillation is fundamentally rooted in the metabolic pathways of yeast, with specific precursors playing pivotal roles in the formation of higher alcohols and related congeners. The Ehrlich pathway is central to the production of fusel alcohols, wherein branched-chain and aromatic amino acids—such as valine, leucine, isoleucine, phenylalanine, tyrosine, and tryptophan—are first transaminated to their corresponding α-keto acids. These α-keto acids are then decarboxylated and reduced to yield higher alcohols, including isoamyl alcohol, isobutanol, and

2-phenylethanol. Methionine, a sulfur-containing amino acid, serves as a precursor for methionol and other sulfurous volatiles. The availability and flux of these amino acids, as well as the activity of key enzymes such as aminotransferases and decarboxylases, directly influence the concentration of higher alcohols in the final distillate. In addition to amino acid catabolism, intermediates of central carbon metabolism, particularly pyruvate and its derivatives, act as crucial precursors for both higher alcohols and aldehydes. The glycolytic pathway, pentose phosphate pathway, and pyruvate metabolism are all implicated in modulating the pool of precursor metabolites available for volatile compound synthesis. Furthermore, the regulation of genes involved in these pathways, such as ADH4, SER33, and GDH2, has been shown to significantly impact the levels of specific higher alcohols, underscoring the genetic and metabolic complexity underlying volatile compound formation in yeast fermentation systems [84–86].

As will be seen in the following chapters, acetaldehyde is one of the most detected pollutants in out-of-spec recovered ethanol. The formation of acetaldehyde from ethanol is a central process in both biological and chemical systems, involving a complex interplay of enzymatic and non-enzymatic mechanisms. In biological contexts, the primary route for ethanol oxidation is catalysed by alcohol dehydrogenase (ADH), a widely distributed enzyme in mammals, bacteria, and yeast. ADH catalyses the reversible oxidation of ethanol to acetaldehyde, utilizing NAD^+ as a cofactor, and its activity is critical for ethanol metabolism in the liver and for fermentative pathways in microorganisms [87]. In addition to ADH, alternative enzymatic pathways contribute to acetaldehyde formation, including the microsomal ethanol oxidizing system (cytochrome P450 2E1) and catalase, both of which become more prominent under conditions of high ethanol exposure or oxidative stress [88]. The catalytic oxidation of ethanol to acetaldehyde is also a key industrial process, where heterogeneous catalysts such as gold or Au/TiO_2 facilitate the oxidative dehydrogenation of ethanol. These catalytic reactions proceed via the

activation of molecular oxygen on the catalyst surface, followed by hydrogen abstraction from ethanol and the formation of acetaldehyde as the primary product, with selectivity and efficiency influenced by catalyst structure and reaction conditions [89]. Furthermore, the Maillard reaction, a non-enzymatic browning process between reducing sugars and amino compounds, can generate acetaldehyde as a volatile intermediate through Strecker degradation and related pathways, particularly in thermally processed foods. Collectively, these mechanisms underscore the multifaceted nature of acetaldehyde formation, with alcohol dehydrogenase playing a pivotal role in biological systems, catalytic oxidation dominating industrial processes, and the Maillard reaction contributing to acetaldehyde generation in food chemistry [87].

The identification of specific precursors and the elucidation of degradation pathways are not only relevant from a mechanistic standpoint but also have practical implications. The presence of trace contaminants in the distillate may affect its reuse potential, regulatory compliance, and long-term stability, ultimately influencing the overall efficiency and sustainability of the recovery process.

1.5 Energy and Environmental Aspects of Wastewater Distillation

1.5.1 Energy Load of Distillation

As already stated earlier in this chapter, distillation remains one of the most energy-intensive operations in the chemical industry, accounting for approximately 40% of the sector's total energy consumption and contributing significantly to CO_2 emissions [90]. The energy load required for distillation is highly dependent on the nature of the mixture, with diluted mixtures—such as those encountered in bioethanol or acetone-butanol-ethanol (ABE) recovery—posing challenges due to the large volumes of liquid that must be vaporized to achieve the separation. For example, conventional distillation of dilute bioethanol streams typically requires 2–

2.5 kWh/kg ethanol, while ABE recovery can demand 11–15 MJ/kg-ABE, with even higher values in less optimized systems [91]. Steam is the primary utility for providing the necessary heat, but its use is associated with high operational costs, significant CO_2 emissions, and process inefficiencies if not carefully managed [92].

Recent advances in distillation technology, such as dividing wall columns (DWC), thermally coupled columns, and heat-integrated designs, have demonstrated substantial potential for reducing energy consumption. For instance, replacing conventional columns with a Kaibel (DWC) column in isopropyl alcohol production reduced reboiler duty by up to 22.8% [93], while heat-integrated and vapor recompression systems in bioethanol and ABE recovery have achieved energy savings of 20–60% compared to traditional setups [94]. These improvements not only lower energy and steam requirements but also reduce CO_2 emissions and operational costs, although they may involve higher capital expenditures and increased process complexity [95].

Table 1.2 summarizes typical energy loads and savings for various distillation processes and configurations.

Table 1.2: Summary of energy loads and savings for industrial distillation processes.

Process/Configuration	**Energy Load/Steam Use**	**Energy Savings Potential**	**Reference**
Conventional IPA distillation	~18,617 kW (total reboiler duty)	—	[93]
Bioethanol (dilute, classic)	2–2.5 kWh/kg ethanol	—	[91]
ABE (dilute, classic)	11–15 MJ/kg-ABE	—	[91]

Heat-integrated/advanced columns	20–60% less energy	20–60%	[94]
Dividing wall/thermally coupled columns	9–23% less energy vs. base case	9–23%	[95]

Distillation has high energy requirements, especially when dealing with diluted mixtures and when steam is used. Process intensification and advanced configurations provide significant opportunities to reduce energy consumption and emissions, supporting the transition toward more sustainable industrial operations.

1.5.2 Associated Environmental Impact

The environmental impact of distillation processes is a critical concern in the chemical and related industries, primarily due to their high energy consumption and associated CO_2 emissions, as well as the challenges of waste treatment. Life Cycle Assessment (LCA) studies consistently demonstrate that the operational phase of distillation, particularly the energy required for heating and separation, dominates the environmental footprint, often accounting for over 90% of the total impacts on human health, ecosystems, and resource depletion. For example, the treatment of pharmaceutical wastewater by distillation emits approximately 0.011 kg CO_2-equivalent per kilogram of effluent, with most emissions arising from energy use rather than equipment manufacturing [96]. Waste treatment is another significant factor, as distillation processes generate both wastewater and organic waste; LCA-based guidelines indicate that the environmental benefit of distillation for solvent recovery depends on the specific solvent, with recovery being preferable for those with high environmental burdens during production, while incineration may be more suitable for solvents with lower impacts [97]. Importantly, there is a well-documented trade-off between achieving high product purity and increasing environmental impact: higher purity typically requires greater energy input, leading to

higher CO_2 emissions and resource use. For instance, LCA studies of hybrid distillation-pervaporation systems for alcohol-water mixtures show that while advanced configurations and heat integration can reduce CO_2 emissions and total annual costs by 15–40%, pursuing very high purity levels significantly increases the environmental burden unless energy efficiency measures and renewable energy sources are implemented. Thus, the design and operation of distillation systems must carefully balance the demands for product purity with the imperative to minimize environmental impacts, as supported by comprehensive LCA evidence [98].

1.5.3 Strategies for Reducing Environmental Impact

A variety of strategies have been developed to reduce the environmental impact of distillation, focusing on minimizing energy consumption, CO_2 emissions, and operational costs. The integration of alternative technologies, such as heat pumps, vacuum distillation, advanced thermal integration, and process regeneration, has proven highly effective. Heat pump-assisted distillation, particularly when combined with pressure-swing and extractive configurations, can reduce Total Annual Costs (TAC) and CO_2 emissions by up to 68% compared to conventional processes, with additional benefits when integrated with feed preconcentration and solvent recovery [99]. Vapor recompression and heat integration further enhance energy efficiency, with reductions in energy use and global warming potential (GWP) often exceeding 50% [100]. Advanced column designs, such as dividing-wall columns and thermally coupled systems, also contribute to significant energy and emission savings [101]. Vacuum distillation, by lowering operating pressures and boiling points, reduces the heat input required, making it especially suitable for heat-sensitive or high-boiling mixtures [102]. Regeneration and pre-treatment steps, such as feed preheating and preconcentration, are critical for improving process efficiency; these measures can lower energy costs by up to 22% and further reduce emissions when combined with heat integration [103]. Membrane-based alternatives and hybrid systems, while not always directly

substitutable for distillation, offer additional pathways for energy and emission reductions, particularly in water and solvent recovery applications [104]. Table 1.3 summarizes the impact reduction potential of these strategies, highlighting their effectiveness in sustainable distillation process design.

Table 1.3: Summary of key strategies and their impact on reducing energy use and emissions in distillation.

Strategy/Technology	**Typical Impact Reduction (Energy/CO_2)**	**Reference**
Heat pump-assisted distillation	Up to 68% CO_2, 51% TAC	[99]
Vapor recompression/heat integration	40–75% energy/CO_2 reduction	[100]
Dividing-wall/thermally coupled columns	20–50% energy/CO_2 reduction	[101]
Vacuum distillation	Lower heat input, reduced emissions	[102]
Pre-treatment (preheating, preconcentration)	22–69% cost/energy reduction	[103]
Membrane/hybrid systems	16–47% energy/CO_2 reduction	[104]

1.5.4 Context of Ecological Transition

The ecological transition in the pharmaceutical sector is strongly influenced by policy frameworks such as the European Green Deal, which aim to

decouple economic growth from resource use and achieve climate neutrality by 2050. Within this context, solvent use and solvent-related emissions represent a major environmental concern, as solvents account for up to 80–90% of the total mass involved in API production and constitute a primary source of life cycle emissions [105]. The Green Deal and related initiatives emphasize circular economy principles, resource efficiency, and the minimization of hazardous emissions, encouraging the adoption of solvent recovery systems, advanced purification technologies, and industrial symbiosis practices [106]. Solvent recovery plays a central role in these strategies: by reducing the need for virgin solvent production and limiting hazardous waste, recovery and reuse pathways contribute substantially to emission reductions while supporting compliance with increasingly stringent regulatory frameworks. LCA demonstrates that such approaches can reduce environmental footprints and greenhouse gas emissions by up to 85% [107], underscoring their relevance for both sustainability and economic performance.

Despite these benefits, the implementation of solvent recovery systems presents important trade-offs. Pharmaceutical manufacturing is governed by strict quality and safety standards, which require that recovered solvents meet high purity criteria to avoid risks to product integrity and patient safety. Achieving these purity levels often necessitates sophisticated purification equipment and continuous process monitoring, increasing operational complexity and costs [105,108]. Moreover, sustainability decision-making in the sector is complicated by data gaps, uncertain environmental impacts, and the need for multi-criteria assessment tools capable of balancing environmental, economic, and social dimensions [108]. Nevertheless, systems-level approaches and sustainability metrics, such as the E factor, Process Mass Intensity (PMI), and LCA, are increasingly used to evaluate the performance of solvent recovery strategies and optimize their integration into manufacturing processes [109]. Overall, solvent recovery emerges as a cornerstone of circular economy strategies in the pharmaceutical industry, enabling significant reductions in GHG emissions,

toxic releases, and resource consumption, while aligning industrial practices with broader ecological transition objectives [105].

In this context, product quality becomes a critical parameter not only from a regulatory and operational standpoint, but also from an environmental one. Distillates that fail to meet internal specifications often require additional treatment steps, such as re-distillation, adsorption on activated carbon, or blending, which increase energy consumption, generate secondary waste streams, and reduce the overall sustainability of the process. Ensuring consistent quality of the recovered ethanol is therefore essential to minimizing the environmental footprint and enabling true circular use within pharmaceutical operations.

1.6 Identified Gaps and Motivation for the Research

1.6.1 Gaps in Current Literature and Technologies

Despite the extensive body of research on solvent recovery in the pharmaceutical sector, several critical gaps remain in the current literature, particularly regarding ethanol recovery from complex waste streams such as those generated by plasma fractionation.

Firstly, while distillation is widely recognized as the most established technology for ethanol separation, conventional systems remain highly energy-intensive, especially when applied to dilute aqueous solutions typical of pharmaceutical effluents. Although energy-saving configurations, such as heat pump-assisted and vacuum distillation systems, have shown significant potential in reducing consumption and emissions, their application to real industrial waste streams remains limited. Most studies are either simulation-based or refer to model mixtures, and only a few provide experimental validation in realistic, high-fouling, or low-concentration contexts.

Secondly, the literature on contaminants in recovered ethanol is often focused on fermentation-derived ethanol or alcoholic beverages, while less is known about volatile and semi-volatile impurities formed during the recovery of ethanol from pharmaceutical effluents, particularly in the presence of complex organic matrices. Although some studies describe degradation products such as aldehydes or furans, the identification of specific precursors and the reaction pathways involved in their formation during distillation is still fragmentary and case dependent.

Finally, while LCA have highlighted the environmental impact of distillation-based recovery, these analyses often treat the system in simplified terms, without integrating product quality, contaminant removal needs, or reprocessing cycles into the overall sustainability evaluation. This leads to an incomplete understanding of the trade-offs between energy use, environmental performance, and solvent purity, especially when high product specifications are required.

1.6.2 Industrial and Sustainability Needs

The pharmaceutical industry operates under strict regulatory, economic, and environmental constraints. From an operational standpoint, the use of large volumes of ethanol, particularly in plasma fractionation processes, makes its efficient recovery essential for reducing raw material costs and minimizing hazardous waste generation. However, the variability of effluent composition, the stringent quality requirements for recovered ethanol, and the sensitivity of pharmaceutical production chains limit the applicability of standard recovery approaches.

In addition to economic considerations, environmental sustainability has become a strategic priority across the sector, driven by policy frameworks such as the European Green Deal and the increasing adoption of LCA tools in process design. Solvent-related emissions represent a major contribution to the industry's environmental footprint, and solvent recovery is recognized as a key strategy to support decarbonization and resource efficiency. Nonetheless, achieving environmental targets is often complicated by the

need for high product purity, which typically requires energy-intensive reprocessing steps and specialized purification technologies, thereby reducing the overall sustainability gains.

Furthermore, circular economy principles encourage the reintegration of recovered materials into the production cycle, but this requires reliability in solvent quality, predictable process performance, and robust contaminant control strategies. These requirements are especially critical in pharmaceutical applications, where recovered ethanol is not simply a commodity but a functional ingredient subject to strict compliance standards.

Therefore, the development of recovery technologies must strike a delicate balance between energy efficiency, environmental impact, product quality, and economic feasibility, a challenge that remains unresolved in the current literature and industrial practice.

1.6.3 Motivation and Objective of this Research

Considering the gaps identified in the literature and the pressing industrial and environmental needs, this research aims to develop and evaluate innovative process configurations for ethanol recovery from pharmaceutical wastewater, specifically from effluents generated during human plasma fractionation. The study focuses on designing a system that is energy-efficient, environmentally sustainable, and capable of producing high-quality ethanol suitable for internal reuse.

The core of the proposed solution is the integration of heat pump-assisted distillation, a technology that offers the potential to significantly reduce energy consumption and CO_2 emissions by recovering and upgrading waste heat within the system. However, beyond energy performance, the research also addresses the critical issue of contaminant formation in the distillate, which currently limits the reusability of recovered ethanol. To this end, a dedicated experimental investigation is carried out to identify the precursors

of volatile and semi-volatile impurities, determine their formation kinetics, and evaluate how operating conditions influence their presence in the distillate.

The methodology combines process simulation, experimental analysis, and techno-economic evaluation to compare different configurations and define optimal operating conditions. Environmental impacts are assessed through energy balance and sustainability indicators, in line with circular economy goals and regulatory expectations.

Ultimately, this work aims to contribute a case-specific, experimentally validated approach to ethanol recovery from complex pharmaceutical effluents, providing both technical insight and practical recommendations for the implementation of low-impact, high-performance recovery systems in industrial settings.

In addition to ethanol recovery, this study investigates a complementary approach for wastewater valorisation. A case study was simulated involving the application of a hydrodynamic cavitation system to the company's existing wastewater treatment plant with the aim of improving the quality of the effluent. This technology has shown promise in degrading persistent organic contaminants, enhancing biodegradability, and reducing toxicity, thus enabling the possibility of reusing treated pharmaceutical effluents for irrigation, including for crops with the most stringent regulatory requirements. This second line of investigation aims to support broader circular economy strategies, expanding the sustainability impact of the proposed process interventions.

2. INDUSTRIAL PROCESS AND PRELIMINARY EXPERIMENTAL EVIDENCE

This chapter describes the industrial and operational context from which the hydroalcoholic waste under study originates, analyzing both the plasma fractionation process and the company's ethanol recovery system.

Some of the information reported comes from technical documentation and internal studies carried out by Takeda Manufaturing Italia in previous years, while the experimental investigation presented here was conducted in collaboration with LabAnalysis Life Science S.r.l.[1] to provide a more in-depth characterization of waste and distillates.

The chapter therefore integrates historical data, plant observations, and experimental results aimed at:

- understanding the compositional variability of waste,
- identifying the potential precursors of volatile compounds,

[1] LabAnalysis Life Science S.r.l. is a private Accredia-certified analysis laboratory that Takeda often relies on for specific analyses of wastewater and products.

- assessing the influence of operating conditions on the formation of contaminants during distillation.

This information forms the basis for the advanced analytical studies reported in Chapter 3. and for the development of the technological solutions proposed in the following chapters.

2.1 The Plasma Fractionation Process and Origin of the Hydroalcoholic Waste

The separation and purification of plasma proteins have been central to the development of modern biotherapeutics, with the Cohn fractionation process representing a pivotal advance in this field. Developed in the 1940s by Edwin J. Cohn and colleagues, this process introduced a systematic approach to plasma protein fractionation using cold ethanol precipitation under carefully controlled conditions of pH, ionic strength, temperature, and protein concentration. The method enabled the selective enrichment of major plasma proteins, such as albumin, immunoglobulins, fibrinogen, and others, into distinct fractions, each with specific therapeutic applications [2,110,111].

The original motivation for the Cohn process was to address urgent clinical needs during World War II, particularly the demand for stable plasma-derived albumin to treat shock and blood loss in wounded soldiers. Over time, the process has been adapted and expanded to support the large-scale production of a variety of plasma-derived medicinal products, including immunoglobulins for immunodeficiency disorders and coagulation factors for bleeding disorders [110,111]. The ability to efficiently utilize a single plasma donation for the extraction of multiple therapeutic proteins has made the Cohn process a cornerstone of the plasma fractionation industry, supporting the treatment of millions of patients worldwide [110,111].

Plasma fractionation today remains fundamentally based on the principles established by Cohn but has evolved to incorporate additional steps and technologies to improve yield, purity, and safety. The process typically begins with cryoprecipitation at 1–4°C to isolate factor VIII, von Willebrand factor, and fibrinogen, followed by sequential cold ethanol precipitation at subzero temperatures (–3°C to –6.5°C) and varying ethanol concentrations (8% to 40% v/v) to separate other major protein fractions [2,110]. For example, in industrial-scale Cohn fractionation, Fraction I is precipitated at 8% ethanol, –3°C, and pH 7.2, with a protein concentration of 51.1 g/L. Fractions II+III are obtained at 25% ethanol, –5°C, and pH 6.8, with a protein concentration of 30.0 g/L. Fraction IV-1 is precipitated at 18% ethanol, –5°C, and pH 5.2, with a protein concentration of 15.8 g/L. The final albumin-rich Fraction V is isolated at 40% ethanol, –5°C, and pH 4.8, with a protein concentration of 7.5 g/L [2]. These precise adjustments of ethanol concentration, temperature, and pH at each step exploit the differential solubility of plasma proteins, enabling their selective precipitation and enrichment.

Modern fractionation plants process plasma in batches of several thousand liters, with global annual plasma fractionation volumes exceeding 23–28 million liters [110]. Analytical methods such as Kjeldahl digestion and digital refractometry are used for in-process monitoring of protein concentrations, ensuring process consistency and product quality [2]. Downstream, chromatographic techniques are increasingly integrated to further purify specific proteins, and robust viral inactivation/removal steps, such as solvent/detergent treatment, pasteurization (60°C for 10 hours), low pH incubation, and nanofiltration, are implemented to ensure product safety [110,111].

In summary, the Cohn fractionation process not only laid the foundation for the plasma protein therapeutics industry but also continues to evolve, driven by the need for efficient, safe, and cost-effective production of life-saving biotherapies. The integration of technical advances and rigorous process control, including specific ethanol concentrations (8–40%), subzero

temperatures (–3°C to –6.5°C), and pH adjustments (7.2 to 4.8) at each fractionation step, has enabled the reliable supply of high-quality plasma-derived medicines to meet global clinical needs [2,110,111].

Hydroalcoholic wastewater mainly comes from the supernatants generated during protein precipitation and subsequent washing of solid fractions. Ethanol, used as a precipitating agent, remains in significant concentrations in waste liquids, together with residues of partially denatured proteins, stabilizers, plasma-derived organic compounds, and potential degradation products.

The composition of these wastes is not constant but varies depending on:

- process operating parameters (temperature, pH, ethanol concentration).
- fractionation process implemented.
- characteristics of the plasma batch treated.
- methods of separation and washing of protein fractions.
- fractionation technologies used, including modern high-yield variants.

This variability has a decisive influence on the behaviour of the waste during distillation and is one of the key elements in understanding the formation of undesirable volatile compounds in the recovered product.

The diagram in Figure 2.1 summarizes the ethanol-based plasma fractionation process Next Generation 1 (NG1) currently adopted at the Takeda production site in Cittaducale. While the exact conditions and parameters remain confidential, the scheme illustrates the sequential precipitation steps, the corresponding separation operations, and the points at which hydroalcoholic waste streams are generated during routine manufacturing of this process.

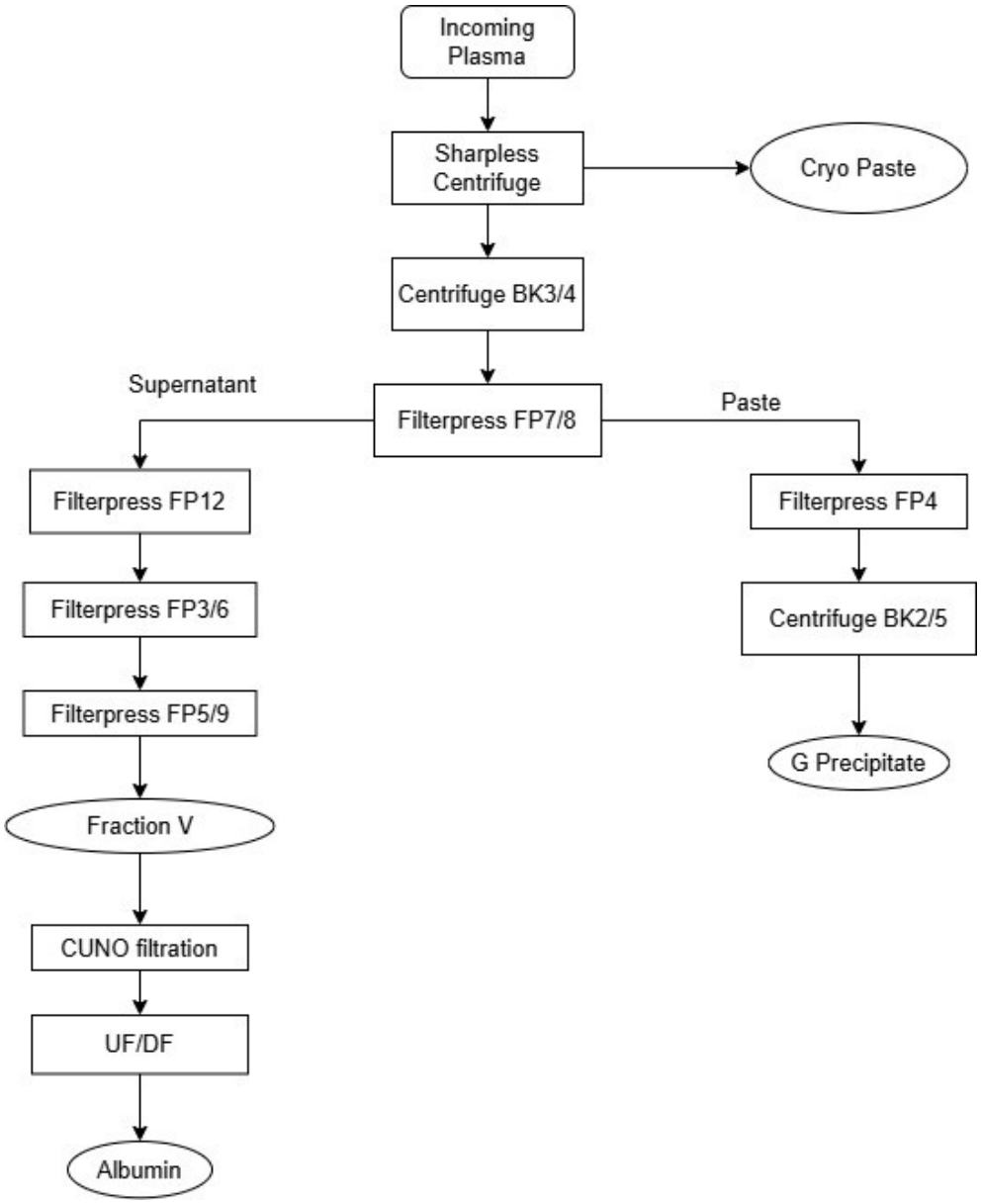

Figure 2.1: Simplified diagram of the fractionation process NG1 implemented at the Takeda plant in Cittaducale (RI), Italy.

2.2 Description of the Ethanol Recovery System

2.2.1 Ethanol Recovery System

The Spent EtOH produced in the various fractionation stages is collected for ethanol recovery. The recovered ethanol will then be reused for the fractionation process. During the NG1 process, the stages highlighted in the diagram in Figure 2.1 produce Spent EtOH with different ethanol

concentrations. These solutions are then treated according to the diagram in Figure 2.2.

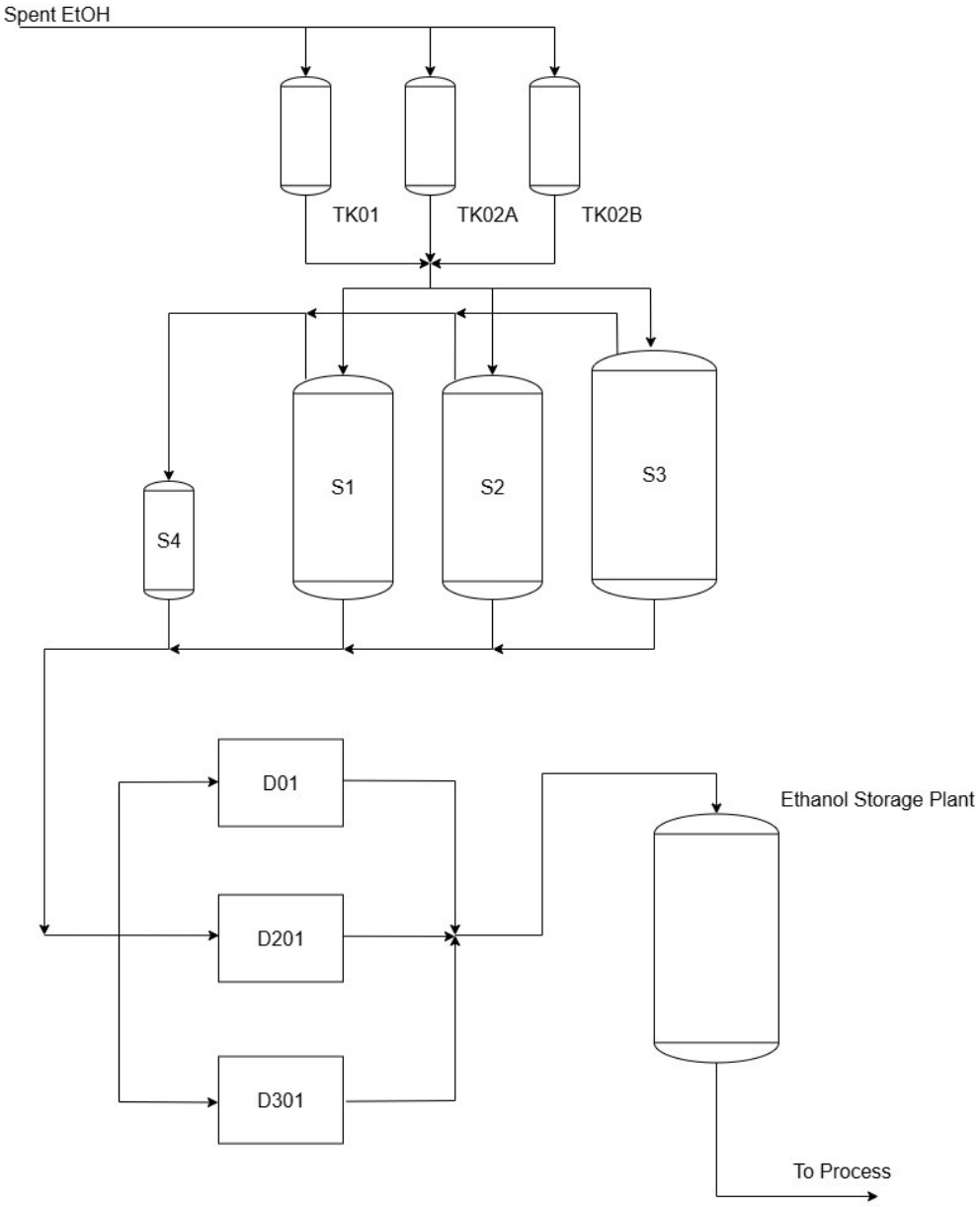

Figure 2.2: Diagram of the Spent EtOH collection and treatment plant and Recovered Ethanol collection plant.

Spent ethanol is first collected in booster tanks (TK01 and TK02A/B) and subsequently transferred to the main storage tanks S1 (100 m^3), S2 (100 m^3), and S3 (150 m^3). From these tanks, the hydroalcoholic solution is fed to the distillation units D01 and, to a larger extent, D301, where the ethanol recovery process is carried out. The recovered ethanol is then directed to dedicated collection tanks, where it remains in quarantine until batch

release. The quarantine and quality-release section of the recovery system falls outside the scope of the present study.

It is important to note that the distillation unit D201 is currently being phased out, and a new plant, D401, is under construction. Once operational, D401 will replace all existing distillation units, enabling full decommissioning of the current recovery infrastructure.

2.2.2 DISTILLATION PLANT

The ethanol recovery system currently in operation at the Takeda facility and object of this study is a two-column distillation unit designed to process hydroalcoholic waste streams originating from plasma fractionation. The plant, referred to as D301, has a nominal capacity of 12,000 L/day of ethanol (100% w/w equivalent) and is optimized to treat mother liquors containing a minimum ethanol concentration of 20% v/v. Figure 2.3 shows the diagram of this system.

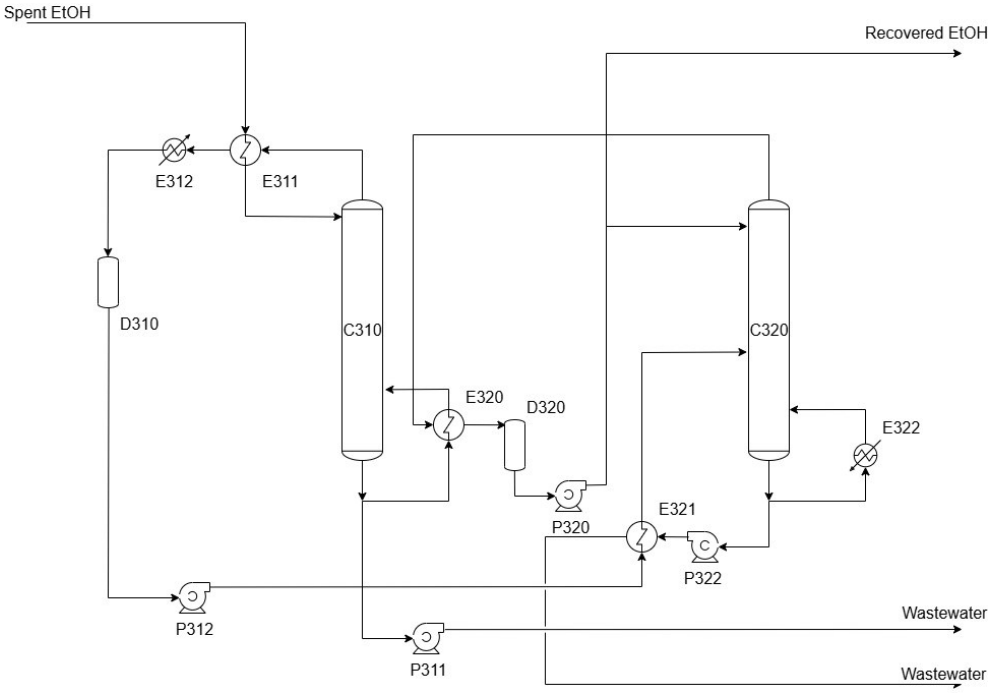

Figure 2.3: Simplified layout of D301.

Because the feed contains thermolabile protein residues and other organic compounds, the system is configured to minimize thermal degradation. For this reason, the first distillation column (C310) operates under deep vacuum,

maintaining a bottom temperature below 60°C. The second column (C320) operates near atmospheric pressure and is responsible for ethanol concentration above 95.1% v/v. The two columns are energetically integrated through a double-effect configuration: the latent heat released by condensing vapors from C320 supplies the thermal duty of C310, resulting in reduced steam consumption and high distillation efficiency.

The process consists of two main stages:

- Alcohol depletion (C310) – Removal of ethanol from the feed until complete exhaustion.
- Alcohol concentration (C320) – Enrichment of ethanol to a final purity above 95.1% v/v.

The mother liquor is pumped by P301 through flow controller FT301 and introduced at the top tray of C310 after preheating in E311, which uses the latent heat of vapors exiting the column. C310 is equipped with valve trays and operates under a vacuum of approximately 10 kPaA at the top and 17 kPaA at the bottom, conditions that allow ethanol to be stripped at temperatures significantly lower than its atmospheric boiling point.

The bottoms stream, depleted with ethanol, is continuously withdrawn by P311 and discharged to waste handling.

Vapors leaving the top of C310 are condensed in a three-stage condenser train (E311, E312, and E313), with E313 connected to a liquid-ring vacuum pump (P310) that maintains sub-atmospheric operation. The condensed stream is collected in drum D310 and pumped to the second column by P312.

The condensate from C310 is fed to tray 12 of C320 after being preheated in the plate exchanger E321 against the bottoms of the same column. In the stripping section of C320, residual ethanol is recovered; the bottoms, now ethanol-free, are removed by P322 after cooling in E321.

In the rectifying section, a reflux stream is supplied from accumulator D320 via pump P320. Under normal operation, the column reaches a head

temperature of 78–79°C and a sensitive plate temperature of 86°C, conditions corresponding to the target purity of >95.1% v/v.

Head vapors are first condensed in E310, which functions simultaneously as the reboiler of C310 (double-effect). Remaining vapor is condensed in the guard condenser E320. The condensate from both exchangers returns to D320, from which part is recycled as reflux and part is withdrawn as final product. The product stream is cooled in heat exchangers E380 and E381 before being sent to ethanol storage tanks. Table 2.1 shows a summary of the material balances for plant D301.

Extraction of the final product is regulated by valve DTCV322, controlled through the temperature difference between the sensitive tray (TT322B) and the top of the column (TT322A), ensuring stable purity and flow conditions.

Steam at 350 kPaA is supplied through the distribution header D300, with E322 serving as the reboiler for C320 during steady-state operation. Cooling is provided by well water (≈18°C) or chilled water (≈7°C), depending on the condenser. A liquid-ring vacuum pump ensures a stable vacuum level for C310, typically set at 10 kPaA, as monitored by PT311/PICA311.

The entire system operates under a computerized control architecture that manages flow, pressure, temperature, levels, and vacuum. The PLC interfaces with all field instruments, providing:

- Real-time trends and historical logging
- Alarm reports
- Automated shutdown and emergency procedures
- Interactive synoptic views for operators

The setup ensures stable and reproducible distillation performance, even with variable feed composition typical of pharmaceutical waste streams.

Table 2.1: Material balance for D301

Stream	Description	T (°C)	P (kPa)	Flowrate (kg/h)	Water and others (kg/h)	Ethanol (kg/h)	Ethanol (% w/w)	Ethanol (% vol.)
1	Feed (Mother liquors)	5	Pump	1957	1557	400	20,44	25
2	Preheated feed	30	Pump	1957	1557	400	20,44	25
3	Vapors from C 310	35	10	941	541	400	42,49	50
4	Stillage (dark discharge from C 310)	56	17	1016	1016	0	0	0
5	Feed to C 320	35	Pump	941	541	400	42,49	50
6	Preheated feed to C 320	70	Pump	941	541	400	42,49	50
7	Vapors from C 320	78	102	2371	180	2191	92,42	95,1
8	Reflux C 320	78	Pump	1398	147	1251	92,42	95,1
9	Final product	78	Pump	433	33	400	92,42	95,1
10	Final product	78	Pump	433	33	400	92,42	95,1
11	Stillage (light discharge from C 320)	105	120	509	509	0	0	0
12	Stillage (light discharge from C 320)	40	40	509	509	0	0	0
13	Steam to E 322	138	350	1140	1140	0	0	0
14	Steam to E 310	138	350	0	0	0	0	0

2.2.3 CRITICAL ISSUES IDENTIFIED

Part of the issue is linked to the intrinsic variability of the hydroalcoholic waste itself. Differences between plasma batches, fractionation conditions, and the introduction of modern high-yield fractionation processes (such as the NG1 workflow) resulted in waste streams with heterogeneous compositions. These streams frequently contain partially denatured proteins, stabilizers, carbohydrates, and other reactive organic species that could act as precursors for volatile compounds formed during heating. As a result, the behavior of the waste during distillation could vary significantly from batch to batch.

Over the years, several recurring quality deviations have been identified in ethanol recovered from hydroalcoholic waste streams. These deviations included the appearance of unexpected volatile and semi-volatile compounds in the distillate, fluctuations in ethanol concentration, and inconsistent performance between batches processed under nominally identical operating conditions. A marked increase in impurities was often observed when the reboiler temperature exceeded specific thresholds, suggesting the activation of thermally driven degradation reactions. However, no studies have been conducted to confirm this phenomenon.

Finally, the analytical capabilities available on site for this utility are not sufficient to elucidate the chemical nature or origin of the contaminants. While GC-FID, spectrophotometry, and routine quality control assays allowed quantitative monitoring of selected parameters, they were unable to identify unknown species, determine whether such compounds originated upstream in the fractionation process, or verify whether they formed thermally during distillation. Moreover, potential precursors could not be detected or characterized with the analytical tools available in-house. These limitations hindered the understanding of the root causes of the observed deviations and justified the need for a comprehensive, advanced analytical investigation.

In addition to the historical issues described above, more recent deviations were observed in hydroalcoholic solutions stored in tank S2, a newly installed vessel within the facility. Several batches of recovered ethanol originating from this tank exhibited out-of-specification results, with analytical evidence indicating a direct correlation between the detected impurities and the material of the tank's internal liner. Although the precise migration mechanism was not fully characterized at the time of occurrence, the nature and distribution of the contaminants strongly suggested leaching phenomena attributable to the internal coating.

Given the stringent quality requirements that characterize pharmaceutical manufacturing environments, the response to this event was immediate. Tank S2 was promptly isolated from the production network, and all hydroalcoholic solutions stored within it were disposed of in full compliance with applicable waste management regulations. This swift action ensured complete containment of the issue and prevented any potential impact on downstream processes or on the quality of the recovered ethanol. The incident further underscored the sensitivity of the recovery system to materials of construction and reinforced the need for careful control of all components in contact with process streams.

2.3 Motivations for In-Plant Analytical Investigation

In recent years, several quality deviations have been documented in the recovered ethanol produced at the Takeda facility. These deviations prompted a series of internal investigations and, subsequently, a dedicated analytical study performed in 2021 by LabAnalysis S.r.l., aimed at characterizing the volatile impurity profile of recovered ethanol batches originating from different fractionation pathways.

The study focused on the quantification of acetaldehyde, ethyl acetal, and octanoic acid, as well as on the untargeted screening of volatile organic compounds. Acceptance criteria were established based on the European

Pharmacopoeia [78] and internal specifications, including limits for methanol, acetaldehyde + acetal, benzene, total other volatile impurities, and UV absorbance thresholds within specified wavelength ranges.

The results presented in the study (summarized in Table 2.2) highlighted a clear difference between ethanol recovered from NG pathways and ethanol recovered from Pathway 1 (PW1) process. In particular:

- Recovered ethanol from PW1 frequently exhibited higher levels of "total other volatile impurities", in some cases approaching or exceeding internal thresholds.
- Acetaldehyde + Acetal levels displayed variability among samples, with PW1 material generally showing higher concentrations.
- UV absorbance between 270–340 nm, although compliant in many cases, showed notable variability and raised questions about its predictive value for the presence of impurities.
- The untargeted volatile screening revealed the presence of additional organic compounds whose identity could not be resolved with the available analytical scope.

Table 2.2: Characterization of ethanol recovered from certain production batches in 2021.

Compounds $\left[\frac{mg}{l}\right]$	**PW1 A**	**PW1 B**	**NG3**	**NG9**	**NG4**	**NG7**	**NG1**
Acetaldehyde	12,6	7,45	7,3	3,16	3,46	3,92	4,28
Ethyl acetate	16,6	8,96	8,77	4,79	5,56	6,58	9,05
Acetone	57	16	76,8	48,2	49,1	59,5	74,5
2,2-Dietoxy propane	2,02	0	0	0	0	0	0
Diethyl acetal	49	16,1	7,68	4,94	4,41	5,19	4,85
Octanoic acid	<1	<1	<1	<1	<1	<1	<1
Tetrahydrofuran	2,46	1,25	2,08	1,91	1,51	2,24	3,76

These findings suggested that the volatile profile of the recovered ethanol was strongly influenced by the upstream process pathway, in line with the

hypothesis that the chemical composition of the hydroalcoholic waste is closely linked to the specific fractionation steps and operational conditions.

The conclusions of the 2021 characterization study highlighted two critical aspects:

1. Recovered ethanol from NG pathways contained fewer impurities, suggesting that differences in the upstream fractionation process significantly affect impurity formation and carryover.
2. PW1-derived ethanol showed recurrent deviations, indicating that the corresponding hydroalcoholic waste streams likely contain precursors or reactive species that promote the formation of volatile impurities during distillation.

The study also recommended the execution of a new characterization campaign involving multiple PW1 batches, strengthening the observation that current knowledge of precursor species and impurity formation mechanisms was insufficient.

The results obtained by LabAnalysis, while valuable, raised several questions that could not be resolved solely through off-site analyses. Most critically:

- It remained unclear whether volatile impurities were already present in the hydroalcoholic waste before entering the distillation system.
- The study did not address whether these compounds were formed thermally during the distillation process.
- The available analytical methods did not allow for the identification of unknown species detected in the untargeted screening.
- No information was available on the role of modern high-yield fractionation processes in influencing the impurity landscape.

These unresolved questions provided the motivation for a deeper, systematic in-plant analytical investigation, designed to characterize the hydroalcoholic waste prior to distillation, monitor its transformation during heating, and identify potential precursor compounds.

This investigation, described in the following sections, aimed to bridge the analytical gaps identified in the 2021 study and provide a mechanistic understanding of impurity formation in the ethanol recovery process.

2.4 EXPERIMENTAL METHOD

Based on the quality deviations documented in recovered ethanol and on the outcomes of previous characterization studies, a targeted experimental campaign was carried out directly at the production site. The main objective of this activity was to investigate the origin of volatile and semi-volatile compounds associated with hydroalcoholic waste streams, to assess their potential formation during distillation, and to generate representative samples for advanced off-site analytical characterization.

2.4.1 SAMPLING ACTIVITY

Sampling activities focused exclusively on hydroalcoholic waste streams generated by NG fractionation workflows, as the PW process is being progressively phased out and will no longer be operated at the facility. This approach ensured that the experimental investigation addressed process configurations representative of current and future industrial operation.

A significant number of samples were collected directly during selected stages of the NG plasma fractionation process. This sampling strategy was adopted to capture the hydroalcoholic streams at the point of generation, prior to mixing, storage, or dilution effects. Collecting samples during fractionation allowed a more representative assessment of the chemical composition of the waste streams and facilitated the identification of potential precursor species originating from specific process steps.

Moreover, sampling at different stages of the NG workflow enabled correlation between upstream processing conditions and downstream behavior during distillation. This approach was essential to distinguish between compounds already present in the hydroalcoholic waste because of fractionation operations and species formed only after thermal treatment, thereby supporting a mechanistic interpretation of impurity formation.

Samples were also collected from selected storage tanks S2 and S3. Care was taken to ensure sample representativeness and compliance with internal Good Manufacturing Practice (GMP) procedures during collection, handling, and storage.

A first subset of samples withdrawn from storage tanks S2 and S3, together with samples collected during NG fractionation operations, was analyzed as received, without any preliminary thermal treatment. These analyses were performed to characterize the native volatile and semi-volatile profiles of the hydroalcoholic solutions prior to distillation, thereby providing information on compounds already present in the waste streams before exposure to elevated temperatures.

2.4.2 Laboratory-Scale Batch Distillation Tests

In addition to direct analysis, aliquots of hydroalcoholic solutions collected from storage tanks S2 and S3 were subjected to batch distillation experiments using a laboratory-scale rotary evaporator. These tests were designed to simulate distillation under controlled conditions, allowing systematic variation of operating pressure and boiling temperature.

By performing distillation at different pressure–temperature combinations, it was possible to reproduce a range of thermal severities representative of industrial operation and to evaluate the formation and evolution of volatile and semi-volatile compounds during the distillation process. The use of a rotary evaporator provided precise control over operating parameters and residence time, enabling reproducible comparison between different experimental conditions.

Laboratory-scale batch distillation tests were carried out using a Heidolph Hei-VAP Value Digital rotary evaporator. The system was equipped with a thermostatic heating bath and a condenser, while vacuum was provided by an external pump. Figure 2.4 shows the apparatus used for the experimental

tests. Although the vacuum level was monitored through an integrated pressure gauge, no active pressure control system was available. Operating conditions were therefore defined and reported in terms of measured pressure and corresponding boiling temperature.

Figure 2.4: Experimental apparatus used for batch distillation in the laboratory.

Hydroalcoholic solutions collected from tank S2 were distilled as received, without any preliminary treatment. Samples withdrawn from tank S3 were subjected to two different preparation approaches: a first set was distilled as received, while a second set was pre-filtered using 3 μm Whatman filters (cat. no. 1444-125) prior to distillation. This additional step was introduced to evaluate the potential influence of suspended solids on the formation of volatile and semi-volatile compounds during thermal treatment.

All distillation tests were performed in batch mode, and the resulting distillates were collected and submitted for subsequent analytical characterization. The adopted setup allowed a controlled and reproducible comparison of distillation behavior under different thermal conditions, while maintaining a simplified configuration representative of industrial batch distillation.

The operating conditions adopted for the laboratory-scale distillation tests are summarized in Table 2.3.

Table 2.3: Batch distillation test plan.

S3: sample name	p [kPa]	T_{eb} [°C]	T_{bath} [°C]
Dist_S3_V_p0	19	50,25	55
Dist_S3_V_p1	39	65,67	70
Dist_S3_V_p2	59	75,33	80
Dist_S3_V_p3	70	79,27	85
Dist_S3_V_p4	atmospheric	85,98	91
S3 filtered: sample name	**p [kPa]**	**T_{eb} [°C]**	**T_{bath} [°C]**
Dist_S3_Settl_V_p0	19	50	55
Dist_S3_Settl_V_p1	43	68	73
Dist_S3_Settl_V_p2	67	78	84
Dist_S3_Settl_V_p3	atmospheric	86	95
S2: sample name	**p [kPa]**	**T_{eb} [°C]**	**T_{bath} [°C]**
Dist_S2_V_p0	19	49,86	55
Dist_S2_V_p1	39	63,98	69
Dist_S2_V_p2	59	73,08	78
Dist_S2_V_p3	70	79,94	85
Dist_S2_V_p4	atmospheric	85,49	90

2.4.3 Analytical Characterization

Advanced analytical characterization of hydroalcoholic samples was carried out by an external specialized laboratory (LabAnalysis Life Science S.r.l.) using screening techniques aimed at the identification and semi-quantitative evaluation of volatile organic compounds (VOC) and semi-volatile organic compounds (SVOC). The applied methodologies are summarized below.

Volatile compounds analysis by HS-GC-MS

Volatile organic compounds were analyzed by headspace gas chromatography coupled with mass spectrometry (HS-GC/MS). Samples were prepared by diluting 1 mL of sample to a final volume of 10 mL with purified water and transferred into 20 mL headspace vials.

The method was applied as a screening approach for VOC detection. Ethyl acetate was used as a surrogate compound to estimate the concentration of identified volatile species. Identification of detected compounds was

performed by comparison with the NIST mass spectral library. A method blank was analyzed to evaluate background signals and exclude analytical artefacts.

Semi-volatile compounds analysis by GC-MS

Semi-volatile organic compounds were analyzed by gas chromatography–mass spectrometry (GC/MS) following liquid–liquid extraction (LLE). For this purpose, 5 mL of sample were extracted with 5 mL of dichloromethane by shaking, and the resulting organic phase was directly injected into the GC/MS system.

The analysis was conducted as a screening method. Bis(2-ethylhexyl) phthalate was used as a surrogate compound for the estimation of SVOC concentrations. Compound identification was achieved by comparison with the NIST mass spectral database, and a method blank was included to account for background contributions.

Instrumental conditions

For SVOC analysis, chromatographic separation was carried out using a 50% phenyl / 50% dimethylpolysiloxane capillary column (30 m × 0.25 mm, 0.15 µm film thickness). The injector was operated in splitless mode at 280°C, with an injection volume of 1 µL. The oven temperature program started at 40°C (5 min), followed by a ramp of 20°C·min^{-1} up to 330°C, with a final hold of 10 min. Helium was used as carrier gas at a constant flow rate of 1 mL·min^{-1}.

The mass spectrometer operated in electron ionization mode (EI, 70 eV) with full-scan acquisition in the 45–450 m/z range. A solvent delay of 5 min was applied to suppress the dichloromethane signal.

Complementary physicochemical analyses

Additional analyses were performed to characterize the non-volatile fraction of the samples. Total protein content (TP) was determined using the

Kjeldahl method (Nx6.25). Particle size distribution (PSD) was measured by laser diffraction using a Malvern Mastersizer 3000. Liquid and particle specific gravity (LSG and PSG) were determined according to Regulation (EC) No. 440/2008, Method A.3. Total suspended solids (TSS) and total dissolved solids (TDS) were quantified following the APAT–CNR IRSA 2090 B method. An overview of the collected samples and the corresponding analytical techniques requested from LabAnalysis is reported in Table 2.4.

All samples intended for VOC and SVOC analyses were stored in dark borosilicate glass bottles to minimize light-induced degradation and adsorption phenomena. Samples were kept at −20°C immediately after collection and maintained at the same temperature throughout storage and shipment to the external laboratory. Temperature-controlled transport was used to preserve sample integrity and limit potential volatilization or chemical transformation prior to analysis.

Samples collected for the determination of total suspended solids (TSS), total dissolved solids (TDS), liquid specific gravity (LSG), particle specific gravity (PSG), and particle size distribution (PSD) were instead transferred into plastic containers, as required by the corresponding analytical protocols. These samples were stored and shipped at ambient temperature, in accordance with standard methods for physicochemical characterization of aqueous suspensions.

Table 2.4: List of samples analyzed.

Sample ID	Source	Treatment	Analysis
CS_BK6/7_TP	Cooling Skid Centrifuge BK6/7	None	TP
CS_BK3/4_TP	Cooling Skid Centrifuge BK3/4	None	TP
Sur_FP5/9_TP_t0	Supernatant Filter press FP5/9 Start time	None	TP
Sur_FP5/9_TP_t1	Supernatant Filter press	None	TP

	FP5/9 Middle time		
Sur_FP5/9_TP_t2	Supernatant Filter press FP5/9 End time	None	TP
CS_BK2/5_TP	Cooling Skid Centrifuge BK2/5	None	TP
Sur_BK2/5_TP	Supernatant Centrifuge BK2/5	None	TP
UF_TP	Ultrafiltration Permeate	None	TP
DF_TP_t0	Diafiltration Permeate, Start time	None	TP
DF_TP_t1	Diafiltration Permeate, Middle time	None	TP
DF_TP_t2	Diafiltration Permeate, End time	None	TP
S3_TP	Tank S3	None	TP
S2_TP	Tank S2	None	TP
CS_BK6/7_SV	Cooling Skid Centrifuge BK6/7	None	GC-MS
CS_BK3/4_SV	Cooling Skid Centrifuge BK3/4	None	GC-MS
PreW_FP7/8_SV	Prewash Filter press FP7/8	None	GC-MS
PreW_FP12_SV	Prewash Filter press FP12	None	GC-MS
PreW_FP3/6_SV	Prewash Filter press FP3/6	None	GC-MS
PreW_FP5/9_SV	Prewash Filter press FP5/9	None	GC-MS
Sur_FP5/9_SV	Supernatant Filter press FP7/8	None	GC-MS
CS_BK2/5_SV	Cooling Skid Centrifuge BK2/5	None	GC-MS
Sur_BK2/5_SV	Supernatant Centrifuge	None	GC-MS

	BK2/5		
UF_SV	Ultrafiltration Permeate	None	GC-MS
DF_SV	Diafiltration Permeate	None	GC-MS
S3_SV	Tank S3	None	GC-MS
S2_SV	Tank S2	None	GC-MS
Dist_S3_SV_p0	Tank S3 p0	Distillation	GC-MS
Dist_S3_SV_p1	Tank S3 p1	Distillation	GC-MS
Dist_S3_SV_p2	Tank S3 p2	Distillation	GC-MS
Dist_S3_SV_p3	Tank S3 p3	Distillation	GC-MS
Dist_S3_SV_p4	Tank S3 p4	Distillation	GC-MS
Dist_S2_SV_p0	Tank S2 p0	Distillation	GC-MS
Dist_S2_SV_p1	Tank S2 p1	Distillation	GC-MS
Dist_S2_SV_p2	Tank S2 p2	Distillation	GC-MS
Dist_S2_SV_p3	Tank S2 p3	Distillation	GC-MS
Dist_S2_SV_p4	Tank S2 p4	Distillation	GC-MS
Dist_S3_Settl_SV_p0	Tank S3 p0	Filtration + Distillation	GC-MS
Dist_S3_Settl_SV_p1	Tank S3 p1	Filtration + Distillation	GC-MS
Dist_S3_Settl_SV_p2	Tank S3 p2	Filtration + Distillation	GC-MS
Dist_S3_Settl_SV_p3	Tank S3 p3	Filtration + Distillation	GC-MS
CS_BK6/7_V	Cooling Skid Centrifuge BK6/7	None	HS-GC-MS
CS_BK3/4_V	Cooling Skid Centrifuge BK3/4	None	HS-GC-MS
PreW_FP7/8_V	Prewash Filter press FP7/8	None	HS-GC-MS
PreW_FP12_V	Prewash Filter press FP12	None	HS-GC-MS
PreW_FP3/6_V	Prewash Filter press FP3/6	None	HS-GC-MS

PreW_FP5/9_V	Prewash Filter press FP5/9	None	HS-GC-MS
Sur_FP5/9_V	Supernatant Filter press FP5/9	None	HS-GC-MS
CS_BK2/5_V	Cooling Skid Centrifuge BK2/5	None	HS-GC-MS
Sur_BK2/5_V	Supernatant Centrifuge BK2/5	None	HS-GC-MS
UF_V	Ultrafiltration Permeate	None	HS-GC-MS
DF_V	Diafiltration Permeate	None	HS-GC-MS
S3_V	Tank S3	None	HS-GC-MS
S2_V	Tank S2	None	HS-GC-MS
Dist_S3_V_p0	Tank S3 p0	Distillation	HS-GC-MS
Dist_S3_V_p1	Tank S3 p1	Distillation	HS-GC-MS
Dist_S3_V_p2	Tank S3 p2	Distillation	HS-GC-MS
Dist_S3_V_p3	Tank S3 p3	Distillation	HS-GC-MS
Dist_S3_V_p4	Tank S3 p4	Distillation	HS-GC-MS
Dist_S2_V_p0	Tank S2 p0	Distillation	HS-GC-MS
Dist_S2_V_p1	Tank S2 p1	Distillation	HS-GC-MS
Dist_S2_V_p2	Tank S2 p2	Distillation	HS-GC-MS
Dist_S2_V_p3	Tank S2 p3	Distillation	HS-GC-

Dist_S2_V_p4	Tank S2 p4	Distillation	HS-GC-MS
Dist_S3_Settl_V_p0	Tank S3 p0	Filtration + Distillation	HS-GC-MS
Dist_S3_Settl_V_p1	Tank S3 p1	Filtration + Distillation	HS-GC-MS
Dist_S3_Settl_V_p2	Tank S3 p2	Filtration + Distillation	HS-GC-MS
Dist_S3_Settl_V_p3	Tank S3 p3	Filtration + Distillation	HS-GC-MS
CS_BK6/7_Solids	Cooling Skid Centrifuge BK6/7	None	TSS, TDS, LSG, PSG
CS_BK3/4_Solids	Cooling Skid Centrifuge BK3/4	None	TSS, TDS, LSG, PSG
PreW_FP7/8_Solids	Prewash Filter press FP7/8	None	TSS, TDS, LSG, PSG
PreW_FP12_Solids	Prewash Filter press FP12	None	TSS, TDS, LSG, PSG
PreW_FP3/6_Solids	Prewash Filter press FP3/6	None	TSS, TDS, LSG, PSG
PreW_FP5/9_Solids	Prewash Filter press FP5/9	None	TSS, TDS, LSG, PSG
Sur_FP5/9_Solids_t0	Supernatant Filter press FP5/9 Start Time	None	TSS, TDS, LSG, PSG
Sur_FP5/9_Solids_t1	Supernatant Filter press FP5/9 Middle Time	None	TSS, TDS, LSG, PSG
Sur_FP5/9_Solids_t2	Supernatant Filter press FP5/9 End Time	None	TSS, TDS, LSG, PSG
CS_BK2/5_Solids	Cooling Skid Centrifuge BK2/5	None	TSS, TDS, LSG, PSG
Sur_BK2/5_Solids	Supernatant Centrifuge BK2/5	None	TSS, TDS, LSG, PSG

UF_Solids	Ultrafiltration Permeate	None	TSS, TDS, LSG, PSG
DF_Solids_t0	Diafiltration Permeate Start Time	None	TSS, TDS, LSG, PSG
DF_Solids_t1	Diafiltration Permeate Middle Time	None	TSS, TDS, LSG, PSG
DF_Solids_t2	Diafiltration Permeate End Time	None	TSS, TDS, LSG, PSG
S3_Solids	Tank S3	None	TSS, TDS, LSG, PSG
S3_PSD	Tank S3	None	PSD
HYHT_BK2_V	New Process Supernatant BK2	None	HS-GC-MS
HYHT_FP5_V	New Process Supernatant FP5	None	HS-GC-MS
HYHT_BK2_SV	New Process Supernatant BK2	None	GC-MS
HYHT_FP5_SV	New Process Supernatant FP5	None	GC-MS
HYHT_BK2_TP	New Process Supernatant BK2	None	TP
HYHT_FP5_t0_TP	New Process Supernatant FP5 Start Time	None	TP
HYHT_FP5_t1_TP	New Process Supernatant FP5 Middle Time	None	TP
HYHT_FP5_t2_TP	New Process Supernatant FP5 End Time	None	TP
HYHT_FP5_t0_Solids	New Process Supernatant FP5 Start Time	None	TSS, TDS, LSG, PSG
HYHT_FP5_t1_Solids	New Process Supernatant FP5 Middle Time	None	TSS, TDS, LSG, PSG
HYHT_FP5_t2_Solids	New Process Supernatant FP5 End Time	None	TSS, TDS, LSG, PSG

HYHT_Sur_BK2_Solids	New Process Supernatant BK2	None	TSS, TDS, LSG, PSG

2.4.4 Limitations of the Experimental Approach

While the experimental campaign provided valuable insights into the behaviour of NG-derived hydroalcoholic waste streams, certain limitations must be acknowledged. The number of samples and operating conditions investigated was constrained by industrial availability and by the need to minimize disruption to routine plant operations. Moreover, although advanced analytical techniques were employed by the external laboratory, the study was primarily qualitative and comparative in nature and did not allow full kinetic modelling or definitive identification of all detected species.

Nevertheless, the combination of in-plant sampling, controlled laboratory-scale distillation, and off-site advanced analysis provided a robust framework to investigate impurity formation mechanisms and to support the more detailed analytical discussion presented in the following sections.

2.5 Results of Real Spent EtOH Analyses

2.5.1 Volatile Compounds Analysis

The results of the volatile organic compounds (VOC) screening performed on as-received hydroalcoholic samples are reported in Table 2.5. For all analysed samples, ethanol was detected as the main volatile component, with measured concentrations ranging approximately from 0.08 to 1.28% w/v, depending on the sampling point and process stream.

Among the other monitored volatile species, octanoic acid ethyl ester and ethyl acetate were consistently reported below the method disregard level (0.001% w/v) for all samples listed in Table 2.5. Styrene was also below the disregard level in most samples; however, a measurable value of 0.002%

w/v was detected in the sample collected from tank S2 (S2_V), while all other samples showed concentrations below the reporting threshold.

Overall, the VOC screening of as-received samples indicates a limited presence of volatile organic compounds other than ethanol, with most detected species remaining below the analytical reporting limit. These results provide a baseline characterization of the volatile fraction present in the hydroalcoholic waste streams prior to any thermal treatment.

Table 2.5: Volatile Organic Compounds found in samples.

Sample	Ethanol (% w/v)	Octanoic acid ethyl ester (% w/v)	Ethyl acetate (% w/v)	Styrene (% w/v)
CS_BK6/7 V	1,086	<0,001	<0,001	<0,001
CS_BK3/4_V	1,282	<0,001	<0,001	<0,001
PreW_FP7/8_V	0,722	<0,001	<0,001	<0,001
PreW_FP12_V	0,602	<0,001	<0,001	<0,001
PreW_FP3/6_V	0,581	<0,001	<0,001	<0,001
PreW_FPS/9_V	0,766	<0,001	<0,001	<0,001
Sur_FPS/9_V	0,082	<0,001	<0,001	<0,001
CS_BK2/S_V	1,12	<0,001	<0,001	<0,001
Sur_BK2/5_V	0,67	<0,001	<0,001	<0,001
UF_V	0,326	<0,001	<0,001	<0,001
DF_V	0,364	<0,001	<0,001	<0,001
S3_V	0,684	<0,001	<0,001	<0,001
S2_V	0,6	<0,001	<0,001	0,002

HYHT_BK2_V	0,609	<0,001	<0,001	<0,001
HYHT_FP5_V	0,76	<0,001	<0,001	<0,001

In addition, it is worth noting that acetaldehyde and acetaldehyde-related acetals were not detected in any of the analyzed as-received samples. For all samples reported in Table 2.5, the concentrations of these compounds were below the method disregard level, indicating their absence within the sensitivity limits of the applied HS-GC/MS screening. This observation confirms that, prior to any thermal treatment, aldehydes and acetals do not represent a detectable contribution to the volatile impurity profile of the hydroalcoholic waste streams.

2.5.2 SEMI VOLATILE COMPOUNDS ANALYSIS

The results of the semi-volatile organic compounds (SVOC) screening performed on as-received hydroalcoholic samples are reported in Table 2.6. The analysis revealed the presence of several semi-volatile compounds across the investigated samples, with concentrations reported above the method disregard level.

Detected SVOCs include compounds belonging to classes such as fatty acids, fatty acid ethyl esters, and sterol-related species, although their occurrence and relative abundance varied among samples. Differences were observed between samples collected from different storage tanks, with samples from tank S3 generally showing a higher number of detected SVOCs compared to those from tank S2, as indicated by the entries reported in Table 2.6.

The reported concentrations reflect the semi-quantitative nature of the applied GC/MS screening method and provide an overview of the semi-volatile fraction present in the hydroalcoholic waste streams prior to any thermal treatment. No additional semi-volatile compounds were detected above the reporting threshold other than those listed in Table 2.6.

Table 2.6:Semi Volatile Organic Compounds found in samples.

Sample	**CS_BK6/7_SV**	**CS_BK3/4_SV**	**PreW_FP7/8_SV**	**PreW_FP12_SV**
Octanoic acid ethyl ester (% w/v)	<0,001	<0,001	<0,001	<0,001
Octanoic acid (% w/v)	<0,001	<0,001	<0,001	<0,001
Hexadecanoic acid, ethyl ester (% w/v)	0,002	0,002	<0,001	<0,001
n-Hexadecanoic acid (% w/v)	0,007	0,008	0,002	0,002
Octadecanoic acid, ethyl ester (% w/v)	0,002	0,002	<0,001	<0,001
Octadecanoic acid (% w/v)	0,005	0,006	0,001	0,001
(Z)-13-Docosenamide (% w/v)	0,002	<0,001	<0,001	<0,001
Cholesterol	<0,001	<0,001	<0,001	<0,001
Cholest-4-en-3-one (% w/v)	<0,001	<0,001	<0,001	<0,001

Sample	**Prew_FP3/6_SV**	**PreW_FPS/9_SV**	**Sur_FPS/9_SV**	**CS_BK2/S_SV**
Octanoic acid ethyl ester (% w/v)	<0,001	<0,001	<0,001	<0,001
Octanoic acid (% w/v)	<0,001	<0,001	<0,001	<0,001
Hexadecanoic acid, ethyl ester (% w/v)	<0,001	<0,001	0,001	0,001

n-Hexadecanoic acid (% w/v)	0,003	0,022	0,018	0,003
Octadecanoic acid, ethyl ester (% w/v)	<0,001	0,001	0,001	0,002
Octadecanoic acid (% w/v)	0,001	0,017	0,014	0,002
(Z)-13-Docosenamide (% w/v)	<0,001	<0,001	<0,001	<0,001
Cholesterol	<0,001	<0,001	<0,001	<0,001
Cholest-4-en-3-one (% w/v)	<0,001	<0,001	<0,001	<0,001

Sample	**Sur_BK2/5_SV**	**UF_SV**	**DF_SV**	**S3_SV**
Octanoic acid ethyl ester (% w/v)	<0,001	<0,001	<0,001	<0,001
Octanoic acid (% w/v)	<0,001	<0,001	<0,001	<0,001
Hexadecanoic acid, ethyl ester (% w/v)	0,001	<0,001	<0,001	<0,001
n-Hexadecanoic acid (% w/v)	<0,001	<0,001	<0,001	0,006
Octadecanoic acid, ethyl ester (% w/v)	0,004	<0,001	<0,001	<0,001
Octadecanoic acid (% w/v)	<0,001	<0,001	<0,001	<0,001
(Z)-13-Docosenamide (% w/v)	0,005	<0,001	<0,001	<0,001

Cholesterol	0,002	<0,001	<0,001	<0,001
Cholest-4-en-3-one (% w/v)	0,002	<0,001	<0,001	<0,001

Sample	**S2_SV**	**HYHT_BK2_SV**	**HYHT_FPS_SV**
Octanoic acid ethyl ester (% w/v)	<0,001	<0,001	<0,001
Octanoic acid (% w/v)	<0,001	<0,001	0,002
Hexadecanoic acid, ethyl ester (% w/v)	<0,001	<0,001	<0,001
n-Hexadecanoic acid (% w/v)	0,003	<0,001	0,008
Octadecanoic acid, ethyl ester (% w/v)	0,003	0,002	<0,001
Octadecanoic acid (% w/v)	<0,001	<0,001	<0,001
(Z)-13-Docosenamide (% w/v)	0,004	0,005	<0,001
Cholesterol	0,001	0,002	<0,001
Cholest-4-en-3-one (% w/v)	0,001	0,002	<0,001

2.5.3 PARTICLE SIZE DISTRIBUTION

The results of the particle size distribution (PSD) analysis performed on hydroalcoholic samples collected from tank S3 are reported in Table 2.7. The data indicate the presence of a measurable particulate fraction in all analyzed S3 samples, with particle sizes distributed over the reported dimensional range.

The PSD analysis was performed exclusively on samples from tank S3, as this tank was actively feeding the distillation system at the time of sampling and was not associated with any quality deviations. This choice was made to obtain a characterization of the hydroalcoholic waste that was as representative as possible of normal operating conditions, avoiding the influence of atypical or off-specification scenarios.

The PSD results show that suspended particles are characterized by a broad size distribution, confirming the heterogeneous nature of the solid fraction present in the hydroalcoholic solutions stored in tank S3. The presence of particles within the micrometric range is consistent across the analyzed samples, as indicated by the reported characteristic diameters.

These findings are supported by the corresponding total suspended solids (TSS) values reported for the same samples, which confirm the presence of a non-negligible amount of suspended material. The combined PSD and TSS data provide a physical characterization of the particulate fraction present in S3 hydroalcoholic waste prior to any filtration or thermal treatment.

Table 2.7: Particle Size Distribution for Spent EtOH in S3.

S3_PSD	**µm**
d0,1	3,27
d0,5	10,075
d0,9	22,18

2.5.4 TOTAL PROTEIN CONTENT

The results of the total protein (TP) determination for the analyzed hydroalcoholic samples are reported in Table 2.8. Measurable protein concentrations were detected in all samples, with values ranging between 0.03% and 0.10%. Samples associated with different process streams showed varying TP levels, with higher values (0.10%) observed in samples CS_BK2/5_TP, SUR_BK2/5_TP, and HYHT_BK2_TP, while lower concentrations were measured in UF_TP (0.03%) and S3_TP (0.04%).

Table 2.8: Total Protein Content of the samples.

Sample	Total Protein
CS_BK6/7_TP	0,05%
CS_BK3/4_TP	0,05%
CS_BK2/5_TP	0,10%
SUR_BK2/5_TP	0,10%
UF_TP	0,03%
S3_TP	0,04%
S2_TP	0,05%
HYHT_BK2_TP	0,10%

The temporal evolution of total protein content in the FP5/9 supernatant is reported in Table 2.9. The TP concentration increased from 0.05% at t_0 to 0.10% at t_1, followed by a slight decrease to 0.08% at t_2. These results indicate a non-monotonic trend in protein content over time during FP5/9 operation.

Table 2.9: Total Protein Content Trend on the FP5/9 Supernatant.

Sample	Time (min)	Total Protein
SUR_FP5/9_TP_t0	0	0,05%
SUR_FP5/9_TP_t1	42	0,10%
SUR_FP5/9_TP_t2	80	0,08%

The total protein content trend for the supernatant from the diafiltration step is reported inTable 2.10. TP concentration decreased progressively from 0.05% at t_0 to 0.04% at t_1, reaching values below the analytical detection limit (<0.0002%) at t_2. This data set highlights a marked reduction in measurable protein content over the monitored time points.

Table 2.10: Total Protein Content Trend for the Supernatant from Diafiltration Step.

Sample	Time (min)	Total Protein
DF_TP_t0	0	0,05%
DF_TP_t1	40	0,04%
DF_TP_t2	55	<0,0002%

Finally, the temporal evolution of total protein content in the FP5/9 supernatant during the High Yield High Throughput (HYHT) process is summarized in Table 2.11. The HYHT process is a new process currently being studied that can be applied to the NG process. This process will increase the production yields of the processes currently in place. In this case, TP concentrations showed limited variation over time, with values of 0.09% at t_0, 0.07% at t_1, and 0.08% at t_2, indicating relatively stable protein levels across the sampled time points.

Table 2.11: Total Protein Content Trend on the FP5/9 Supernatant during the HYHT Process.

Sample	Time (min)	Total Protein
HYHT_FP5_t0_TP	0	0,09%
HYHT_FP5_t1_TP	42	0,07%
HYHT_FP5_t2_TP	80	0,08%

2.5.5 LIQUID PROPERTIES

The results of the liquid specific gravity (LSG), total suspended solids (TSS), and total dissolved solids (TDS) measurements for the analyzed hydroalcoholic samples are reported in Table 2.12. The data show a wide variability among samples collected from different process streams.

Table 2.12: Liquid Specific Gravity, Total Suspended Solids and Total Dissolved Solids of the samples.

Sample	LSG	TSS	TDS
	g/l	mg/l	mg/l
CS_BK6/7_Solids	906	0,5	56
CS_BK3/4_Solids	882	60	215
CS_BK2/5_Solids	906	3	274
PreW_FP7/8_Solids	970	2	305
PreW_FP12_Solids	970	8	7337
Prew_FP3/6_Solids	988	8	9
PreW_FP5/9_Solids	952	3	9683
Sur_BK2/5_Solids	946	900	8376
UF_Solids	984	33	31726
HYHT_Sur_BK2_Solids	934	1840	6400

LSG values ranged from 882 g/l to 988 g/l. Lower values were observed for samples such as CS_BK3/4_Solids (882 g/l) and CS_BK6/7_Solids (906

g/l), while higher values were measured for PreW_FP3/6_Solids (988 g/l) and UF_Solids (984 g/l).

TDS values spanned a broad range, from 9 mg/l in PreW_FP3/6_Solids up to 31,726 mg/l in UF_Solids, highlighting significant differences in dissolved solid content among the investigated streams.

The temporal evolution of LSG, TSS, and TDS for the supernatant of FP5/9 is reported in Table 2.13. LSG values remained constant between t_0 and t_1 (936 g/l) and increased slightly at t_2 (942 g/l). TSS values increased from 390 mg/l at t_0 to 450 mg/l at t_1, followed by a decrease to 190 mg/l at t_2. TDS values decreased from 12,062 mg/l at t_0 to 10,346 mg/l at t_1 and then increased slightly to 10,692 mg/l at t_2.

Table 2.13: Liquid Specific Gravity, Total Suspended Solids and Total Dissolved Solids Trends for the Supernatant of FP5/9.

Sample	Time	LSG	TSS	TDS
	min	g/l	mg/l	mg/l
Sur_FP5/9_Solids_t0	0	936	390	12062
Sur_FP5/9_Solids_t1	42	936	450	10346
Sur_FP5/9_Solids_t2	80	942	190	10692

The temporal trends of liquid properties for the supernatant of the diafiltration step are summarized in Table 2.14. LSG values decreased progressively from 996 g/l at t_0 to 984 g/l at t_1, reaching 968 g/l at t_2. TSS concentrations also decreased over time, from 26 mg/l at t_0 to 16 mg/l at t_1 and 6 mg/l at t_2. A consistent decreasing trend was observed for TDS values, which declined from 28,147 mg/l at t_0 to 15,404 mg/l at t_1 and 4,642 mg/l at t_2.

Table 2.14: Liquid Specific Gravity, Total Suspended Solids and Total Dissolved Solids Trends for the Supernatant of the Diafiltration Step.

Sample	Time	LSG	TSS	TDS
	min	g/l	mg/l	mg/l
DF_Solids_t0	0	996	26	28147
DF_Solids_t1	40	984	16	15404
DF_Solids_t2	55	968	6	4642

The temporal evolution of LSG, TSS, and TDS for the supernatant of FP5/9 during the HYHT process is reported in Table 2.15. LSG values remained unchanged between t_0 and t_1 (919 g/l) and increased slightly at t_2 (929 g/l). TSS values showed limited variation, with 640 mg/l at t_0, 660 mg/l at t_1, and 540 mg/l at t_2. TDS values decreased progressively from 9,750 mg/l at t_0 to 9,580 mg/l at t_1 and 9,080 mg/l at t_2.

Table 2.15: Liquid Specific Gravity, Total Suspended Solids and Total Dissolved Solids Trends for the Supernatant of FP5/9 during the HYHT Process.

Sample	Time	LSG	TSS	TDS
	min	g/l	mg/l	mg/l
HYHT_FP5_t0_Solids	0	919	640	9750
HYHT_FP5_t1_Solids	42	919	660	9580
HYHT_FP5_t2_Solids	80	929	540	9080

2.5.6 Results of Laboratory-Scale Distillation Tests

The results reported in Table 2.16 refer to hydroalcoholic samples subjected to laboratory-scale batch distillation. The analyzed distillates were obtained from hydroalcoholic solutions originating from tank S3, characterized by an ethanol concentration of approximately 19% v/v prior to distillation.

The table summarizes the volatile and semi-volatile compounds detected in the distillates, as identified by the applied screening methods. Compared to the corresponding as-received samples, the distillates show the presence of

additional volatile species reported above the method disregard level, indicating a modification of the volatile profile following thermal treatment.

It should be noted that distillation time was not considered a relevant parameter in this experimental campaign, as the objective of the laboratory-scale tests was not to evaluate distillation kinetics or separation efficiency. Instead, the experiments were specifically designed to assess the formation of volatile compounds under elevated temperature conditions, independently of the duration of the distillation process.

The results reported in Table 2.16 therefore provide a qualitative and semi-quantitative description of the volatile compounds present in the distillates obtained from S3 hydroalcoholic solutions under high-temperature laboratory-scale distillation conditions.

Table 2.16: VOC and SVOC for the Distilled Samples from S3 Tank before filtration.

Sample	**Dist_S3_V_p0**	**Dist_S3_V_p1**	**Dist_S3_V_p2**	**Dist_S3_V_p3**	**Dist_S3_V_p4**
p (kPa)	19	39	59	70	amb
T eb (°C)	50,25	65,67	75,33	79,27	85,98
T bath	55	70	80	85	91
VOC					
Ethanol (% w/v)	0,651	0,649	0,627	0,562	0,933
Octanoic acid ethyl ester (% w/v)	<0,001	<0,001	<0,001	<0,001	<0,001
Ethyl acetate (% w/v)	<0,001	<0,001	<0,001	<0,001	<0,001
Styrene (% w/v)	0,001	<0,001	<0,001	<0,001	<0,001
SVOC					
Octanoic acid ethyl	<0,001	<0,001	<0,001	0,001	<0,001

ester (% w/v)					
Octanoic acid (% w/v)	0,001	<0,001	0,001	<0,001	0,002
Hexadecanoic acid, ethyl ester (% w/v)	<0,001	<0,001	<0,001	<0,001	<0,001
n-Hexadecanoic acid (% w/v)	0,005	0,003	0,004	0,003	0,006
Octadecanoic acid, ethyl ester (% w/v)	<0,001	<0,001	<0,001	<0,001	0,001
Octadecanoic acid (% w/v)	<0,001	<0,001	<0,001	<0,001	<0,001
(Z)-13-Docosenamide (% w/v)	<0,001	<0,001	<0,001	<0,001	<0,001
Cholesterol	<0,001	<0,001	<0,001	<0,001	<0,001
Cholest-4-en-3-one (% w/v)	<0,001	<0,001	<0,001	<0,001	<0,001

The results reported in Table 2.17 refer to laboratory-scale batch distillation tests performed on hydroalcoholic solutions from tank S3 subjected to pre-filtration prior to distillation. As for the other distillation experiments, the initial ethanol concentration of the S3 solutions was approximately 19% v/v.

The table summarizes the volatile and semi-volatile compounds detected in the distillates obtained from filtered S3 samples. Compared to the results reported for unfiltered S3 solutions (Table 2.16), the distillates derived from filtered samples exhibit a slightly reduced number of detected compounds and, for several species, lower reported semi-quantitative levels.

The results reported in Table 2.17 document the effect of pre-filtration on the chemical profile of the distilled solutions highlighting differences in the

volatile and semi-volatile composition of distillates obtained from filtered and unfiltered hydroalcoholic solutions under otherwise comparable laboratory-scale distillation conditions.

Representative photographs of S3 hydroalcoholic solutions before and after filtration, together with the solid residues retained on the filter, are shown in Figure 2.5 and Figure 2.6. These visual observations provide qualitative support to the analytical differences reported in Table 2.17.

As for the other laboratory-scale distillation tests, the duration of the distillation was not considered a relevant variable, since the experimental objective was limited to assessing the presence and formation of volatile compounds under high-temperature conditions.

Table 2.17: VOC and SVOC for the Distilled Samples from S3 Tank after filtration.

Sample	**Dist_S3_Settl_V_p0**	**Dist_S3_Settl_V_p1**	**Dist_S3_Settl_V_p2**	**Dist_S3_Settl_V_p3**
p (kPa)	19	43	67	amb
T eb (°C)	50	68	78	86
T bath (°C)	55	73	84	95
VOC				
Ethanol (% w/v)	0,586	0,474	0,556	0,752
Octanoic acid ethyl ester (% w/v)	<0,001	<0,001	<0,001	<0,001
Ethyl acetate (% w/v)	<0,001	0,002	<0,001	<0,001
Styrene (% w/v)	<0,001	<0,001	<0,001	<0,001
SVOC				
Octanoic acid ethyl ester (% w/v)	<0,001	0	<0,001	<0,001

Octanoic acid (% w/v)	<0,001	0,002	0,001	0,002
Hexadecanoic acid, ethyl ester (% w/v)	<0,001	<0,001	<0,001	<0,001
n-Hexadecanoic acid (% w/v)	0,002	0,004	0,003	0,004
Octadecanoic acid, ethyl ester (% w/v)	<0,001	<0,001	<0,001	<0,001
Octadecanoic acid (% w/v)	<0,001	<0,001	<0,001	<0,001
(Z)-13-Docosenamide (% w/v)	<0,001	<0,001	<0,001	<0,001
Cholesterol	<0,001	<0,001	<0,001	<0,001
Cholest-4-en-3-one (% w/v)	<0,001	<0,001	<0,001	<0,001

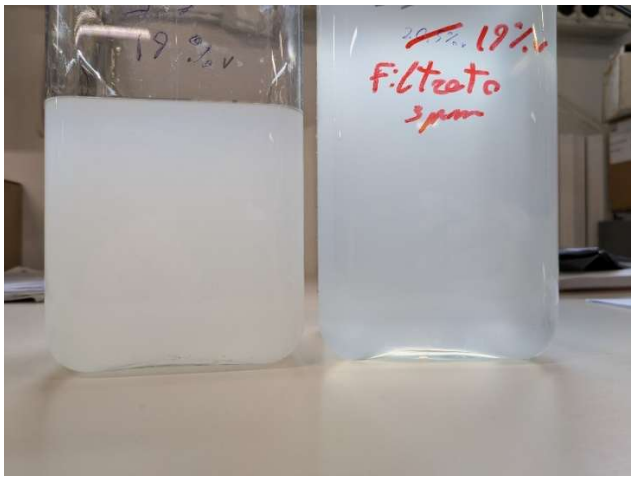

Figure 2.5: Hydroalcoholic Solution from S3 before and after filtration.

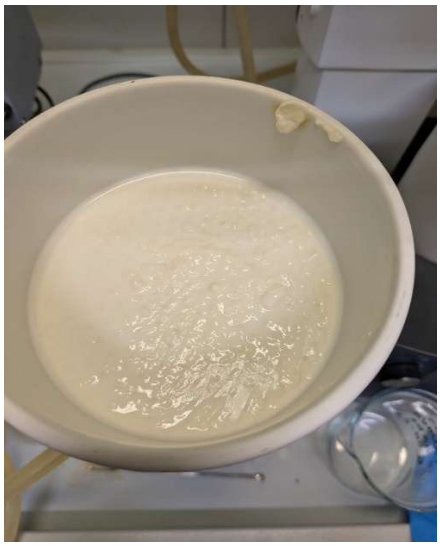

Figure 2.6: Solid residue retained by the filter.

The results reported in Table 2.18 refer to laboratory-scale batch distillation tests performed on hydroalcoholic samples originating from tank S2, characterized by an ethanol concentration of approximately 21% v/v prior to distillation.

Among the volatile compounds detected in the distilled samples reported in Table 2.18, the presence of styrene is clearly observed at high temperature, with concentrations reported above the method disregard level. This finding is particularly noteworthy when compared to the corresponding as-received samples discussed in Section 2.5.1, in which styrene was detected in S2 solutions.

In addition to styrene, other volatile and semi-volatile compounds were detected at varying semi-quantitative levels, as documented in Table 2.18. The reported data indicates a modification of the volatile profile following laboratory-scale distillation under the applied experimental conditions.

Overall, the results are summarized in the table document the volatile composition of distillates obtained from S2 hydroalcoholic solutions at elevated temperatures, with styrene representing one of the compounds detected in the distilled fraction under the investigated conditions.

Table 2.18: VOC and SVOC for the Distilled Samples from S2 Tank.

Sample	**Dist_S2_V_p0**	**Dist_S2_V_p1**	**Dist_S2_V_p2**	**Dist_S2_V_p3**	**Dist_S2_V_p4**
p (kPa)	19	39	59	70	amb
T eb (°C)	49,86	63,98	73,08	79,94	85,49
T bath	55	69	78	85	90
VOC					
Ethanol (% w/v)	0,834	0,652	0,638	0,574	0,896
Octanoic acid ethyl ester (% w/v)	0,007	<0,001	<0,001	<0,001	0,006
Ethyl acetate (% w/v)	<0,001	<0,001	<0,001	<0,001	0,001
Styrene (% w/v)	<0,001	<0,001	<0,001	<0,001	0,003
SVOC					
Octanoic acid ethyl ester (% w/v)	<0,001	<0,001	<0,001	<0,001	<0,001
Octanoic acid (% w/v)	0,001	<0,001	<0,001	<0,001	0,001
Hexadecanoic acid, ethyl ester (% w/v)	<0,001	<0,001	<0,001	<0,001	<0,001
n-Hexadecanoic acid (% w/v)	0,002	<0,001	<0,001	<0,001	0,002
Octadecanoic acid, ethyl ester (% w/v)	<0,001	<0,001	<0,001	<0,001	0,001
Octadecanoic acid (% w/v)	<0,001	<0,001	<0,001	<0,001	<0,001

(Z)-13-Docosenamide (% w/v)	<0,001	<0,001	<0,001	<0,001	<0,001
Cholesterol	<0,001	<0,001	<0,001	<0,001	<0,001
Cholest-4-en-3-one (% w/v)	<0,001	<0,001	<0,001	<0,001	<0,001

2.5.7 SUMMARY OF KEY OBSERVATIONS

The results presented in the previous sections provides a comprehensive experimental overview of the chemical and physical characteristics of the hydroalcoholic waste streams and their behaviour under laboratory-scale distillation conditions.

Screening of volatile organic compounds in as-received samples showed that ethanol was the dominant volatile component, while other monitored VOCs were generally detected at very low levels or below the method disregard threshold. Acetaldehyde and acetaldehyde-related acetals were not detected in any of the as-received samples within the sensitivity limits of the applied analytical methods.

The analysis of semi-volatile organic compounds revealed the presence of several SVOCs in the hydroalcoholic waste prior to distillation, with samples from tank S3 generally exhibiting a broader SVOC profile compared to those from tank S2. These results indicate a higher chemical complexity of the S3 hydroalcoholic solutions before any thermal treatment.

Physical characterization highlighted the presence of a particulate fraction in S3 samples, as confirmed by particle size distribution and total suspended solids measurements. The PSD analysis was intentionally performed on S3 samples collected under normal operating conditions, providing a representative description of the hydroalcoholic waste stream in the absence of quality deviations.

Measurements of total protein content showed detectable protein levels in all analysed samples, with values varying among different process streams. Temporal monitoring revealed distinct trends depending on the specific unit operation, including progressive increases, decreases, or relatively stable protein concentrations over time, as documented for the FP5/9 supernatant, diafiltration supernatant, and HYHT-related streams.

Similarly, liquid specific gravity, total suspended solids, and total dissolved solids exhibited substantial variability across samples and distinct temporal trends depending on the process step. While LSG values remained within a relatively narrow range, TSS and TDS showed more pronounced changes over time for several streams.

Laboratory-scale batch distillation tests demonstrated clear differences between as-received and distilled samples, with distillates generally exhibiting a more complex volatile and semi-volatile profile. Differences were observed between samples originating from tanks S2 and S3, as well as between filtered and unfiltered S3 solutions. Notably, styrene was detected in distilled samples, including those obtained from S2 hydroalcoholic solutions.

2.6 Discussion and Connection to Advanced Studies

2.6.1 General Results

The experimental evidence presented in this chapter provides an initial framework for understanding the chemical nature of hydroalcoholic waste streams generated during plasma fractionation and their behaviour under thermal treatment. The combined analysis of as-received samples, physicochemical characterization, and laboratory-scale distillation tests highlights both the strengths and the intrinsic limitations of the adopted experimental approach.

The screening of as-received hydroalcoholic solutions showed that, prior to any thermal treatment, acetaldehyde and acetaldehyde-related acetals were not detected within the sensitivity limits of the applied HS-GC/MS methods. This observation indicates that these compounds do not represent a detectable fraction of the volatile impurity profile under ambient or storage conditions. However, the laboratory-scale distillation experiments were performed using a rotary evaporator, a configuration that may not be fully suitable for the reliable detection of highly volatile species. Compounds such as acetaldehyde, with a normal boiling point of approximately 20 °C, can be partially or fully lost during sample handling, pressure reduction, or condensation inefficiencies.

Consequently, the absence of acetaldehyde and acetals in the distillates cannot be interpreted as definitive evidence of their non-formation during thermal treatment but rather highlights a methodological limitation of the adopted laboratory setup for VOC assessment. While the rotary evaporator experiments were effective in demonstrating qualitative changes in the volatile and semi-volatile profiles at elevated temperatures, they are not sufficient to conclusively address the formation pathways of the most volatile impurities. This limitation directly motivates the adoption of more advanced and controlled analytical approaches, which are introduced and discussed in the following chapter.

A second key outcome of this study concerns the presence of styrene. Styrene was detected at low levels in the as received hydroalcoholic solution from tank S2, and its presence was further confirmed in the corresponding distilled samples obtained at high temperature. This observation establishes a clear link between the chemical composition of the hydroalcoholic waste stored in S2 and the volatile profile of the resulting distillate and motivated a focused investigation on the characteristics of this storage system.

The differences observed between samples originating from tanks S2 and S3, as well as between filtered and unfiltered S3 solutions, further emphasize the role of upstream process conditions, storage environment, and suspended material in shaping the impurity landscape of hydroalcoholic

waste streams. These findings support the hypothesis that precursor species may already be present in the waste prior to distillation, and that their transformation during heating depends on both chemical composition and thermal severity.

2.6.2 S2 CASE STUDY

A further element emerging from the analysis concerns the materials of construction of tank S2, from which styrene was detected in the as-received hydroalcoholic solution and subsequently confirmed in the corresponding distillates. An investigation of the construction characteristics of this tank revealed that the internal liner is made of an epoxy vinyl ester resin, specifically DERAKANE® MOMENTUM 411-350.

According to information provided by the tank manufacturer, the selected epoxy vinyl ester resin is commonly employed as an internal liner material due to its ability to cure at ambient temperature and compatibility with the solution stored in it. This characteristic significantly simplifies the manufacturing and installation process of lined storage tanks, avoiding the need for elevated curing temperatures and complex thermal treatments. As such, the use of ambient temperature curing resins represents a practical and widely adopted solution in industrial applications, particularly for large vessels and on-site lining operations.

While this property offers clear advantages from a construction and operational standpoint, the presence of styrene in the resin formulation, as indicated in the material datasheet, becomes a relevant factor when such materials are used in prolonged contact with hydroalcoholic solutions. According to the technical datasheet provided by the manufacturer, DERAKANE MOMENTUM 411-350 is formulated with a styrene content of approximately 45% by weight. This information is particularly relevant considering the analytical results presented in this chapter, as it identifies the liner material as a potential source of styrene in contact with the hydroalcoholic waste stored in tank S2.

The release of styrene from vinyl ester epoxy resins into hydroalcoholic solutions is a multifaceted process governed by both the physicochemical properties of the resin and the characteristics of the contacting medium. Styrene, commonly employed as a reactive diluent to reduce resin viscosity and facilitate processing, is known to migrate from the polymer matrix under certain environmental conditions. The emission rate of styrene is significantly influenced by factors such as the initial styrene content, temperature, and exposed surface area, with diffusion and evaporation coefficients exhibiting a strong temperature dependence [112,113].

In aqueous and hydroalcoholic environments, the presence of alcohol can further facilitate styrene leaching due to its higher solubility and potential swelling or partial hydrolysis of the resin matrix, which increases the mobility of small molecules [114]. While the present study does not allow a definitive attribution of the detected styrene to migration phenomena from the liner, the coexistence of (i) measurable styrene in the S2 hydroalcoholic solution, (ii) its persistence in the corresponding distillates, and (iii) the documented presence of styrene in the liner resin formulation strongly suggests that the internal coating of tank S2 represents the primary suspect associated with the observed contamination.

At this stage, the available data allow only a qualitative correlation between the liner material and the detected styrene, without providing direct evidence of migration mechanisms, kinetics, or influencing factors such as temperature, ethanol concentration, or contact time.

3. CONTAMINANTS AND PRECURSORS

3.1 INTRODUCTION AND SCOPE OF THE STUDY

The recovery and reuse of ethanol represent a critical aspect of the plasma fractionation process, both from an economic and regulatory perspective. As discussed in Chapter 2, the quality of recovered ethanol is primarily constrained by the presence of volatile and semi-volatile contaminants, among which acetaldehyde and acetaldehyde-related acetals are subject to particularly strict limits (10 ppm) according to the European Pharmacopoeia [78]. Although several operational strategies, such as operating the first distillation column under vacuum to limit reboiler temperature, have been implemented at industrial scale, episodes of off-specification ethanol continue to occur intermittently and without a clear correlation with specific production campaigns.

Previous investigations and routine quality controls have mainly focused on the analysis of contaminants already present in the recovered ethanol or in the spent ethanol streams prior to distillation. However, this approach alone does not fully explain the sporadic nature of contamination events, nor does it provide sufficient insight into the underlying mechanisms responsible for

the formation of acetaldehyde during thermal treatment. Historical plant observations suggest that acetaldehyde is often generated within the distillation system rather than being present in significant amounts in the feed streams, indicating the possible involvement of chemical or biochemical precursors activated under process conditions.

In this context, the identification and characterization of acetaldehyde precursors represent a necessary step toward a deeper understanding of contaminant formation phenomena. Unlike conventional contaminants originating from alcoholic fermentation, the spent ethanol streams generated during plasma fractionation are characterized by a complex and atypical chemical matrix. These streams consist of hydroalcoholic solutions containing inorganic ions, buffering species, and residual organic matter originating from the processing of human plasma, which may create favourable conditions for secondary reactions during heating. No systematic study had previously been conducted to assess the role of such species as potential precursors or promoters of acetaldehyde formation in ethanol recovery systems.

The objective of the present chapter is therefore to investigate the origin of acetaldehyde contamination from a precursor-oriented perspective. The study combines a broad chemical characterization of spent ethanol streams with a series of controlled laboratory experiments designed to evaluate the influence of key variables, including pH, temperature, buffer composition, and the presence of enzymatic systems, on acetaldehyde formation. Attention is given to distinguishing between purely thermal degradation pathways and enzymatic or pseudo-enzymatic mechanisms that may be activated under the mild temperatures typical of industrial distillation under reduced pressure.

Rather than developing a formal kinetic model, this chapter adopts an experimental and parametric approach aimed at identifying the dominant factors and interactions governing acetaldehyde formation. The resulting framework provides a qualitative and semi-quantitative basis for interpreting plant behaviour and for defining operational strategies to

mitigate the risk of ethanol contamination. The findings presented here establish the conceptual and experimental foundation for the subsequent discussion on process optimization and contaminant prevention in ethanol recovery systems.

The results presented in this chapter are based on experimental activities carried out at the Universidad Complutense de Madrid and constitute the basis for ongoing scientific dissemination.

3.2 Characterization of Spent Ethanol Streams

3.2.1 Scope and Analytical Dataset

The analytical activities discussed in this section aim to provide a broad chemical characterization of spent ethanol streams beyond the volatile and semi-volatile fraction addressed in Chapter 2. The purpose of this characterization is to identify non-volatile species and matrix components that may play a role as chemical precursors or promoters in the formation of acetaldehyde and related contaminants during thermal treatment.

The dataset considered in this section is based on analytical investigations carried out in 2022 on representative samples of spent ethanol collected from the ethanol recovery system. Two samples, collected by tank S1 and S3, were selected as representative of typical hydroalcoholic waste streams generated during the plasma fractionation process. These samples were characterized within an external analytical campaign commissioned to obtain a comprehensive chemical fingerprint of the spent ethanol matrix. The analyses were carried out by the Lab Analysis S.R.L. laboratory.

A multi-technique analytical approach was adopted to capture the different chemical fractions present in the samples. The applied techniques included gas chromatography with flame ionization detection (GC/FID) for ethanol quantification, ion chromatography (IC) for inorganic anions and buffering species, inductively coupled plasma mass spectrometry (ICP/MS) for

elemental impurities, and ultra-high-performance liquid chromatography coupled with high-resolution mass spectrometry (UHPLC-HRMS) for the screening of non-volatile organic compounds. In addition, screenings of volatile and semi-volatile organic compounds were performed as part of the same analytical campaign; however, these results are discussed separately in Chapter 2. and are not reiterated here.

Although the analyses were conducted on samples collected during an earlier production period, the investigated streams are representative of the spent ethanol generated by the plasma fractionation process in terms of ethanol concentration, ionic strength, and overall matrix complexity. As such, the results provide a reliable basis for interpreting the chemical environment in which secondary reactions and precursor activation phenomena may occur during ethanol recovery operations.

3.2.2 Ethanol Content and General Composition

The ethanol content of the spent ethanol streams was determined by GC/FID analysis as part of the 2022 analytical campaign. Both analysed samples (S1 and S3) exhibited an ethanol concentration of approximately 25% by volume, corresponding to 25.0% and 25.2%, respectively. These values are fully consistent with the expected composition of mother liquors generated during the plasma fractionation process and confirm the representativeness of the selected samples.

The relatively high ethanol concentration plays a dual role in the context of contaminant formation. On one hand, ethanol represents the target compound to be recovered and reused; on the other hand, it constitutes a reactive substrate that may undergo chemical or biochemical transformation under suitable conditions. In the presence of buffering species, residual organic matter, and potential catalytic environments, ethanol cannot be regarded as chemically inert, particularly during thermal treatment.

From an experimental perspective, the measured ethanol content is also relevant for the interpretation of the laboratory-scale tests discussed in the following sections. The ethanol concentrations employed in controlled experiments were selected to be compatible, on a mass basis, with those measured in the spent ethanol streams, thereby ensuring coherence between the industrial matrix and the model systems investigated. This alignment supports the validity of using simplified laboratory mixtures to study precursor activation mechanisms occurring in the industrial ethanol recovery process.

3.2.3 Inorganic Ions and Buffering Species

The inorganic ionic composition of the spent ethanol streams was investigated by ion chromatography (IC) to assess the presence of buffering species and inorganic ions that may influence secondary reaction pathways during thermal treatment. The results obtained for samples S1 and S3 are summarized in Table 3.1.

Table 3.1: Inorganic Ion Composition of Spent EtOH.

Compound	Spent EtOH from S1 [mg/l]	Spent EtOH from S3 [mg/l]
Fluoride	< 0.50	< 0.50
Chloride	1982	1996
Acetate	3691	3586
Nitrite	< 5.0	< 5.0
Bromide	< 5.0	< 5.0
Nitrate	< 5.0	< 5.0
Phosphate	103	101
Sulfate	10	11

Both samples exhibited a significant ionic content, with chloride and acetate identified as the dominant anions. Chloride concentrations were close to 2.0 g/l in both cases, while acetate was present at concentrations of approximately 3.6–3.7 g/l. These values indicate a relatively high ionic

strength of the hydroalcoholic matrix, consistent with the extensive use of ethanol and buffering agents during the plasma fractionation process.

Of relevance is the presence of phosphate ions at concentrations of about 100 mg/l in both samples. Although substantially lower than acetate, phosphate is known to play a critical role in acid–base buffering and to interact with enzymatic and pseudo-enzymatic systems in aqueous and hydroalcoholic environments. Even at moderate concentrations, phosphate species can influence reaction equilibria, proton transfer mechanisms, and the stability of enzyme–cofactor complexes.

Sulfate was detected only at low concentrations (approximately 10–11 mg/l), while nitrate, nitrite, bromide, and fluoride were below the respective detection limits. The limited presence of oxidizing inorganic species further suggests that non-enzymatic oxidative pathways are unlikely to dominate under the investigated conditions.

Overall, the IC results highlight that spent ethanol streams are characterized by a strongly buffered chemical environment, dominated by acetate and supplemented by measurable amounts of phosphate. This ionic composition is particularly relevant when considering the activation of acetaldehyde formation pathways that are sensitive to pH control, buffer identity, and proton availability. As discussed in the following sections, the presence of phosphate emerges as a key factor in modulating ethanol oxidation phenomena observed under controlled experimental conditions.

3.2.4 Elemental Impurities

The presence of elemental impurities in the spent ethanol streams was investigated by inductively coupled plasma mass spectrometry (ICP/MS) to assess the possible contribution of metal-catalysed pathways to acetaldehyde formation. The results obtained for samples S1 and S3 are reported in Table 3.2.

Table 3.2: Elemental Impurities found in Spent EtOH.

Compound	Spent EtOH from S1 [mg/l]	Spent EtOH from S3 [mg/l]
Cd	< 0.30	< 0.30
Pb	< 0.75	< 0.75
As	< 2.3	< 2.3
Hg	< 0.45	< 0.45
Co	< 0.75	< 0.75
Tl	< 1.2	< 1.2
V	< 1.5	< 1.5
Ni	< 3.0	< 3.0
Au	< 15	< 15
Pd	< 1.5	< 1.5
Ir	< 1.5	< 1.5
Rh	< 1.5	< 1.5
Ru	< 1.5	< 1.5
Se	< 12	< 12
Ag	< 1.5	< 1.5
Pt	< 1.5	< 1.5
Li	< 38	< 38
Sb	< 14	< 14
Ba	< 105	< 105
Mo	< 225	< 225
Cu	< 45	< 45
Sn	< 90	< 90
Cr	< 165	< 165

All analysed elements were found to be below the respective detection limits of the method. Transition metals commonly associated with redox activity or catalytic oxidation reactions, such as iron, copper, nickel, cobalt, chromium, palladium, platinum, and other noble metals, were not detected at concentrations that could reasonably promote catalytic processes.

Similarly, toxic heavy metals and metalloids, including cadmium, lead, mercury, and arsenic, were also below detection limits.

The absence of detectable transition metals is a relevant finding in the context of contaminant formation mechanisms. Metal-catalysed oxidation of ethanol to acetaldehyde is a well-known pathway in both heterogeneous and homogeneous systems; however, the ICP/MS results indicate that such mechanisms are unlikely to play a significant role in the studied spent ethanol streams. This observation supports the exclusion of metal-driven redox reactions as a primary source of acetaldehyde under the investigated conditions.

Consequently, the formation of acetaldehyde observed during ethanol recovery operations and laboratory-scale experiments is more plausibly attributed to alternative pathways, such as enzymatic or matrix-mediated processes, rather than to direct metal-catalysed oxidation. This conclusion further narrows the range of plausible precursor activation mechanisms and provides a clearer framework for interpreting the experimental results discussed in the subsequent sections.

3.2.5 Non-Volatile Organic Fraction

The non-volatile organic fraction of the spent ethanol streams was investigated by UHPLC-HRMS to assess the presence of organic species that are not detectable by conventional GC-based techniques but may nonetheless influence the chemical behaviour of the matrix during thermal treatment. This analysis provides insight into the overall complexity of the spent ethanol streams and into the potential presence of macromolecular or highly functionalized compounds originating from the plasma fractionation process.

The UHPLC-HRMS screening revealed the presence of a heterogeneous set of organic compounds spanning a wide molecular weight range. In both samples collected from S1 and S3, several signals were associated with polyethylene glycol (PEG)-like species, identified through characteristic mass spacing and used as reference compounds for semi-quantitative

estimation. PEG-related signals were detected at concentrations ranging from approximately 10 to 50 mg/l, indicating the presence of polymeric or oligomeric structures in the spent ethanol matrix.

In addition to PEG-related species, multiple high-molecular-weight compounds with partially assigned elemental compositions were detected. These compounds typically exhibited molecular masses between approximately 700 and 1900 m/z and contained combinations of carbon, hydrogen, nitrogen, oxygen, phosphorus, and, in some cases, sulphur. Although definitive structural identification was not possible within the scope of this screening analysis, the elemental compositions suggest the presence of complex organic species potentially derived from plasma proteins, processing aids, or auxiliary chemicals used during fractionation and purification steps.

The concentration of individual non-volatile organic species was generally within the range of 10–30 mg/l, with similar qualitative profiles observed for both S1 and S3 samples. This consistency indicates that the presence of such compounds is not an isolated occurrence but rather a characteristic feature of the spent ethanol streams generated by the plasma fractionation process.

From a mechanistic standpoint, the detection of a substantial non-volatile organic fraction highlights that spent ethanol cannot be considered a simple ethanol–water mixture. Instead, it represents a chemically complex medium in which macromolecular and multifunctional organic species coexist with inorganic ions and buffering agents. Such a matrix may provide favourable conditions for secondary reactions, stabilization of reactive intermediates, or interaction with enzymatic systems, even in the absence of high temperatures or strong oxidizing agents.

These findings further support the hypothesis that acetaldehyde formation during ethanol recovery may be influenced by matrix effects and precursor activation phenomena rather than by purely thermal degradation of ethanol.

The implications of this complex organic background are explored in the following sections through targeted experimental investigations.

3.2.6 VOLATILE AND SEMI-VOLATILE COMPOUNDS

The screening of volatile and semi-volatile organic compounds in spent ethanol streams was performed as part of the same analytical campaign and is discussed in detail in Chapter 2. For this reason, the corresponding results are not repeated here.

The identification of volatile and semi-volatile species provides essential information on the contaminants already present in the spent ethanol matrix prior to thermal treatment. However, as demonstrated in Chapter 2. , key compounds of concern, such as acetaldehyde and acetaldehyde-related acetals, were not detected at significant levels in the as-received streams. This observation supports the hypothesis that these contaminants are predominantly formed during ethanol recovery rather than being directly introduced with the feed.

Within the context of the present chapter, the volatile and semi-volatile screening results are therefore considered only to contextualize the broader chemical environment of the spent ethanol matrix. The focus is shifted toward non-volatile species and matrix components that may act as precursors or promoters of contaminant formation during thermal treatment, as discussed in the following sections.

3.2.7 SUMMARY AND IMPLICATIONS FOR PRECURSOR ACTIVATION

The results presented in this section demonstrate that spent ethanol streams generated during plasma fractionation are characterized by a chemically complex matrix that extends well beyond a simple ethanol–water system. While the volatile and semi-volatile fraction has been addressed separately in Chapter 2. the broader characterization performed here highlights the presence of inorganic ions, buffering species, and non-volatile organic

matter that may significantly influence secondary reaction pathways during thermal treatment.

The ethanol concentration, close to 25% by volume, confirms the representativeness of the investigated streams and establishes ethanol as both the target compound for recovery and a potential reactive substrate. Ion chromatography revealed a strongly buffered environment, dominated by acetate and accompanied by measurable concentrations of phosphate. The latter, although present at lower levels than acetate, is known to interact with acid–base equilibria and enzymatic systems, suggesting a possible role in modulating ethanol oxidation phenomena.

At the same time, ICP/MS analyses excluded the presence of transition metals at concentrations capable of promoting catalytic oxidation of ethanol. This finding allows metal-driven pathways to be reasonably ruled out and narrows the range of plausible mechanisms responsible for acetaldehyde formation. In parallel, UHPLC-HRMS screening revealed a heterogeneous non-volatile organic fraction, including polymeric and high-molecular-weight species containing heteroatoms such as nitrogen, phosphorus, and sulphur, further confirming the chemical richness of the spent ethanol matrix.

Taken together, these observations support the hypothesis that acetaldehyde formation during ethanol recovery is not governed solely by temperature but may result from the activation of specific precursor pathways within a buffered and chemically active medium. In particular, the coexistence of ethanol, phosphate species, and residual organic matter creates conditions potentially favourable to enzymatic or matrix-mediated oxidation mechanisms. This framework provides the basis for the targeted experimental investigations presented in the following sections, which aim to isolate and evaluate the role of selected precursors under controlled laboratory conditions.

3.3 Hypotheses on Acetaldehyde Precursor Formation

The broad chemical characterization of spent ethanol streams discussed in Section 3.2 highlights that the investigated matrices are characterized by a buffered and chemically complex environment, in which ethanol coexists with inorganic ions, non-volatile organic matter, and residual biological components. These features suggest that acetaldehyde formation during thermal treatment cannot be attributed solely to temperature effects but may involve the activation of specific precursor pathways under favorable chemical conditions. On this basis, the following section formulates and discusses the main hypotheses regarding the origin of acetaldehyde contamination in recovered ethanol.

Analyses conducted on spent ethanol streams have highlighted that acetaldehyde is generally formed in modest quantities within the distillation column rather than being present in significant amounts in the feed. This observation suggests that acetaldehyde contamination is primarily associated with in-process formation phenomena activated under specific chemical and thermal conditions.

Acetaldehyde is a volatile compound that can originate from a variety of organic precursors through chemical, thermal, or biological pathways. The main precursors reported in the literature include ethanol, α-amino acids (such as alanine and cysteine), α-keto acids (e.g., pyruvic acid), α-ketoacyl peptides, and chromophoric dissolved organic matter (CDOM). The relevance of each pathway strongly depends on temperature, pH, oxidizing conditions, and the chemical environment in which the reactions occur.

From α-keto acids and α-ketoacyl peptides, acetaldehyde can be generated through degradation reactions such as the Strecker degradation, particularly at elevated temperatures. Literature data indicate that these reactions typically require temperatures on the order of 150 °C in water or diluted acetic acid to proceed at appreciable rates [115]. Similarly, ethanol can yield

acetaldehyde through dehydrogenation reactions, which are enhanced in the presence of catalysts such as phosphoric acid, ammonia, or water under supercritical conditions [116], or through steam reforming and microbial degradation pathways in aquatic environments [117].

α-Amino acids, including alanine and cysteine, are also reported to generate acetaldehyde under oxidative conditions or upon heating, with reaction mechanisms that are strongly influenced by pH, temperature, and the nature of the oxidizing agent. α-Keto acids may additionally contribute to acetaldehyde formation through transamination reactions [118,119]. In natural aquatic systems, CDOM has been shown to release acetaldehyde through photochemical processes driven by light exposure [120]. However, many of these pathways involve conditions, such as strong oxidation, photochemical activation, or high temperatures, that are not fully representative of industrial ethanol distillation under reduced pressure.

To assess the potential contribution of protein-derived precursors under conditions relevant to the studied system, albumin and γ-globulins were selected as model compounds. These proteins represent the main products of plasma fractionation, and it is reasonable to assume that trace amounts may be present in spent ethanol streams. Albumin and γ-globulins contain amino acids that have been identified as potential acetaldehyde precursors upon heating, thus enabling the simulation of the behaviour of biological residues during the distillation process.

In parallel, ethanol itself represents a highly relevant precursor due to its abundance and chemical reactivity. In biological systems, ethanol is primarily converted into acetaldehyde through the action of alcohol dehydrogenase (ADH) in conjunction with the cofactor nicotinamide adenine dinucleotide (NAD^+). This enzymatic reaction constitutes the initial and rate-limiting step of ethanol oxidative metabolism in the liver. ADH catalyses the reversible oxidation of primary and secondary alcohols into their corresponding aldehydes or ketones [121]. In the specific case of ethanol, ADH oxidizes ethanol to acetaldehyde while NAD^+ is reduced to

NADH [122]. Although this reaction is reversible in vitro [123,124], it is strongly driven toward acetaldehyde formation in vivo, as aldehyde dehydrogenases rapidly convert acetaldehyde into acetate [125].

Plasma and blood concentrations of ADH and NAD^+ are generally low but play a crucial role in determining reaction rates. ADH is predominantly localized in the liver, where its activity is significantly higher than in other tissues [126,127]. In human plasma, average ADH activity is reported to be approximately 0.08 ± 0.06 U/L, although values as high as 1.51 U/L have been observed under specific conditions such as chronic alcohol consumption or liver damage, with typical ranges between 0.54 and 0.81 U/L [128]. NAD^+ concentrations in human plasma are approximately 1.34 μM, with reported values ranging from 0.44 to 2.88 μM. The NAD^+/NADH ratio is a critical indicator of metabolic redox state and directly affects the efficiency of ADH-catalysed reactions [129].

The catalytic mechanism of ADH varies depending on the organism and isoenzyme. Yeast alcohol dehydrogenase (YADH) follows a partially random order mechanism [130], whereas horse liver and human isoforms operate according to a sequential Bi–Bi mechanism in which NAD^+ binds first and NADH is released last [131]. In all isoforms, the release of NADH often represents the rate-limiting step, thereby influencing the overall ethanol conversion rate [132]. Enzymatic activity is also strongly affected by environmental conditions such as pH and temperature. Human ADH exhibits maximum activity in the alkaline range (pH 9–11), while gastric isoforms show optimal activity near neutral pH (pH 7.7) [125,133]. YADH remains active over a broader pH range, from approximately 4.9 to 9.9 [134]. Temperature increases from 25 °C to 37 °C can double or triple reaction rates, although higher temperatures may also promote enzyme deactivation, by-product formation, or acetaldehyde evaporation. For this reason, liver perfusion studies are often conducted at temperatures close to 25 °C [135].

To investigate whether ethanol present in the studied hydroalcoholic matrix could be converted into acetaldehyde under conditions comparable to those

of an industrial distillation column, experiments were conducted using ADH and NAD^+ as a model enzymatic system. Controlled pH and temperature conditions were selected to simulate those encountered in the first distillation column, allowing the evaluation of potential acetaldehyde formation under operationally relevant conditions.

Notably, the experimental study employed concentrations of ADH and NAD^+ higher than those typically reported in the literature. This approach was adopted to enhance the detectability of acetaldehyde formation within practical experimental timeframes. Furthermore, it cannot be excluded that the plasma fractionation process, by selectively removing specific protein fractions, may result in the relative enrichment of enzymes and cofactors such as ADH and NAD^+ in the spent ethanol streams compared to native plasma.

3.4 Experimental Strategy

The experimental activity described in this chapter was designed to investigate the possible precursor pathways responsible for acetaldehyde formation under conditions representative of industrial ethanol recovery. Based on the hypotheses formulated in Section 3.3, a set of controlled laboratory experiments was carried out using simplified model systems, with the objective of isolating the effect of specific chemical and biochemical factors while maintaining relevance to the industrial process.

The experimental approach was intentionally parametric rather than kinetic. This choice reflects the exploratory nature of the study and the need to identify dominant factors and interaction effects governing acetaldehyde formation, rather than to derive intrinsic kinetic parameters. The resulting experimental dataset was subsequently analysed using a factorial design framework to extract multivariate trends and response surfaces, as discussed in the following sections.

3.4.1 Model Systems and Reagents

Model systems were selected to represent the main classes of potential acetaldehyde precursors identified in Section 3.3. Protein-derived pathways were investigated using albumin and gamma globulins as model compounds. These proteins are the primary products of plasma fractionation and may be present in trace amounts in spent ethanol streams. Their use allowed the assessment of whether residual biological material could contribute to acetaldehyde formation under mild thermal conditions.

Ethanol was considered both as the target compound of the recovery process and as a potential direct precursor of acetaldehyde. To evaluate ethanol-centered pathways under biologically plausible conditions, alcohol dehydrogenase (ADH) and nicotinamide adenine dinucleotide (NAD^+) were employed as a model enzymatic system. This choice was motivated by the well-established role of ADH/NAD^+ in ethanol oxidation and by the potential persistence or relative enrichment of enzymatic components in spent ethanol matrices.

All reagents were selected to ensure chemical purity and reproducibility of the experimental conditions, while maintaining compatibility with the analytical techniques used for acetaldehyde detection.

3.4.2 Experimental Variables

The experimental campaign was structured to evaluate the influence of key variables identified as potentially relevant for precursor activation. The investigated parameters included pH, temperature, incubation time, ethanol concentration, and the concentration of enzymatic components (ADH and NAD^+), as well as the nature of the buffering system.

Experiments were conducted over ranges of pH, temperature, and residence time chosen to be representative of conditions encountered in the first stage of industrial ethanol distillation, particularly under reduced-pressure operation. Concentration levels of ethanol, ADH, and NAD^+ were varied to

assess both individual effects and combined influences on acetaldehyde formation.

The incubation times adopted in the experimental trials were selected based on the estimated residence times in the reboilers of the industrial distillation columns. These values were calculated using the actual equipment volumes and representative operating flow rates and are summarized in Table 3.3.

Table 3.3: Residence Time for the Equipment.

Equipment	Residence Time (min)
C310	4.34
E310	44.52
C320	7.26
E320	15.19

Although the experiments were not originally designed as a formal design of experiments, the collected dataset was sufficiently structured to allow subsequent analysis using a factorial design approach. This ex-post application of DOE techniques enabled the identification of interaction effects and the construction of response surfaces describing acetaldehyde formation as a function of the investigated variables.

3.4.3 Analytical Methods

The concentration of acetaldehyde formed during the experimental runs was identified and quantified by headspace gas chromatography. Analyses were performed using a gas chromatograph equipped with a mass spectrometry detector (GC–MS, Hewlett Packard HP6890 series) for heavier compound identification and confirmation, while acetaldehyde quantitative measurements were additionally supported by gas chromatography with flame ionization detection (GC–FID, Agilent 8860, Santa Clara, CA, USA).

For headspace analysis, 10 mL of the reaction solution were transferred into 20 mL sealed vials. Samples were then heated and agitated at controlled temperatures for different incubation times, depending on the specific

experimental conditions. These parameters were selected to simulate the thermal exposure experienced by the hydroalcoholic matrix during ethanol recovery operations.

Chromatographic separation in GC/FID was achieved using an HP-INNOWAX capillary column (60 m × 320 μm × 0.25 μm). A headspace volume of 2.5 mL was injected in split mode (10:1). Hydrogen was used as the carrier gas under constant flow conditions (2 mL min-1). The injector temperature was set at 140 °C. The oven temperature program started at 40 °C (held for 1.5 min), followed by a ramp of 30 °C min^{-1} up to 220 °C, which was maintained for 6 min. The FID temperature was set at 300 °C, using hydrogen, air and nitrogen as fuel, oxidant and make-up gases, respectively.

3.5 Assessment of Protein-Derived Precursors

The potential contribution of protein-derived precursors to acetaldehyde formation was investigated using albumin and γ-globulins as model compounds. These proteins represent the main products of plasma fractionation and were selected to simulate the behavior of residual biological material potentially present in spent ethanol streams.

Preliminary experiments were carried out by subjecting aqueous solutions containing albumin or γ-globulins to thermal treatment under acidic conditions, using acetic acid to adjust the pH to values representative of those encountered in the industrial process. The samples were incubated at temperatures up to 70 °C for time intervals consistent with the estimated residence times in the reboilers of the distillation columns. Protein concentrations were kept constant within each experimental series, as the objective of these tests was to assess the qualitative feasibility of protein-derived acetaldehyde formation under representative thermal and pH conditions.

Under all tested conditions, no detectable formation of acetaldehyde or other volatile carbonyl compounds was observed. Analytical measurements confirmed that the concentrations of acetaldehyde remained below the detection limits of the applied HS-GC/MS method. This result was consistent across different protein concentrations and incubation times.

At first glance, these findings may appear counterintuitive, as albumin and γ-globulins contain amino acids, such as alanine and cysteine, that have been reported in the literature as potential acetaldehyde precursors through degradation reactions. However, available studies indicate that such transformations typically require substantially higher temperatures and/or strongly oxidative environments. For example, Strecker-type degradation pathways and thermal decomposition of sulfur-containing amino acids are generally reported to occur at temperatures exceeding 120–150 °C, conditions that are not representative of the vacuum-assisted distillation process considered in this study.

The absence of acetaldehyde formation under the investigated conditions therefore suggests that protein-derived pathways do not play a significant role in contaminant formation during ethanol recovery. This finding allows the contribution of residual plasma proteins to be reasonably excluded as a primary source of acetaldehyde in the studied system.

Based on these results, subsequent experimental efforts were focused on alternative precursor pathways, with particular emphasis on ethanol-centered mechanisms and the role of the surrounding chemical environment. These aspects are addressed in the following sections.

3.6 Enzymatic Pathway: Ethanol Oxidation via ADH/NAD^+

Following the exclusion of protein-derived pathways under the investigated conditions, attention was focused on ethanol-centered mechanisms as a potential source of acetaldehyde formation. Among the possible routes,

enzymatic oxidation of ethanol mediated by alcohol dehydrogenase (ADH) in the presence of the nicotinamide adenine dinucleotide cofactor (NAD^+) represents a well-established and chemically plausible pathway capable of operating under mild thermal conditions.

It is worth noting that most literature studies on ADH-mediated ethanol oxidation are conducted under conditions markedly different from those investigated in the present work. Reported experiments typically involve physiological or near-physiological temperatures and cofactor concentrations and are aimed at characterizing enzymatic activity rather than evaluating contaminant formation under process-relevant thermal conditions. In contrast, the experimental conditions adopted in this study were selected to reflect the temperature and residence time ranges encountered during industrial ethanol recovery, thereby extending the investigation of ADH/NAD^+-mediated ethanol oxidation beyond the regimes commonly addressed in the literature.

To evaluate the feasibility of this mechanism within the context of ethanol recovery, a series of controlled laboratory experiments was carried out using ADH and NAD^+ as a model enzymatic system. These experiments were designed to assess whether ethanol oxidation to acetaldehyde could occur under pH, temperature, and residence time conditions representative of those encountered in the first distillation column, and to identify the key factors governing the extent of acetaldehyde formation.

Preliminary control experiments were performed to exclude non-enzymatic contributions to acetaldehyde formation. Tests conducted with ethanol alone, as well as with individual components of the enzymatic system (ADH or NAD^+ in the absence of the complementary species), did not result in detectable acetaldehyde formation across the investigated temperature range. This confirms that, under the tested conditions, ethanol does not undergo significant thermal or spontaneous oxidation, and that acetaldehyde formation requires the simultaneous presence of both ADH and NAD^+.

Subsequent experiments demonstrated that, when ethanol, ADH, and NAD^+ were present together, acetaldehyde formation could be observed under specific chemical environments. The extent of acetaldehyde production was found to be strongly dependent on environmental parameters rather than on enzyme presence alone, indicating that matrix effects play a critical role in activating or inhibiting the enzymatic pathway.

In particular, pH and buffer composition emerged as decisive factors. Experiments conducted under acidic conditions, adjusted using acetic acid, did not result in detectable acetaldehyde formation, consistent with the known inhibition of ADH activity at low pH values. Similarly, no acetaldehyde formation was observed in unbuffered aqueous systems. In contrast, measurable acetaldehyde production was observed when phosphate buffer systems were employed, suggesting a synergistic effect between the enzymatic system and the surrounding chemical environment. This behaviour is consistent with literature reports describing the role of phosphate species in stabilizing enzyme–cofactor complexes and facilitating proton transfer during ethanol oxidation.

Temperature and residence time further modulated acetaldehyde formation. Increasing temperature enhanced the extent of ethanol oxidation, particularly in the range between 50 and 60 °C, while longer incubation times led to increased acetaldehyde concentrations up to a plateau value. These trends indicate that enzymatic activity remains operative under moderately elevated temperatures, although saturation effects and possible enzyme deactivation limit further acetaldehyde accumulation at prolonged exposure times.

The influence of reagent concentrations was also investigated. Variations in ADH concentration alone did not lead to proportional changes in acetaldehyde formation, suggesting that the enzyme was not the limiting factor under the tested conditions. In contrast, NAD^+ concentration exhibited a pronounced effect, with higher cofactor availability resulting in increased acetaldehyde production. This observation is consistent with the

ordered Bi–Bi mechanism of ADH, in which NAD^+ binding precedes ethanol oxidation and NADH release constitutes a rate-limiting step.

Overall, these results demonstrate that enzymatic oxidation of ethanol via the ADH/NAD^+ system represents a viable precursor pathway for acetaldehyde formation under conditions relevant to industrial ethanol recovery. The activation of this pathway is not governed solely by temperature but is critically dependent on the chemical environment, particularly buffer composition and cofactor availability. These findings provide a mechanistic basis for interpreting the intermittent occurrence of acetaldehyde contamination observed at industrial scale and set the stage for a multivariate analysis of interaction effects and response surfaces presented in the following sections.

3.7 Effect of pH and Buffer Systems

The effect of pH and buffer composition on acetaldehyde formation was systematically investigated to clarify the role of the chemical environment in activating or inhibiting the enzymatic oxidation of ethanol. As discussed in the previous sections, alcohol dehydrogenase activity is strongly dependent on pH and on the surrounding matrix, and these factors were therefore examined independently from temperature and reagent concentration effects.

A first set of experiments was carried out under acidic conditions, using acetic acid to adjust the pH in the range 3.00–3.26. These conditions are representative of the acidic environment commonly encountered in spent ethanol streams generated during plasma fractionation. Under all tested acidic conditions, no detectable acetaldehyde formation was observed, regardless of temperature, ethanol concentration, or incubation time. This behaviour is consistent with the known inhibition of ADH activity at low pH values, where protonation of active-site residues and destabilization of the enzyme–cofactor complex significantly reduces catalytic efficiency.

Additional experiments were performed at mildly acidic pH (approximately 5.6), adjusted using sulfuric acid. Also in this case, acetaldehyde concentrations remained below the detection limit of the analytical method. These results indicate that, in the absence of a buffering system capable of stabilizing the enzymatic reaction environment, ethanol oxidation via ADH/NAD^+ is strongly suppressed, even at temperatures where enzymatic activity might otherwise be expected.

Experiments conducted in unbuffered Milli-Q water at near-neutral to slightly alkaline pH (approximately 8.2) similarly did not lead to detectable acetaldehyde formation. Although this pH range is generally more favourable for ADH activity than acidic conditions, the lack of buffering capacity likely resulted in local pH fluctuations during incubation, limiting sustained enzymatic activity.

In contrast, measurable acetaldehyde formation was consistently observed when phosphate buffer systems were employed. Under these conditions, acetaldehyde production occurred across a range of temperatures and incubation times, demonstrating that the presence of phosphate plays a critical role in enabling the enzymatic oxidation of ethanol. Notably, acetaldehyde formation was observed even at moderate temperatures, confirming that buffer composition, rather than pH alone, governs the activation of the pathway.

The concentration of phosphate buffer was also investigated to assess whether buffer strength influenced acetaldehyde formation. Within the explored range, variations in phosphate concentration did not result in significant differences in acetaldehyde production, suggesting that the mere presence of phosphate, rather than its absolute concentration, is sufficient to stabilize the enzymatic system under the investigated conditions.

The promoting effect of phosphate buffers can be rationalized considering their dual role as pH-controlling agents and as facilitators of proton transfer processes. Phosphate species are known to interact with enzyme–cofactor systems, potentially stabilizing intermediate states and lowering the

effective activation barrier for ethanol oxidation. These observations agree with literature reports describing enhanced ADH activity in phosphate-containing media compared to unbuffered systems.

Overall, these results demonstrate that acetaldehyde formation via the ADH/NAD^+ pathway is not governed solely by temperature or enzyme presence, but is critically dependent on the chemical environment, particularly on buffer identity. The strong dependence on phosphate buffers provides a mechanistic link between the chemical composition of spent ethanol streams and the intermittent occurrence of acetaldehyde contamination observed in industrial ethanol recovery operations.

3.8 Effects of Individual Variables on Acetaldehyde Formation

Following the identification of buffer composition as a key enabling factor for enzymatic ethanol oxidation, the influence of temperature, incubation time, and reagent concentrations on acetaldehyde formation was systematically investigated. The experimental results discussed in this section are based on the dataset generated using the ADH/NAD^+ model system under phosphate-buffered conditions, as reported in the experimental campaign carried out at Universidad Complutense de Madrid.

The objective of this analysis was to quantify the relative importance of individual variables and to identify possible interaction effects governing acetaldehyde formation, without developing a formal kinetic model. The results are therefore interpreted in terms of trends, sensitivities, and saturation behaviours relevant to industrial ethanol recovery conditions. For clarity and ease of comparison, the experimental results in this section are presented using bar charts summarizing acetaldehyde concentrations under discrete experimental conditions.

3.8.1 Effect on Temperature and Incubation Time

Temperature was found to be one of the dominant factors influencing acetaldehyde formation. Across all tested conditions, increasing temperature led to a marked increase in acetaldehyde concentration, particularly in the range between 50 and 60 °C. At lower temperatures (around 40 °C), acetaldehyde formation remained limited even after prolonged incubation, indicating reduced enzymatic activity.

Incubation time further modulated the effect of temperature. At 40 °C, acetaldehyde concentration increased only slightly with time, remaining well below critical levels even after 40 minutes. At 50 °C, a more pronounced time dependence was observed, with acetaldehyde formation increasing progressively from 10 to 40 minutes. At 60 °C, acetaldehyde production occurred rapidly and approached a plateau within the first 10–20 minutes, suggesting that either enzyme saturation, cofactor limitation, or partial deactivation limited further conversion.

These results indicate that temperature not only accelerates ethanol oxidation but also reduces the characteristic time required to reach near-steady acetaldehyde levels. This behaviour is consistent with enzymatic systems operating close to their thermal tolerance limits.

Figure 3.1 shows results obtained from tests conducted with 50 ppm ADH, 663 ppm NAD^+, 3156 ppm ethanol, incubation temperature of 40, 50 and 60°C for 10, 20 and 40 minutes.

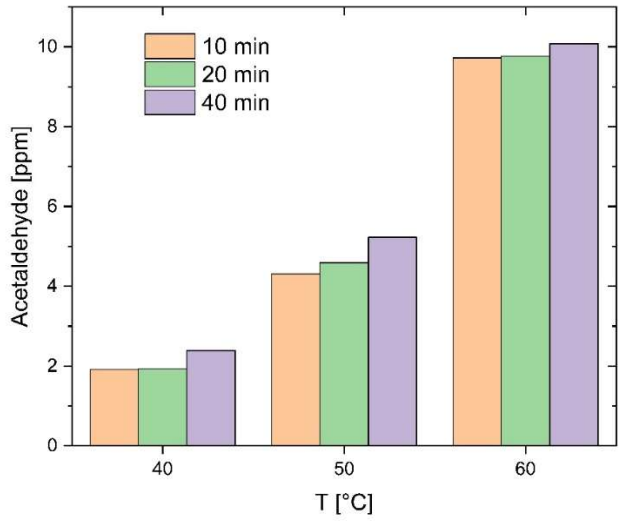

Figure 3.1: Acetaldehyde concentration obtained with tests conducted with 50 ppm of ADH, 663 ppm of NAD^+ and 3156 ppm of EtOH.

3.8.2 Effect of ADH Concentration

The influence of alcohol dehydrogenase concentration on acetaldehyde formation was evaluated over the range explored in the experimental campaign (typically 5–20 ppm). Under otherwise identical conditions of ethanol concentration, NAD^+ availability, temperature, and incubation time, variations in ADH concentration did not result in proportional changes in acetaldehyde production.

This behaviour indicates that, within the investigated range, ADH was not the limiting factor for ethanol oxidation. Once a minimum enzyme concentration was present, the reaction rate appeared to be controlled by other parameters, such as cofactor availability or environmental conditions.

This observation is consistent with enzymatic systems operating under conditions where substrate or cofactor limitation dominates over enzyme concentration effects.

Figure 3.2 groups all tests conducted with ADH concentrations of 5, 10 and 20 ppm, NAD^+ concentration of 530 ppm, and EtOH concentration of 3156 ppm for an incubation time of 10 minutes.

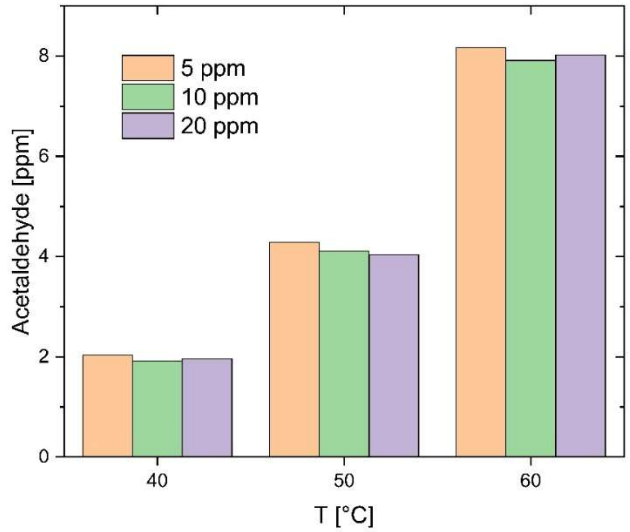

Figure 3.2: Effect of ADH variation at different Temperatures. 530 ppm NAD^+, 3156 ppm of EtOH and 10 min of incubation time.

3.8.3 Effect of NAD^+ Concentration

In contrast to ADH, the concentration of the nicotinamide adenine dinucleotide cofactor (NAD^+) exerted a strong influence on acetaldehyde formation. Increasing NAD^+ concentration consistently resulted in higher acetaldehyde production under all tested temperatures and incubation times.

This effect was particularly evident when comparing experiments conducted at low and high NAD^+ levels, where acetaldehyde concentrations differed by several ppm under otherwise identical conditions. The observed trend confirms that NAD^+ availability represents a limiting factor for ethanol oxidation in the investigated system.

This finding agrees with the ordered Bi–Bi mechanism of alcohol dehydrogenase, in which NAD^+ binding precedes ethanol oxidation and NADH release often constitutes the rate-limiting step of the catalytic cycle.

Figure 3.3 shows the results obtained in tests carried out with 20 ppm of ADH, 3156 ppm of EtOH, and 10 minutes of incubation time in a range of temperature between 40 and 60 °C and a range of NAD^+ between 128 and 1060 ppm.

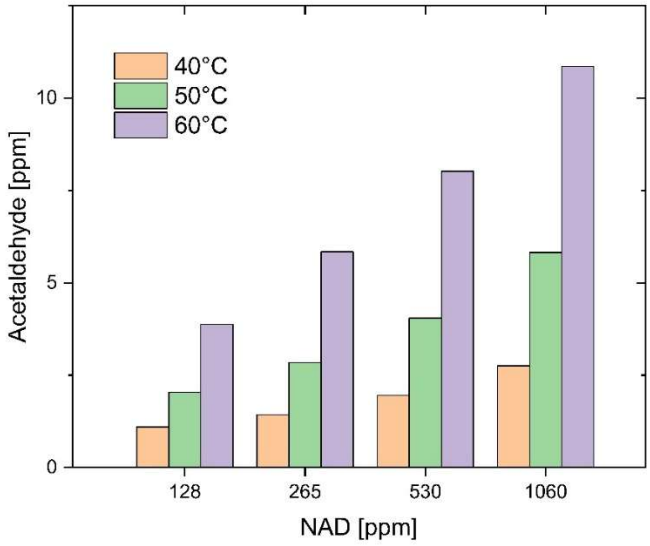

Figure 3.3: Acetaldehyde concentration obtained in tests with 20 ppm of ADH, 3156 ppm of EtOH and 10 min of incubation time.

3.8.4 Effect of Ethanol Concentration

The effect of ethanol concentration on acetaldehyde formation was evaluated over a broad concentration range representative of spent ethanol streams. In all tested configurations, increasing ethanol concentration led to higher acetaldehyde production, confirming ethanol as the primary substrate driving the reaction.

However, at higher ethanol concentrations, the increase in acetaldehyde formation tended to level off, particularly at elevated temperatures. This saturation behaviour suggests that, beyond a certain threshold, ethanol availability no longer limits the reaction rate, which becomes controlled by enzyme activity or cofactor regeneration.

Such trends are qualitatively consistent with Michaelis–Menten-type behaviour, although no kinetic parameters were derived in the present study.

Figure 3.4 shows the results obtained for tests with 50 ppm ADH, 663 ppm NAD^+, incubation temperature 40, 50 and 60°C for 10 minutes at ethanol concentrations of 789, 1578, 2367, 3156 and 4734 ppm.

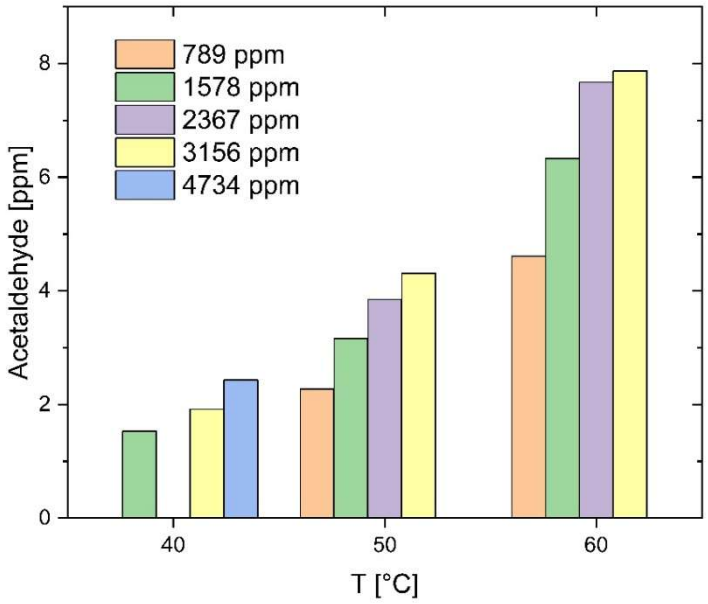

Figure 3.4: Results obtained for tests with 50 ppm ADH, 663 ppm NAD, and 10 minutes of incubation time.

3.8.5 MULTIVARIATE INTERPRETATION

Taken together, these results demonstrate that acetaldehyde formation via the ADH/NAD^+ pathway is governed by a hierarchy of influencing factors. Temperature and NAD^+ availability emerge as the dominant variables, while ADH concentration plays a secondary role once present above a minimum threshold. Ethanol concentration controls the reaction rate at low levels but leads to saturation effects at higher concentrations.

The strong dependence on temperature, time, and cofactor availability provides a mechanistic explanation for the variability observed at industrial scale, where small fluctuations in operating conditions or matrix composition may lead to disproportionate changes in acetaldehyde formation.

3.9 Multivariate Interpretation and Operational Maps

3.9.1 Scope and Methodological Framework

The experimental results discussed in Sections 3.6 - 3.8 highlight that acetaldehyde formation via the ADH/NAD^+ pathway is governed by the combined effect of several operating variables, rather than by a single dominant factor. To systematically interpret these multivariate effects and to identify relevant interactions between process variables, the experimental dataset was analysed using a factorial design approach.

A full factorial design with three factors at two levels (2^3) was applied as a data analysis tool to extract quantitative information from the experimental results. It is important to note that the design of experiments was not used a priori to plan the experimental campaign but was instead applied ex post to interpret an already structured dataset. This approach is appropriate in exploratory and process-oriented studies, where the objective is to identify dominant variables, interaction effects, and operational trends rather than to derive intrinsic kinetic parameters.

Although no formal kinetic modelling was performed, the experimental dataset allows the identification of multivariate trends and interaction effects. These effects can be represented as response surfaces, providing an engineering-oriented interpretation of acetaldehyde formation under the investigated conditions.

For each factorial plan, the response variable was defined as the acetaldehyde concentration measured at the end of the incubation period. A linear factorial model including main effects, two-factor interactions, and the three-factor interaction was considered in the analysis. The relative importance of the effects was evaluated using standardized effect estimates and graphical tools, while the sign of each effect was interpreted based on the corresponding response trends.

Because the experimental focus and operating conditions differed across the investigated cases, the factors included in each 2^3 design were not identical in all factorial plans. For this reason, the definition of the factors and their corresponding low and high levels is provided separately for each plan in the following sections. This plan-by-plan approach allows the factorial analysis to remain closely tied to the specific experimental context, facilitating a clear and physically meaningful interpretation of the results.

Overall, the application of factorial analysis in this chapter serves as a bridge between single-variable interpretations and a more integrated understanding of acetaldehyde formation under process-relevant conditions. The results of the five factorial plans are presented and discussed individually in the following sections, followed by a comparative analysis to identify general trends and robust conclusions.

For consistency across all factorial plans, effects associated with a statistical significance below 95% were considered non-significant and were not discussed further. The interpretation therefore focuses exclusively on dominant main effects and physically meaningful two-factor interactions.

For fitted models derived from the analysis of experimental data, Y indicates the concentration of acetaldehyde, while the independent variables A, B, C, etc. represent the coded variables (-1;+1) of the significant factors used in the model.

Across all investigated factorial plans, the three-factor interaction term (ABC) was found to be negligible or not statistically significant. Consequently, the interpretation of the results focuses on main effects and relevant two-factor interactions, which capture the dominant behavior of the system within the explored experimental domain.

3.9.2 Effect of constant NAD^+/ADH Ratio, Incubation Time and Temperature.

This factorial plan was aimed at investigating the combined influence of enzymatic, thermal, and temporal variables on acetaldehyde formation

under conditions representative of the ADH/NAD^+-mediated ethanol oxidation pathway. In all experiments, ethanol concentration was fixed at 3156 ppm, and the NAD^+/ADH molar ratio was maintained at 13.26 to isolate the effect of absolute enzyme concentration while preserving constant cofactor availability.

A full factorial design with three factors at two levels (2^3) was considered. Factor A corresponded to alcohol dehydrogenase concentration (20–70 ppm), factor B to incubation time (10–40 min), and factor C to incubation temperature (40–60 °C). Acetaldehyde concentration measured at the end of the incubation period was used as the response variable. This configuration enabled the identification of dominant main effects and relevant interaction effects within the explored experimental domain.

The results of the factorial analysis are summarized in Table 3.4, which reports the estimated effects and their associated statistical significance.

Table 3.4: Factorial Analysis for Effects of ADH concentration (A), incubation time (B), and incubation temperature (C).

	A	**B**	**C**	**Y**		
	ADH	**t inc**	**T inc**	**Acetaldehyde**	**Effect**	**Significance**
	[ppm]	**[min]**	**[°C]**	**[ppm]**		
1	20	10	40	1,96		
a	**70**	**10**	**40**	**2,39**	**1,885**	**96,29%**
b	20	40	40	2,03	0,495	86,08%
ab	70	40	40	2,57	0,165	62,57%
c	**20**	**10**	**60**	**8,02**	**7,72**	**99,09%**
ac	**70**	**10**	**60**	**11,03**	**1,4**	**95,01%**
bc	20	40	60	8,61	0,37	81,60%

abc	70	40	60	12,17	0,11	50,00%

The analysis reported in Table 3.4 highlights a clear hierarchy among the investigated factors. Incubation temperature (factor C) exhibits the largest effect magnitude and the highest statistical significance, confirming temperature as the dominant variable controlling acetaldehyde formation under the investigated conditions. Increasing the incubation temperature from 40 to 60 °C results in a pronounced increase in acetaldehyde concentration, regardless of the levels of the other factors.

Alcohol dehydrogenase concentration (factor A) also shows a statistically significant positive effect. Since the NAD^+/ADH molar ratio was kept constant, this result indicates that increasing the absolute enzyme concentration enhances acetaldehyde formation, suggesting that the system is not fully enzyme-saturated within the explored concentration range.

Among the interaction terms, only the interaction between ADH concentration and temperature (AC) exceeds the adopted significance threshold. This interaction indicates that the positive effect of increasing ADH concentration is amplified at higher temperatures, pointing to a synergistic coupling between enzymatic activity and thermal activation. All remaining effects, including incubation time (factor B) and the AB, BC, and ABC interactions, were found to be below the adopted significance threshold and were therefore considered non-significant within the investigated experimental space.

Figure 3.5 shows the main effects of ADH concentration (A) and incubation temperature (C) on acetaldehyde formation for the first factorial plan. Both factors exhibit a positive effect on the response, as indicated by the increasing trend in mean acetaldehyde concentration when moving from the low (−1) to the high (+1) factor level.

Incubation temperature (factor C) displays a markedly steeper slope compared to ADH concentration, confirming temperature as the dominant

factor controlling acetaldehyde formation under these conditions. In contrast, the effect of ADH concentration, while statistically significant, is comparatively moderate, indicating a secondary but non-negligible contribution when the NAD^+/ADH ratio is kept constant.

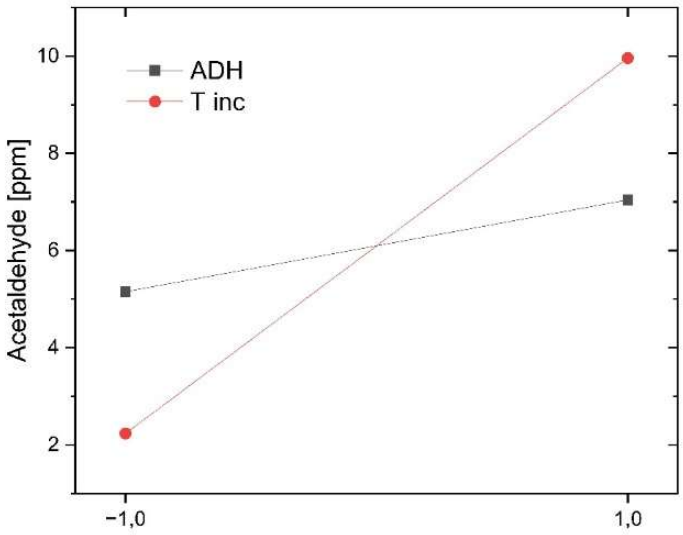

Figure 3.5: Main Effects of ADN concentration (A) and incubation Temperature (C).

Figure 3.6 illustrates the interaction between ADH concentration (A) and incubation temperature (C) on acetaldehyde formation. The non-parallel trends observed for the two temperature levels indicate a significant interaction between the two factors, in agreement with the factorial analysis results.

At low temperature (40 °C), increasing ADH concentration leads to a moderate increase in acetaldehyde formation. In contrast, at high temperature (60 °C), the same increase in ADH concentration results in a substantially larger rise in acetaldehyde concentration. This behaviour confirms that the effect of enzyme concentration is strongly amplified at higher temperatures.

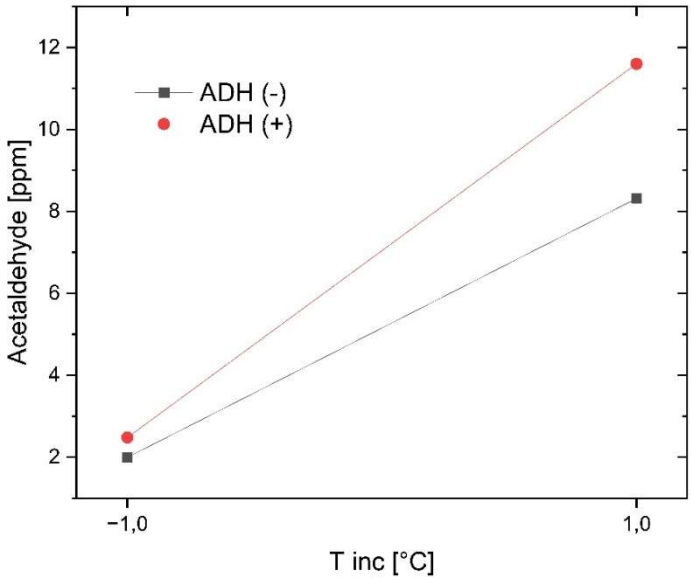

Figure 3.6: Interaction between ADH concentration (A) and incubation temperature (C).

Figure 3.7 reports the scatter plot comparing experimentally measured acetaldehyde concentrations with the values calculated using the factorial model. The close alignment of the data points along the parity line indicates an excellent agreement between experimental and predicted responses.

The fitted model, expressed as

$$Y = 6.10 + 0.94A + 3.86C + 0.70AC \qquad \textit{(Equation 3.1)}$$

captures the dominant contributions of the main effects and the significant interaction identified in the factorial analysis. In particular, the large coefficient associated with temperature (C) and the presence of the AC interaction term are consistent with the trends observed in the main effects and interaction plots.

The high coefficient of regression ($R^2 = 0.998$) confirms that the model provides an accurate representation of the experimental response within the investigated domain.

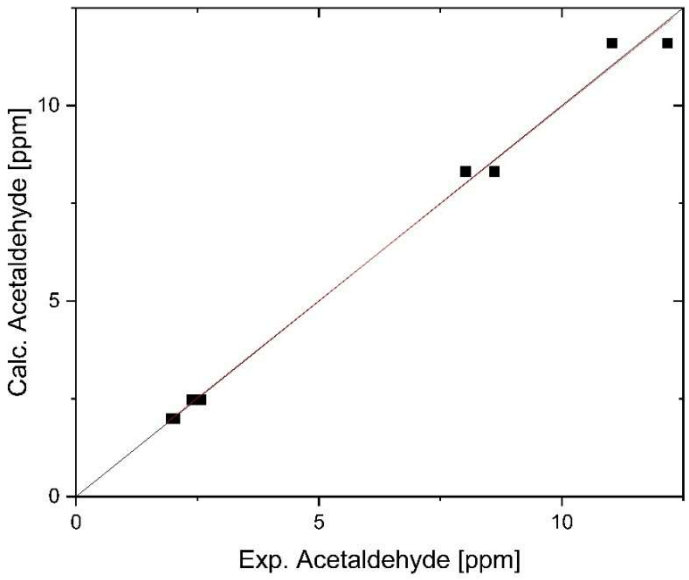

Figure 3.7: Scatter Plot for constant NAD^+/ADH Concentration, Incubation Time and Temperature.

Figure 3.8 presents the response surface describing acetaldehyde formation as a function of ADH concentration and incubation temperature, at fixed ethanol concentration and constant NAD^+/ADH ratio. The surface clearly illustrates the combined and synergistic effect of the two variables, with acetaldehyde concentration increasing monotonically toward the region of high temperature and high enzyme concentration.

The pronounced slope along the temperature axis confirms temperature as the dominant controlling factor, while the inclination along the ADH axis reflects the secondary but significant contribution of enzyme concentration. The curvature of the surface is limited, indicating that within the investigated experimental domain the system behaviour is well described by a first-order factorial model including the AC interaction term.

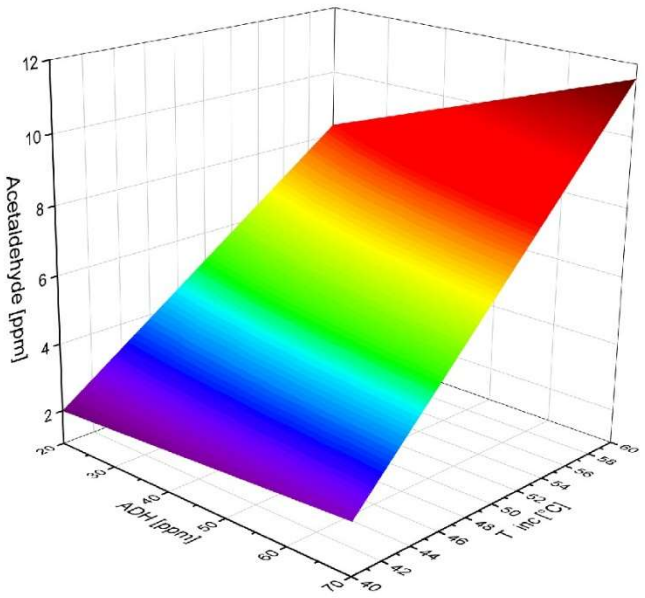

Figure 3.8: Response surface for ADH concentration and incubation temperature.

3.9.3 Effect of NAD^+ Concentration, Incubation Time, and Temperature

In this factorial plan, ethanol concentration was fixed at 3156 ppm and alcohol dehydrogenase concentration was kept constant at 20 ppm to isolate the effect of cofactor availability on acetaldehyde formation. The analysis focused on the role of NAD^+ concentration, incubation time, and incubation temperature under conditions representative of the enzymatic oxidation pathway.

A full factorial design with three factors at two levels (2^3) was considered. Factor A corresponded to NAD^+ concentration (265–530 ppm), factor B to incubation time (10–40 min), and factor C to incubation temperature (50–60 °C). Acetaldehyde concentration measured at the end of the incubation period was used as the response variable. This configuration allowed the assessment of whether acetaldehyde formation in this regime is limited by cofactor availability, thermal activation, or their combined effects.

The results of the factorial analysis are summarized in Table 3.5.

Table 3.5: Factorial Analysis for Effects of NAD concentration (A), incubation time (B), and incubation temperature (C).

	A	**B**	**C**	**Y**		
	NAD^+	**t inc**	**T inc**	**Acetaldehyde**	**Effect**	**Significance**
	[ppm]	**[min]**	**[°C]**	**[ppm]**		
1	265	10	50	2,84		
a	**530**	**10**	**50**	**4,04**	**1,75**	**95,28%**
b	265	40	50	3,33	0,41	80,45%
ab	530	40	50	4,39	0,06	27,53%
c	**265**	**10**	**60**	**5,84**	**3,48**	**97,62%**
ac	530	10	60	8,02	0,62	86,84%
bc	265	40	60	6,05	-0,01	4,89%
abc	530	40	60	8,61	0,13	50,00%

The analysis reported in Table 3.5 shows that both NAD^+ concentration (factor A) and incubation temperature (factor C) exhibit statistically significant positive effects on acetaldehyde formation, exceeding the adopted significance threshold of 95%. Among these, incubation temperature remains the dominant factor, confirming its primary role in activating the enzymatic pathway even within the narrower temperature range explored in this plan (50–60 °C).

The positive and significant effect associated with NAD^+ concentration indicates that, at fixed ADH concentration, acetaldehyde formation is partially limited by cofactor availability. Increasing NAD^+ concentration from 265 to 530 ppm leads to a measurable increase in acetaldehyde production, supporting the interpretation that NAD^+ availability governs the extent of ethanol oxidation under these conditions.

Incubation time (factor B), as well as all two-factor and three-factor interaction terms, exhibit significance levels below the adopted threshold and were therefore considered non-significant. This suggests that, within the investigated experimental space, acetaldehyde formation is controlled primarily by instantaneous operating conditions, namely temperature and NAD^+ concentration, rather than by residence time or higher-order coupling effects.

Figure 3.9 shows the main effects of NAD^+ concentration (A) and incubation temperature (C) on acetaldehyde formation for the second factorial plan. Both factors exhibit a positive effect on the response, as indicated by the increase in mean acetaldehyde concentration when moving from the low to the high factor level.

Incubation temperature (factor C) displays a steeper slope compared to NAD^+ concentration, confirming temperature as the dominant variable within the investigated range. Nevertheless, the positive trend associated with NAD^+ concentration highlights the role of cofactor availability in promoting ethanol oxidation when ADH concentration is fixed.

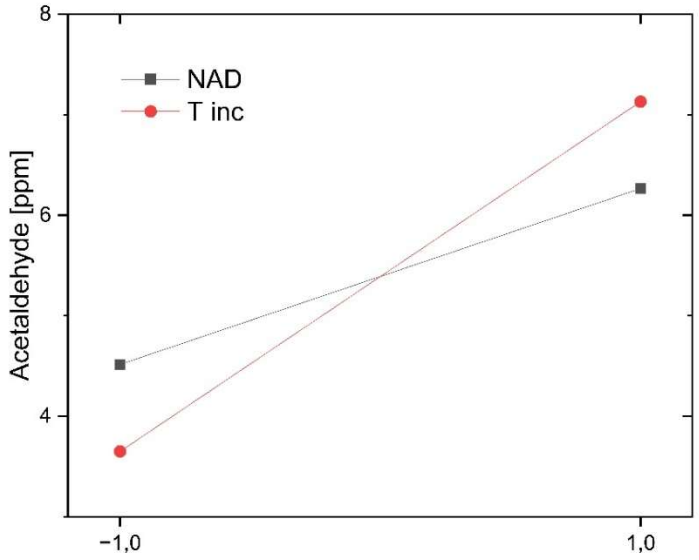

Figure 3.9: Main Effect of NAD concentration (A) and incubation temperature (C).

Figure 3.10 shows the scatter plot comparing experimentally measured acetaldehyde concentrations with values calculated using the factorial model. The close alignment of the data points along the parity line indicates a very good agreement between experimental and predicted responses.

The fitted model, expressed as

$$Y = 5.39 + 0.87A + 1.74C \qquad \textit{(Equation 3.2)}$$

captures the dominant contribution of incubation temperature and the secondary but significant effect of NAD^+ concentration, in line with the trends identified in the factorial analysis. The absence of interaction terms in the model is consistent with the lack of statistically significant interactions in this factorial plan.

The high coefficient of regression ($R^2 = 0.9957$) confirms that the simplified factorial model provides an accurate representation of the experimental response within the investigated domain, supporting its use for response surface visualization and engineering interpretation.

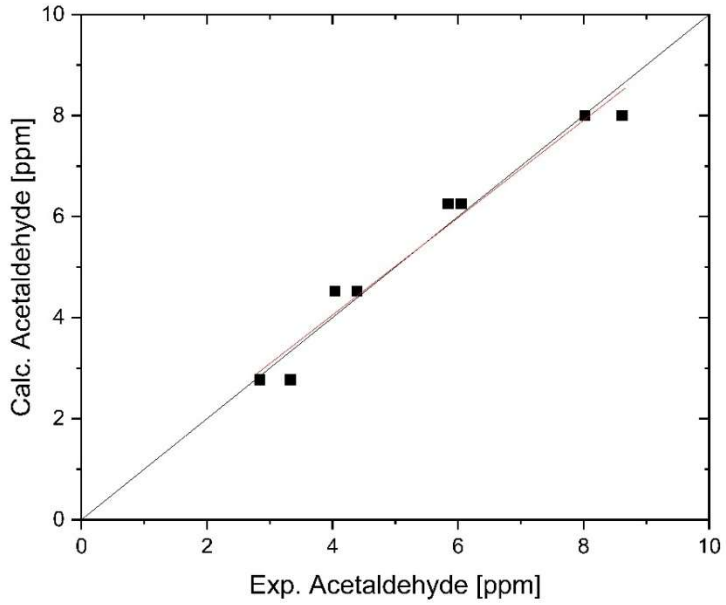

Figure 3.10: Scatter Plot for NAD^+ Concentration, Incubation Time, and Temperature.

Figure 3.11 shows the response surface describing acetaldehyde formation as a function of NAD^+ concentration and incubation temperature at fixed ethanol and ADH concentrations. The surface exhibits a nearly planar profile, indicating an approximately additive contribution of the two factors within the investigated experimental domain.

The slope along the temperature axis is more pronounced than that along the NAD^+ axis, confirming incubation temperature as the dominant variable, while NAD^+ concentration provides a secondary but measurable contribution. The absence of curvature or pronounced interaction features is consistent with the lack of statistically significant interaction terms identified in the factorial analysis.

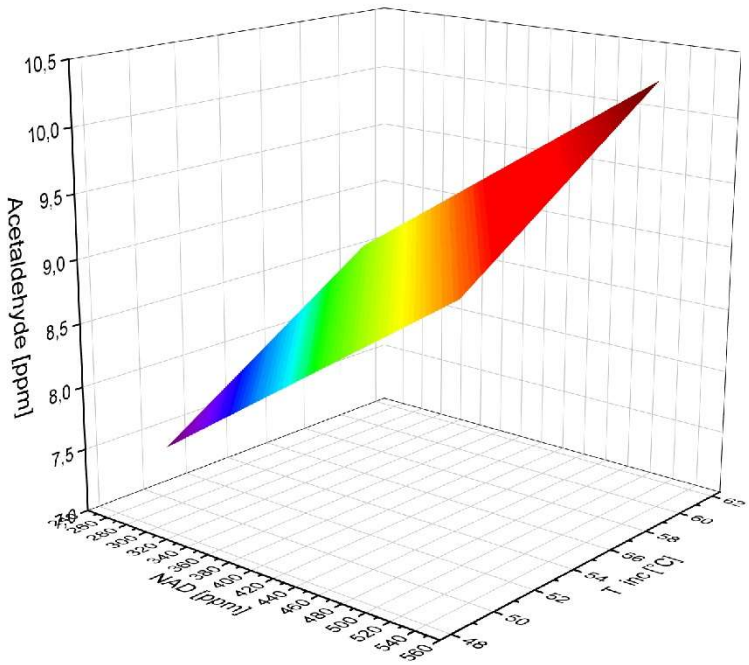

Figure 3.11: Response surface for NAD^+ concentration and incubation temperature.

3.9.4 Effect of Ethanol Concentration, NAD^+ Concentration, and Temperature

In this factorial plan, incubation time was fixed at 10 min and ADH concentration at 20 ppm, while ethanol concentration (A: 1578–3156 ppm), NAD^+ concentration (B: 265–530 ppm), and incubation temperature (C: 50–

60 °C) were varied. Acetaldehyde concentration was used as the response variable.

The factorial analysis reported in Table 3.6 indicates that all three main factors, ethanol concentration (A), NAD^+ concentration (B), and incubation temperature (C), exhibit statistically significant positive effects on acetaldehyde formation, exceeding the adopted significance threshold. Among them, incubation temperature shows the largest effect magnitude, confirming its dominant role also in this experimental configuration.

Table 3.6: Factorial Analysis for Effects of EtOH concentration (A), NAD^+ concentration (B), and incubation temperature (C).

	A	**B**	**C**	**Y**		
	EtOH	**NAD^+**	**T inc**	**Acetaldehyde**	**Effect**	**Significance**
	[ppm]	**[ppm]**	**[°C]**	**[ppm]**		
1	1578	265	50	2,57		
a	**3156**	**265**	**50**	**2,84**	**1,33**	**99,76%**
b	**1578**	**530**	**50**	**2,93**	**1,275**	**99,75%**
ab	**3156**	**530**	**50**	**4,04**	**0,415**	**99,23%**
c	**1578**	**265**	**60**	**4,28**	**2,85**	**99,89%**
ac	**3156**	**265**	**60**	**5,84**	**0,64**	**99,50%**
bc	**1578**	**530**	**60**	**5,64**	**0,495**	**99,36%**
abc	3156	530	60	8,02	-0,005	50,00%

In addition to the main effects, the two-factor interactions AB, AC, and BC are all statistically significant, indicating that acetaldehyde formation in this regime is governed by a strong coupling between substrate availability, cofactor concentration, and temperature. In contrast, the three-factor

interaction (ABC) is negligible and was therefore considered non-significant.

Overall, this factorial plan highlights a multivariate regime in which acetaldehyde formation is simultaneously controlled by ethanol concentration, cofactor availability, and thermal activation, with significant interaction effects emerging when all three variables are allowed to vary.

Figure 3.12 shows the main effects of EtOH concentration (A), NAD^+ concentration (B), and incubation temperature (C) on acetaldehyde formation. All three factors exhibit a positive effect on the response, with mean acetaldehyde concentration increasing when moving from the low to the high factor level.

Among the investigated variables, incubation temperature (factor C) displays the steepest slope, confirming it as the dominant factor. Ethanol concentration and NAD^+ concentration show comparable but less pronounced effects, indicating that substrate availability and cofactor concentration both contribute to acetaldehyde formation when temperature is sufficiently high.

Overall, the main effects plot is consistent with the factorial analysis results, confirming a multivariate regime in which acetaldehyde formation is controlled by the combined influence of temperature, ethanol concentration, and NAD availability.

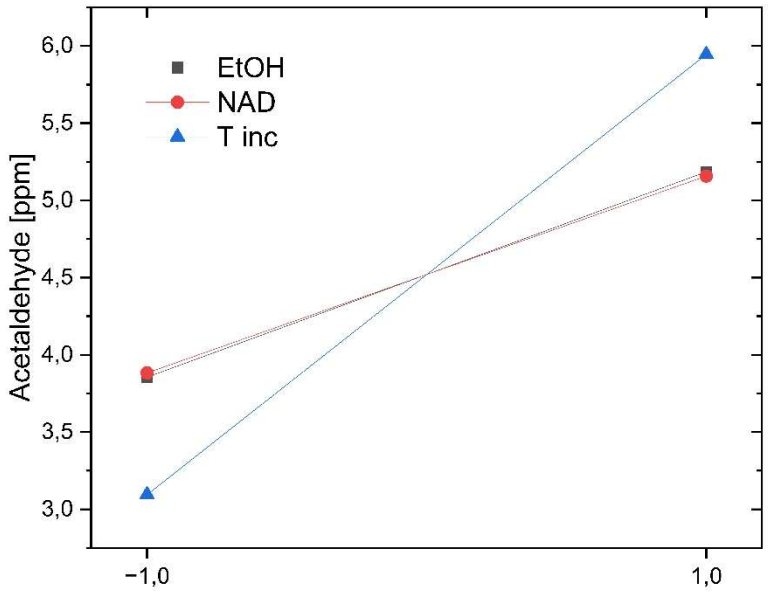

Figure 3.12: Main effects of ethanol concentration (A), NAD concentration (B), and incubation temperature (C).

Figure 3.13 to Figure 3.15 show the interaction plots for the A–C, A–B, and B–C factor pairs. In all cases, non-parallel trends are observed, confirming the presence of statistically significant two-factor interactions, in agreement with the factorial analysis results.

The interaction between ethanol concentration and temperature (A–C) appears particularly pronounced, indicating that the effect of increasing ethanol concentration is strongly amplified at higher temperatures. Similarly, the A–B and B–C plots highlight that the influence of ethanol and NAD concentration on acetaldehyde formation becomes more relevant as temperature increases.

These interaction plots confirm that acetaldehyde formation in this experimental regime cannot be attributed to independent factor effects alone, but arises from a coupled interaction between substrate availability, cofactor concentration, and thermal activation.

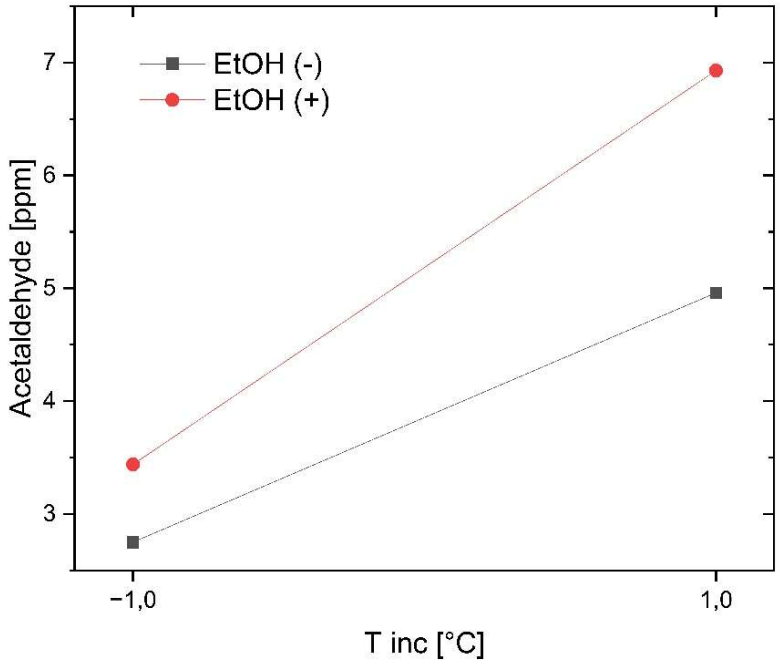

Figure 3.13: Interaction plot between EtOH concentration (A) and incubation Temperature (C).

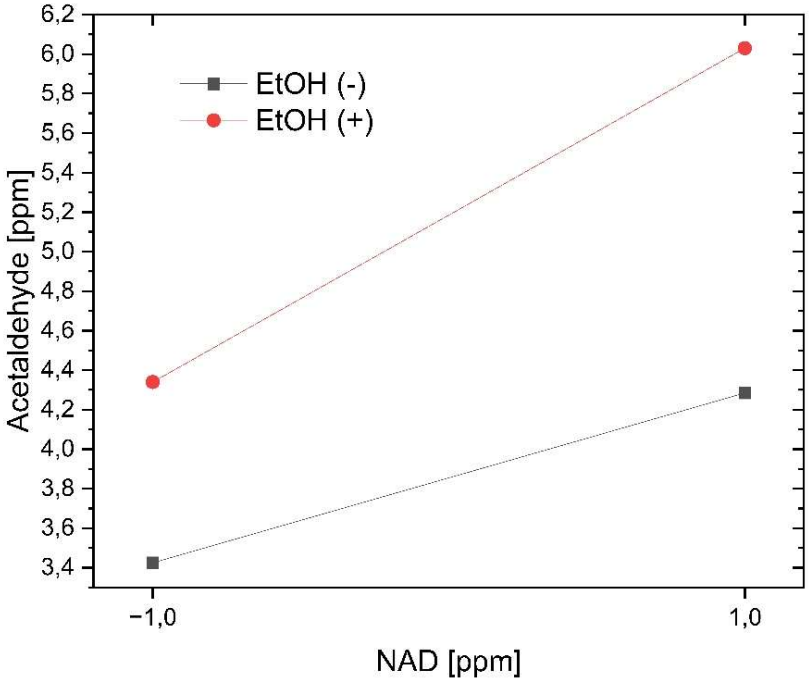

Figure 3.14: Interaction plot between EtOH concentration (A) and NAD^+ concentration (B).

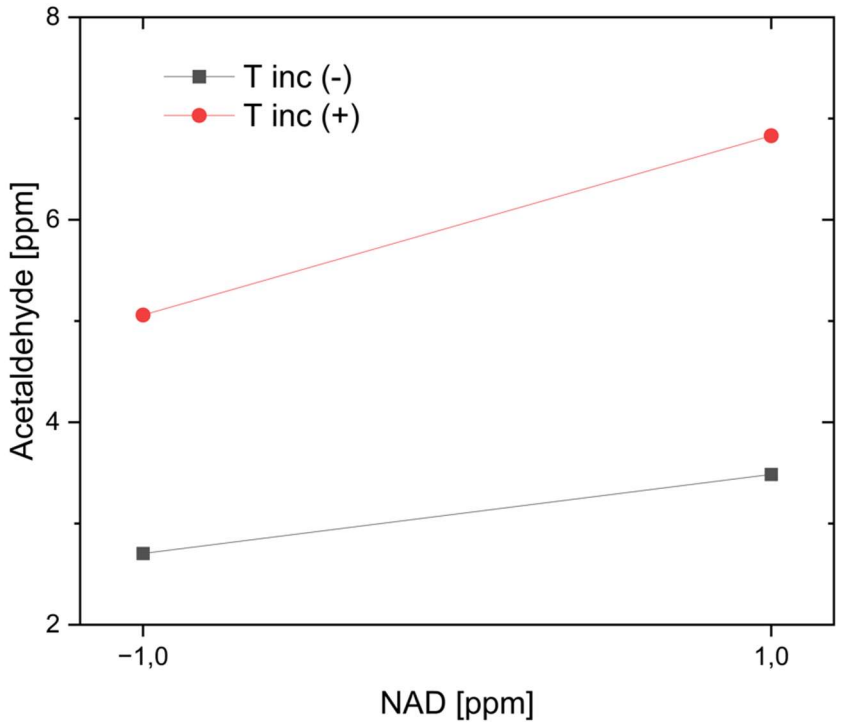

Figure 3.15: Interaction plot between NAD+ concentration (B) and incubation temperature (C).

Figure 3.16 reports the scatter plot comparing experimental and calculated acetaldehyde concentrations for the third factorial plan. The data points lie on the parity line, indicating an excellent agreement between experimental observations and model predictions.

The fitted factorial model,

$$Y = 4.52 + 0.67A + 0.64B + 0.21AB + 1.42C + 0.32AC + 0.25BC \quad \textit{(Equation 3.3)}$$

captures both the main effects and the relevant two-factor interactions identified in the factorial analysis. In particular, the larger coefficient associated with temperature (C) confirms its dominant role, while the presence of multiple interaction terms reflects the coupled influence of ethanol concentration, NAD^+ availability, and thermal activation.

The coefficient of regression ($R^2 = 1$) indicates that the model provides an exact representation of the experimental dataset within the investigated domain.

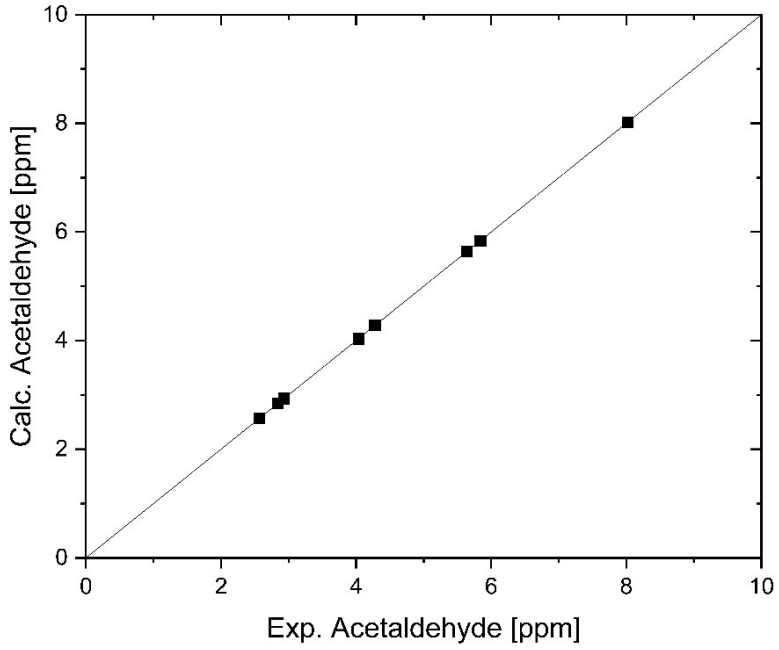

Figure 3.16: Scatter plot for Ethanol Concentration, NAD^+ Concentration, and Temperature effect.

Figure 3.17 to Figure 3.19 show the response surfaces describing acetaldehyde formation as a function of ethanol concentration, NAD^+ concentration, and incubation temperature, with incubation time fixed at 10 min and ADH concentration fixed at 20 ppm. All surfaces exhibit a monotonic increase in acetaldehyde concentration toward regions of higher temperature, confirming thermal activation as the dominant driving force.

The surfaces involving ethanol concentration highlight that increasing substrate availability enhances acetaldehyde formation, particularly at elevated temperature and NAD^+ levels, indicating a coupled effect between substrate concentration and enzymatic activity. Similarly, the NAD^+–temperature surface shows that cofactor availability amplifies acetaldehyde formation mainly under high-temperature conditions, whereas its influence remains limited at lower temperatures.

The response surfaces confirm a strongly multivariate regime in which acetaldehyde formation results from the combined and interacting effects of ethanol concentration, NAD^+ availability, and temperature. These

visualizations provide a clear identification of operating regions associated with elevated acetaldehyde formation and support the factorial interpretation discussed above.

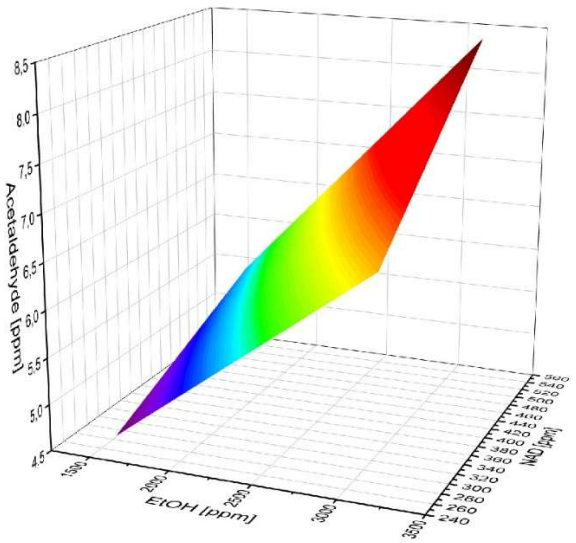

Figure 3.17: Response surface for EtOH and NAD^+ concentration.

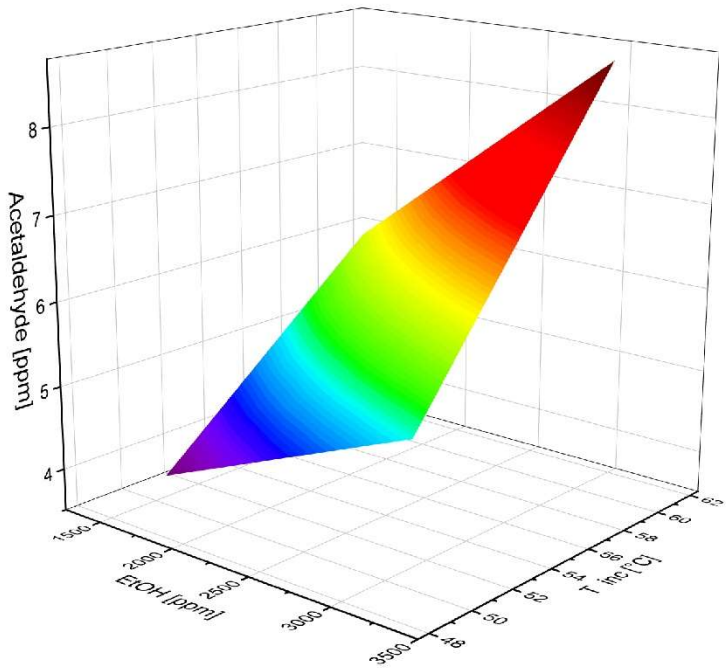

Figure 3.18: Response surface for EtOH concentration and incubation temperature.

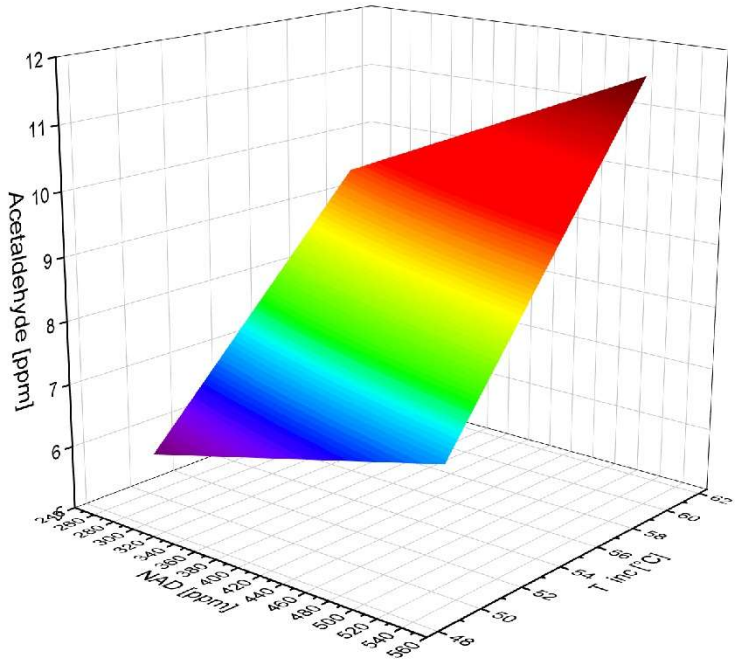

Figure 3.19: Response surface for NAD⁺ concentration and incubation temperature.

3.9.5 Effect of ADH Concentration, Incubation Temperature, and Incubation Time

In this factorial plan, ethanol concentration was fixed at 3156 ppm and NAD⁺ concentration was kept constant at 530 ppm, to investigate the role of enzyme availability under conditions of high cofactor excess. The analysed factors were ADH concentration (A: 10–20 ppm), incubation temperature (B: 40–60 °C), and incubation time (C: 10–40 min), with acetaldehyde concentration as the response variable.

The factorial analysis reported in Table 3.7 shows that incubation temperature (factor B) exhibits the strongest and most statistically significant effect on acetaldehyde formation, clearly exceeding the adopted significance threshold. Increasing temperature from 40 to 60 °C leads to a pronounced increase in acetaldehyde concentration, confirming temperature as the dominant controlling variable under these conditions.

Table 3.7: Factorial analysis for Effect of ADH concentration, incubation temperature, and incubation time.

	A	**B**	**C**	**Y**		
	ADH	**T inc.**	**t inc**	**Acetaldehyde**	**Effect**	**Significance**
	[ppm]	**[°C]**	**[min]**	**[ppm]**		
1	10	40	10	1,92		
a	20	40	10	1,96	0,035	90,97%
b	**10**	**60**	**10**	**7,91**	**6,29**	**99,95%**
ab	20	60	10	8,02	0,03	89,49%
c	**10**	**40**	**40**	**2,06**	**0,37**	**99,14%**
ac	20	40	40	2,03	-0,04	92,08%
bc	**10**	**60**	**40**	**8,59**	**0,265**	**98,80%**
abc	3156	530	60	8,02	-0,005	50,00%

Incubation time (factor C) also shows a statistically significant positive effect, indicating that longer residence times promote acetaldehyde accumulation when sufficient cofactor is available. In contrast, ADH concentration (factor A) does not reach the adopted significance threshold and was therefore considered non-significant within the investigated range, suggesting that enzyme concentration is no longer a limiting factor under conditions of high NAD^+ availability.

Among interaction terms, only the interaction between temperature and incubation time (BC) is statistically significant, indicating that the effect of residence time becomes more pronounced at higher temperatures. All remaining interaction terms, including those involving ADH concentration, are below the significance threshold and were therefore neglected.

Figure 3.20 shows the main effects of incubation temperature (B) and incubation time (C) on acetaldehyde formation for this factorial plan. Incubation temperature exhibits a pronounced positive effect, confirming it as the dominant variable under conditions of fixed ethanol and excess NAD^+ concentration.

In contrast, incubation time shows a much weaker effect, with only a slight increase in mean acetaldehyde concentration across the explored range. This behaviour indicates that residence time plays a secondary role compared to temperature when cofactor availability is not limiting.

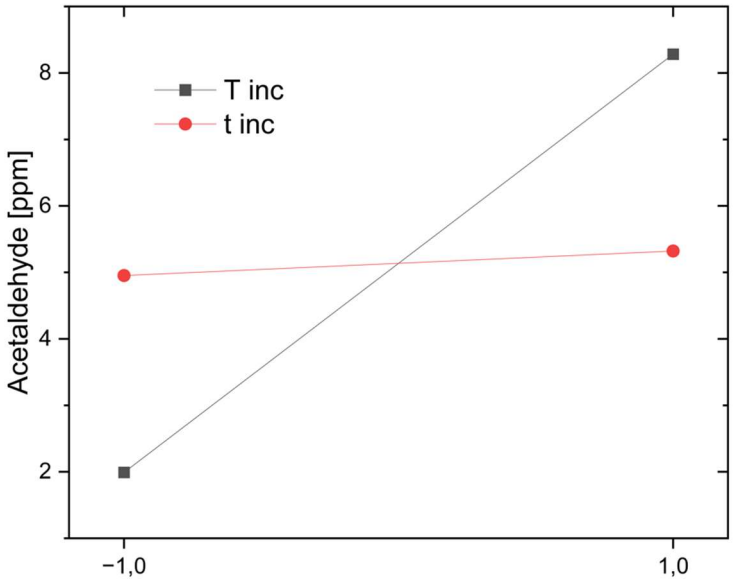

Figure 3.20: Main effects plot for incubation temperature (B) and incubation time (C).

Figure 3.21 shows the interaction plot between incubation temperature (B) and incubation time (C). The non-parallel trends observed indicate a significant interaction between the two factors, in agreement with the factorial analysis results.

At higher temperature levels, increasing incubation time leads to a more pronounced increase in acetaldehyde formation, whereas at lower temperatures the effect of time remains limited. This behaviour confirms that residence time becomes relevant mainly when sufficient thermal activation is provided.

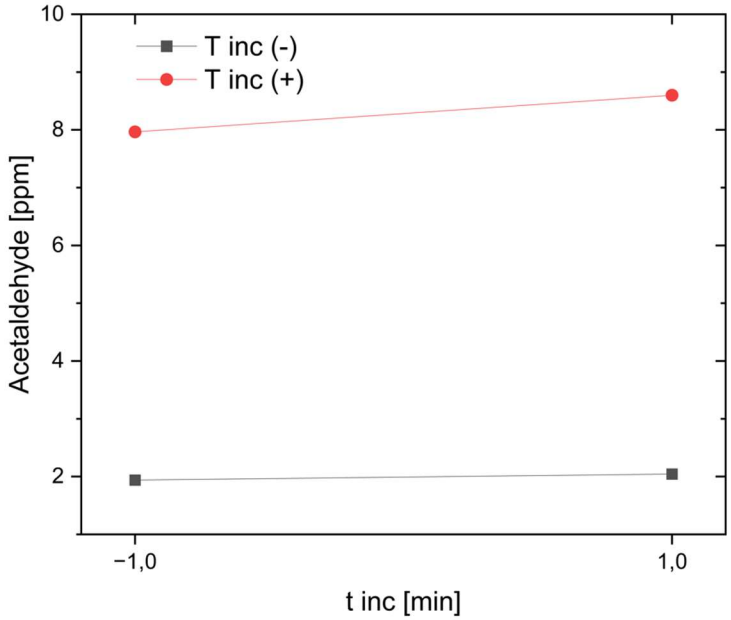

Figure 3.21: Interaction plot between incubation temperature (B) and time(C).

Figure 3.22 shows the scatter plot comparing experimental and calculated acetaldehyde concentrations for this factorial plan. The data points lie on the parity line, indicating an excellent agreement between experimental observations and model predictions.

The fitted factorial model,

$$Y = 5.14 + 3.15B + 0.185C + 0.13BC \qquad \textit{(Equation 3.4)}$$

captures the two effects of the incubation temperature (B), incubation time (C), and the combined effect of the two factors (BC). The coefficient of factor B (incubation temperature) is much higher than the others, demonstrating the effect of the factor.

The coefficient of regression ($R^2 = 1$) confirms that the factorial model accurately describes the experimental response within the investigated domain. This result supports the adequacy of the selected main effects and interaction terms for representing acetaldehyde formation under conditions of fixed ethanol concentration and excess NAD^+ availability.

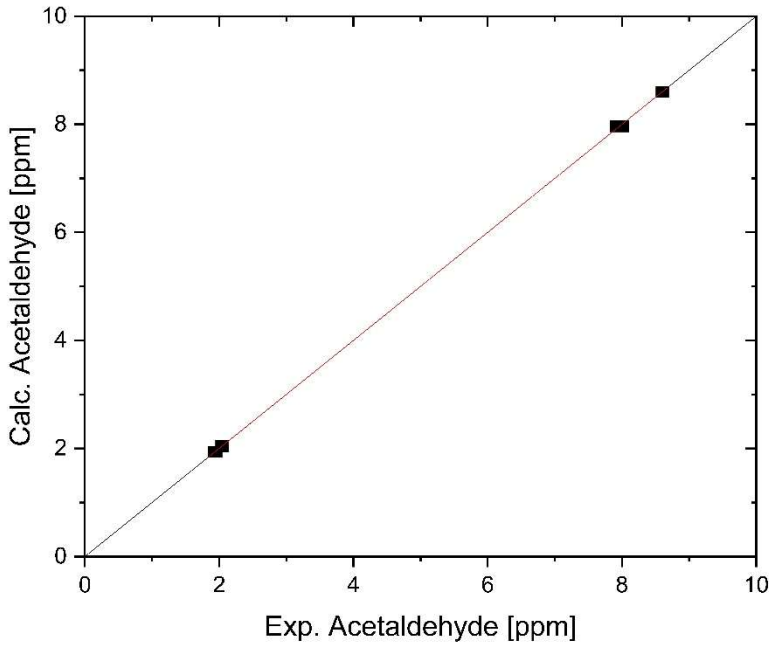

Figure 3.22: Scatter plot for ADH concentration, incubation temperature and incubation time.

Figure 3.23 shows the response surface describing acetaldehyde formation as a function of incubation temperature and incubation time, at fixed ethanol concentration and excess NAD^+ availability. The surface highlights a strong monotonic increase in acetaldehyde concentration with temperature, confirming thermal activation as the dominant driving force in this regime.

The effect of incubation time is comparatively weaker and becomes appreciable mainly at higher temperatures, consistent with the significant temperature–time interaction identified in the factorial analysis. At lower temperatures, increasing residence time has a limited impact on acetaldehyde formation.

Overall, the response surface confirms that under conditions of sufficient cofactor availability, acetaldehyde formation is primarily controlled by temperature, with residence time acting as a secondary factor whose influence is enhanced at elevated temperatures.

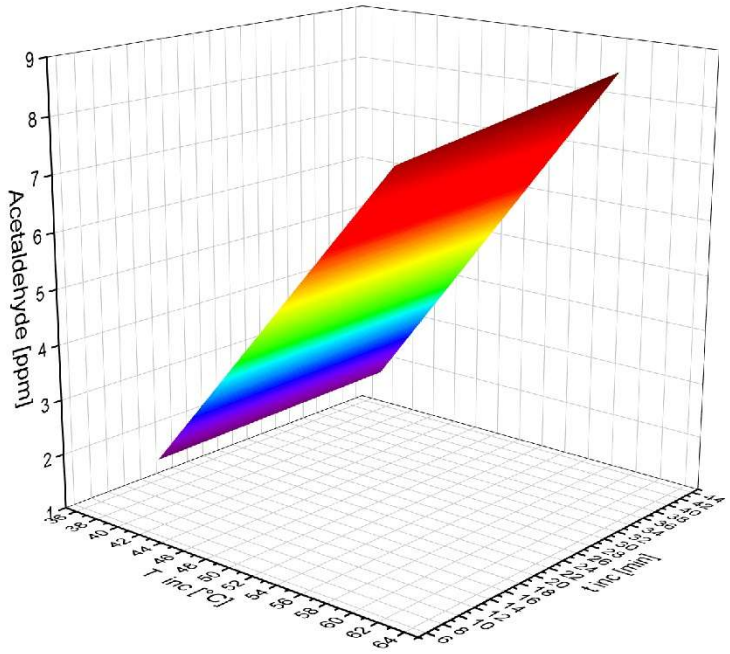

Figure 3.23: Surface response plot for incubation temperature and time.

3.9.6 Effect of NAD^+/ADH Ratio, Incubation Temperature, and Incubation Time

In this factorial plan, ethanol concentration was fixed at 3156 ppm, while the effect of the NAD^+/ADH ratio was investigated by varying factor A between 13.26 and 53. These values correspond to two different enzymatic regimes, obtained by changing ADH concentration from 70 ppm (low NAD^+/ADH ratio) to 10 ppm (high NAD/ADH ratio). Incubation temperature (factor B) was varied between 40 and 60 °C, and incubation time (factor C) between 10 and 40 min. Acetaldehyde concentration was used as the response variable.

The results of the factorial analysis reported in Table 3.8 indicate that incubation temperature (factor B) exhibits the strongest and most statistically significant positive effect on acetaldehyde formation, confirming once again temperature as the dominant controlling variable. Increasing temperature from 40 to 60 °C leads to a marked increase in acetaldehyde concentration, regardless of the NAD^+/ADH ratio.

The NAD^+/ADH ratio (factor A) also shows a statistically significant effect, with a negative sign. This indicates that increasing the NAD^+/ADH ratio, corresponding to lower absolute ADH concentration, results in reduced acetaldehyde formation. This behaviour confirms that, even in the presence of sufficient cofactor, lowering enzyme availability limits the overall oxidation capacity.

Among interaction terms, only the interaction between NAD^+/ADH ratio and incubation temperature (AB) exceeds the adopted significance threshold. This interaction suggests that the impact of enzyme availability becomes more pronounced at higher temperatures, where catalytic activity is otherwise enhanced. Incubation time (factor C) and all remaining interaction terms are below the significance threshold and were therefore considered non-significant.

Table 3.8: Factorial Analysis on Effect of NAD^+/ADH ratio, incubation temperature, and incubation time.

	A	**B**	**C**	**Y**		
	NAD^+/ ADH	**T inc. [°C]**	**t inc [min]**	**Acetaldehyde [ppm]**	**Effect**	**Significance**
1	13,26	40	10	2,39		
a	**53**	**40**	**10**	**1,92**	**-1,92**	**96,52%**
b	**13,26**	**60**	**10**	**11,03**	**7,69**	**99,13%**
ab	**53**	**60**	**10**	**7,91**	**-1,43**	**95,33%**
c	13,26	40	40	2,57	0,535	87,66%
ac	53	40	40	2,06	-0,125	55,52%
bc	13,26	60	40	12,17	0,375	82,62%
abc	53	60	40	8,59	-0,105	50,00%

Figure 3.24 shows the main effects of the NAD^+/ADH ratio (A) and incubation temperature (B) on acetaldehyde formation. Incubation temperature exhibits a strong positive effect, confirming once again its dominant role in promoting acetaldehyde formation.

In contrast, the NAD^+/ADH ratio shows a negative main effect, indicating that increasing the ratio, corresponding to lower absolute ADH concentration, leads to reduced acetaldehyde formation. This trend reflects the limiting role of enzyme availability when the cofactor-to-enzyme ratio is increased.

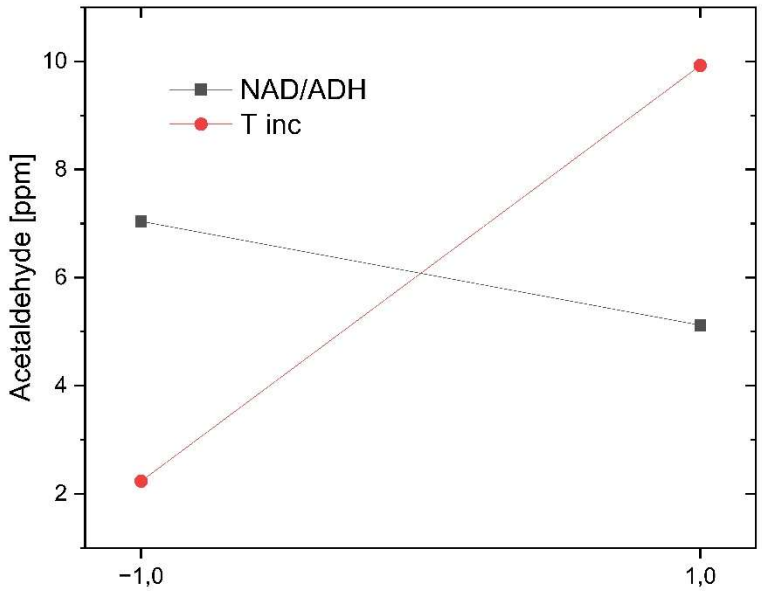

Figure 3.24: Main effects of NAD^+/ADH ratio (A) and incubation temperature (B).

Figure 3.25 shows the interaction plot between the NAD^+/ADH ratio (A) and incubation temperature (B). The non-parallel trends indicate a statistically significant interaction between the two factors, in agreement with the factorial analysis.

At high temperature (B = +1), increasing the NAD^+/ADH ratio, corresponding to a decrease in absolute ADH concentration, leads to a marked reduction in acetaldehyde formation. In contrast, at low temperature

(B = −1), acetaldehyde levels remain low and only weakly affected by changes in the NAD^+/ADH ratio.

This behaviour confirms that enzyme availability becomes a limiting factor primarily under thermally activated conditions, where higher temperatures would otherwise promote ethanol oxidation.

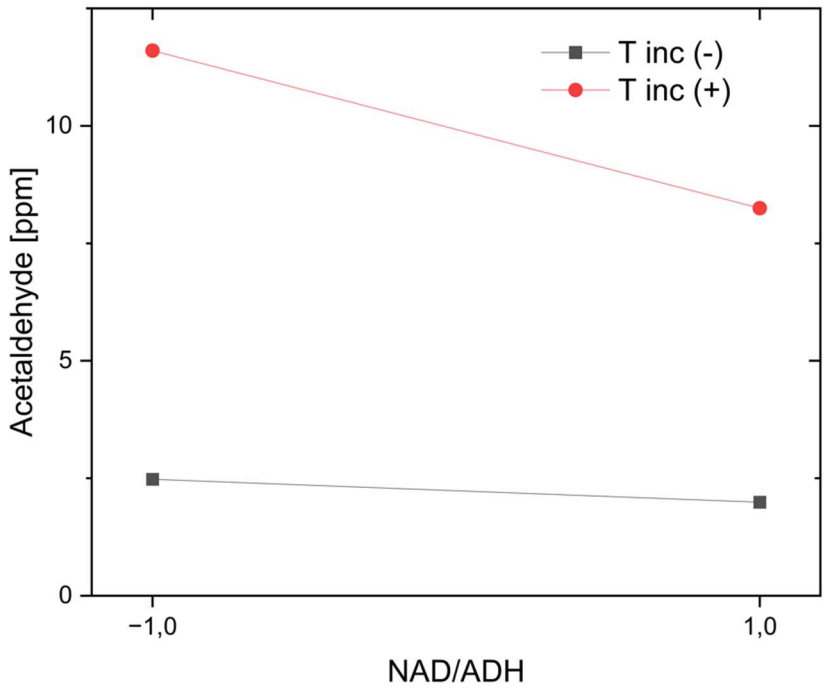

Figure 3.25: Interaction between NAD/ADH ratio (A) and incubation temperature (B).

Figure 3.26 shows the scatter plot comparing experimentally measured and calculated acetaldehyde concentrations for this factorial plan. The close alignment of the data points along the parity line indicates an excellent agreement between experimental results and model predictions.

The fitted model,

$$Y = 6.08 - 0.96A + 3.85B + -0.72AB \qquad \textit{(Equation 3.5)}$$

captures the dominant positive contribution of incubation temperature and the negative effect associated with increasing NAD^+/ADH ratio. The

presence of the AB interaction term is consistent with the significant coupling between enzyme availability and thermal activation identified in the factorial analysis.

The high coefficient of determination ($R^2 = 0.9979$) confirms that the model provides an accurate representation of the experimental response within the investigated domain, supporting its use for response surface visualization and engineering interpretation.

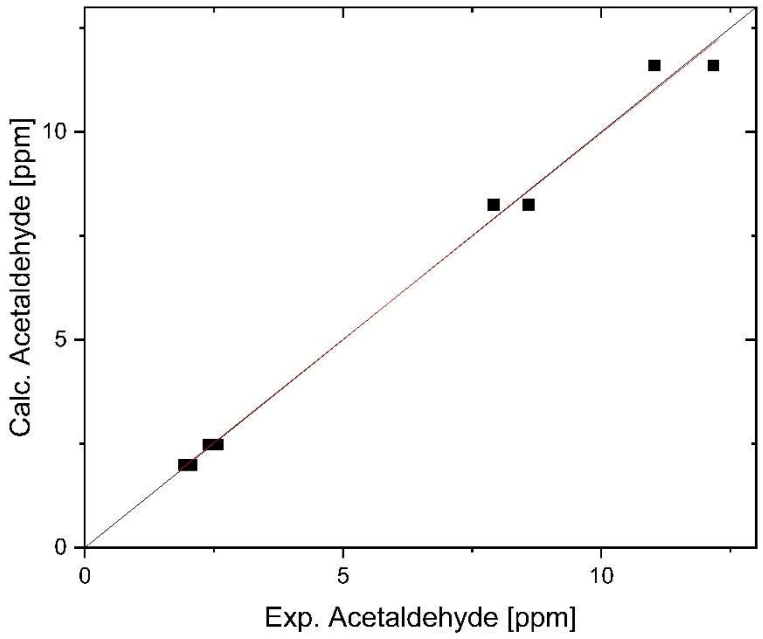

Figure 3.26: Scatter plot for Effect of NAD/ADH ratio, incubation temperature, and incubation time.

Figure 3.27 shows the response surface describing acetaldehyde formation as a function of the NAD^+/ADH ratio and incubation temperature at fixed ethanol concentration. The surface highlights a strong positive dependence on temperature, confirming thermal activation as the dominant driving force across the explored domain.

In contrast, increasing the NAD^+/ADH ratio leads to a systematic decrease in acetaldehyde concentration, reflecting the limiting effect of reduced enzyme availability when the ratio is increased. The combined visualization

confirms the presence of a coupled effect, in which the influence of enzyme availability becomes particularly relevant at higher temperatures.

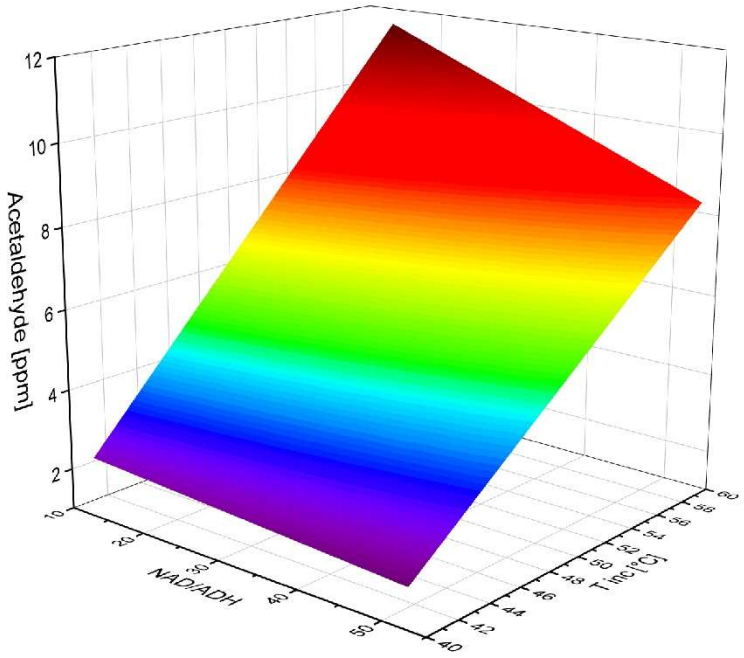

Figure 3.27: surface response for NAD+/ADH factor (A) and incubation temperature (B).

3.10 CONCLUSIONS AND IMPLICATIONS

The results presented in this chapter demonstrate that acetaldehyde formation during ethanol recovery is not an intrinsic or unavoidable consequence of distillation, but rather the outcome of specific chemical and biochemical conditions that activate precursor-driven pathways. In particular, the experimental evidence consistently indicates that ethanol oxidation mediated by the ADH/NAD^+ system represents a viable and process-relevant route for acetaldehyde generation under mild thermal conditions, provided that a suitable chemical environment is present.

Among all investigated variables, incubation temperature emerges as the dominant factor governing acetaldehyde formation across all factorial plans. Increasing temperature systematically enhances acetaldehyde production, while also amplifying the effects of enzymatic and cofactor-related variables. NAD^+ availability plays a secondary but significant role, acting as

a limiting factor when ADH concentration is fixed, whereas ADH concentration becomes limiting only under conditions of low enzyme availability or high NAD^+/ADH ratios. Incubation time generally exhibits a weaker influence, becoming relevant mainly at elevated temperatures through interaction effects.

The factorial analysis highlights that acetaldehyde formation is inherently multivariate. In regimes where ethanol concentration, NAD^+ availability, and temperature are simultaneously varied, significant two-factor interactions arise, confirming that contaminant formation cannot be interpreted through single-variable trends alone. Conversely, three-factor interactions were consistently negligible, indicating that the system behaviour within the explored domain can be adequately described using linear models with selected interaction terms.

From an operational perspective, these findings imply that acetaldehyde contamination can be mitigated by controlling the chemical environment rather than relying solely on thermal management. Minimizing exposure to high temperatures in the presence of active phosphate-buffered systems and enzymatic components, as well as avoiding conditions that favour high effective NAD^+ availability, appears critical. The results provide an engineering-oriented framework for identifying operating windows associated with increased acetaldehyde risk and form the basis for the process optimization strategies discussed in the following chapters.

Overall, this chapter establishes a mechanistic link between matrix composition, enzymatic activity, and operating conditions, offering a coherent interpretation of plant-scale observations and supporting targeted interventions to reduce contaminant formation during ethanol recovery.

While this chapter focused on the chemical quality of the recovered ethanol and on the mechanisms governing contaminant formation, the following chapter shifts the perspective from product quality to process performance. In particular, the distillation system is analysed from an energy, environmental, and economic standpoint, with the aim of evaluating the

overall sustainability of ethanol recovery from hydroalcoholic waste streams.

4. DEVELOPMENT, ANALYSIS, AND EVALUATION OF THE DISTILLATION PLANT

4.1 INTRODUCTION TO THE CASE STUDY

This chapter describes the optimization of the process of ethanol extraction from human plasma fractionation processes wastewater. This is a stream with considerable ethanol concentrations and a variable composition, and its treatment has two goals: first, to recover a solvent with high economic value, and second, to reduce the environmental and energy impact associated with current steam-powered distillation operations.

As part of the industrial collaboration that motivated this study, it was deemed necessary to define a reference case that was representative of the real industrial plant but, at the same time, did not violate information covered by industrial confidentiality. For this reason, the actual mixture was replaced with a model stream consisting of a 35% by volume water-ethanol solution. This choice allows the thermodynamic behavior and operational requirements of the industrial process to be faithfully reproduced, while maintaining the general structure of the plant layout unchanged. Replacing the actual mixture with this representative solution does not entail any significant changes in either the process configuration or the expected

energy performance, thus allowing results to be obtained that are fully transferable to the actual case.

The objective of this study is to evaluate different plant configurations to improve the energy efficiency of distillation, with particular attention to the integration of heat pump systems as an alternative to industrial steam. The analysis was developed through process simulations, energy and economic assessments, and a systematic comparison of multiple energy cost scenarios. The results presented in this chapter have also been collected and discussed in a scientific article currently under review.

4.2 Description of the Reference System

4.2.1 Methodology

The process simulations were performed using Aspen Plus® V11. Due to the highly non-ideal behaviour of the water-ethanol system and the refrigerant of the heat pump cycle, particular attention was given to the choice of thermodynamic models.

The liquid-vapor equilibrium of the water-ethanol mixture fed into the distillation plant was modeled using the UNIQUAC (UNIversal QUasi Chemical) model. The hydrogen bonds in the mix are responsible for its strong non-ideality. This is why the mixture has a low boiling azeotrope at 95.6% v/v at atmospheric pressure [136]. Unlike models such as Peng-Robinson or Soave-Redlich-Kwong, which are not well suited to this type of mixture, the UNIQUAC model provides accurate predictions of azeotropic behavior and activity coefficients [137].

The thermochemical properties of the refrigerant chosen for heat pumps (R-1234ze - Trans-1,3,3,3-Tetrafluoroprop-1-ene) were calculated using the REFPROP database (NIST Reference Fluid Thermodynamic and Transport Properties). This database uses equations of state based on the Helmholtz energy formulation. It is widely recognized for providing highly accurate

data on enthalpy, entropy, heat capacities, and transport properties of refrigerants and pure fluids [138].

The combination of these two thermodynamic models (UNIQUAC for distillation columns and REFPROP for heat pumps) guarantees reliable predictions of the system's separation performance and energy requirements.

Modeling assumptions

The main assumptions used in the model are:

- steady-state operating conditions.
- constant plate efficiency.
- isotropic compressor efficiency defined according to typical values in the literature.
- absence of chemical reactions in the water-ethanol mixture.

These assumptions are consistent with both industrial practice and the approach adopted in the reference work.

Preliminary validation

The model obtained was verified by comparing:

- the expected purities at the top and bottom.
- the temperatures at the top and bottom of the column.
- the thermal consumption (reboilers and condensers).

The results predicted by the simulation are consistent with typical industrial values and with the company's internal dataset, confirming the adequacy of the representative model.

4.2.2 Composition and Characteristics of the Streams

The feed stream to the distillation column in the base case consists of a 35% by volume water-ethanol solution, chosen as a representative mixture of industrial waste resulting from the fractionation of human plasma. This

solution adequately reproduces the thermodynamic behavior of the real mixture, characterized by a high ethanol content and an aqueous matrix containing residual organic compounds in low concentrations.

The decision to use a simplified mixture was motivated by the need to use a modeling system that was faithful to the real process while ensuring the protection of company information. The selected composition allows the typical operating conditions of the industrial plant to remain unchanged and, through simulation, to obtain a separation profile that is comparable to that observed in real operation.

From a thermodynamic point of view, the water-ethanol system is widely characterized in the literature and represents a non-ideal mixture. The presence of the azeotrope at approximately 95.6% ethanol by mass (97.2% by volume) is a relevant factor in the design of operations, as it limits the maximum purity that can be obtained by simple atmospheric distillation. However, the purity of ethanol that can be used for the manufacture of medicines in the European Union is dictated by the Pharmacopoeia [78]. According to the guidelines provided therein, the volume concentration of ethanol must be between 95.1% and 96.9% by volume for use in pharmaceuticals. Table 4.1 summarizes the characteristics of the input and the distillate stream.

Table 4.1: Characteristics of the Input Stream and Recovered Ethanol Stream.

Stream	**Value**
Feed [kg/h]	2000
EtOH [% v/v]	35
Temperature [°C]	20
Pressure [bar]	2
Recovered EtOH [kg/h]	608 – 625
EtOH [% v/v]	95.1 – 96.9

4.2.3 Process Configuration of the Case Study 1 – Base Case

The base case adopted in this study corresponds to the reference industrial configuration used by the partner company, suitably simplified for reasons of confidentiality but fully representative from a thermodynamic and operational point of view. The plant has a configuration with two distillation columns in series, designed to work with the conditions depicted in Table 4.1.

The configuration is illustrated in Figure 4.1 and consists of:

- Column C101, operating under vacuum conditions (0.18 bar),
- Column C102, operating at atmospheric pressure (1 bar),
- two reboilers (E-101 and E-103),
- two total condensers (E-102 and E-104),
- collection tanks and pumps for transferring intermediate streams.

This architecture allows the separation to be divided into two stages, with thermal and qualitative advantages. The first column reduces the boiling temperature and limits the formation of thermal contaminants in the reboiler; the second allows the required purity to be achieved.

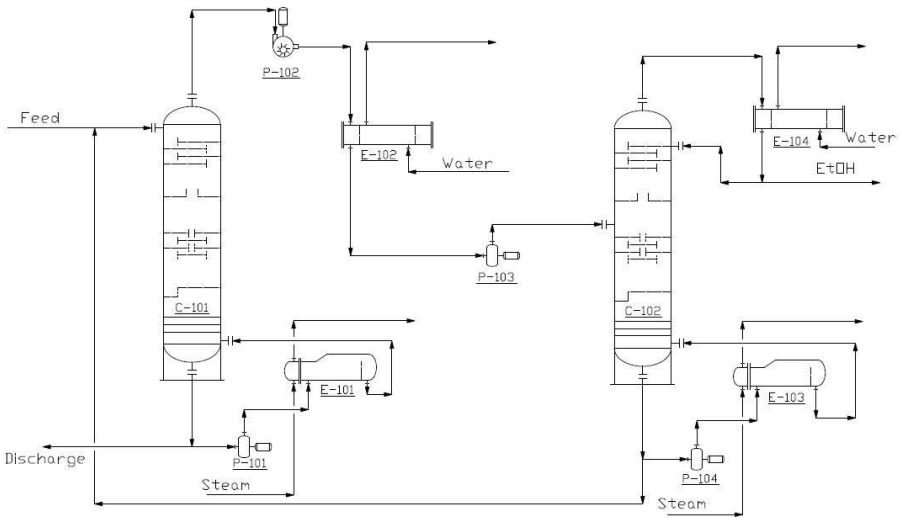

Figure 4.1: Case Study 1: Basic Plant layout.

Column C101 – Vacuum distillation

Column C101 constitutes the first stage of separation and is designed to operate at 0.18 bar, a condition that significantly reduces the temperature in reboiler E-101. This choice responds to the need to:

- limit the thermal degradation of the residual organic components present in the mixture.
- reduce the formation of volatile contaminants, in particular aldehydes, which tend to increase at high temperatures.
- decrease the thermal requirement compared to atmospheric distillation.

The column is equipped with:

- 9 theoretical stages,
- feed to the first tray,
- reflux operating in “once-through” conditions (reflux ratio = 0), as reported in the draft.

The E-101 reboiler requires a heat duty of 360 kW, while the E-102 condenser removes 342 kW, values derived from basic simulations.

Column C102 – Atmospheric distillation

The second column, C102, completes the separation process and produces a distillate with a purity between 95.1 and 96.9% v/v. It operates at atmospheric pressure (1 bar) and is the most energy-intensive part of the plant.

Its main characteristics are:

- 35 theoretical stages,
- feed to tray 24,
- reflux ratio of 2.8,
- E-103 reboiler with a duty of 588 kW,
- E-104 condenser with a duty of 549 kW.

This column dominates the consumption of the base case and is the main point of intervention for the energy integration strategies evaluated in the following scenarios.

The overall layout of the base case reflects solutions commonly adopted in industrial plants dedicated to solvent recovery, especially in the pharmaceutical sector, where contaminant management and final product quality play a critical role.

The two columns share:

- a common feed system.
- intermediate tanks for distillate and bottoms management.
- standard utility networks (steam for reboilers and process water for condensers).

From an energy perspective, the base case is characterized by:

- high steam consumption in reboilers,
- high demand for industrial water for condensers,
- classical heat recovery.

This configuration was used as a reference to evaluate, in the following chapters, the benefits introduced by Vapor Recompression (VR) systems, closed-cycle Heat Pumps (HP), and hybrid configurations (HP + VR), as presented in the draft.

4.2.4 Characteristic Dimensions of the Case Study 1 – Base Case

The preliminary sizing of the base case was obtained directly from the rigorous simulation conducted in Aspen Plus®, which made it possible to identify the fundamental operating parameters of the two distillation columns and the related heat exchangers. The dimensions, shown in Table 4.2 for the columns and Table 4.3 for the Reboilers and Condensers, represent the technical basis for the subsequent configurations analyzed (VR, HP, and HP+VR), as they uniquely determine the thermal conditions

and energy requirements on which the integration systems are based. The duty values, flow rates, theoretical stages, and operating pressures are those reported in the validated model and correspond to the conditions of the representative industrial case used in the study.

Table 4.2: Main features of the columns for the Case Study 1

Parameter	C101	C102
Operative Pressure	0.18 bar	1 bar
Theoretical Stages	9	35
Feed Stage	1	24
Reflux Ratio	0	2.8
Reboiler Duty	E-101: 360 kW	E-103: 588 kW
Condenser Duty (Total)	E-102: 342 kW	E-104: 549 kW
Estimated Diameter [m]	0.8	0.8
Estimated Height [m]	5.4	21

Table 4.3: Main features of the heat exchangers for the Case Study 1.

Equipment	Type	Duty [kW]	Pressure [bar]	Utility
E-101	Reboiler	360	0.18	Steam
E-102	Condenser	342	0.18	Well Water
E-103	Reboiler	588	1	Steam
E-104	Condenser	549	1	Well Water

4.3 Definitions of New Plant Configuration

Starting from the base case described in the previous section, three alternative configurations were developed with the aim of improving the energy efficiency of the distillation process. The configurations analyzed—Vapor Recompression (VR), Closed-Cycle Heat Pump (HP), and HP + VR Hybrid System—represent three thermal integration strategies that have

been extensively studied in the literature and are now the subject of growing interest in the pharmaceutical and chemical industries.

The different configurations were designed using the same operating parameters and dimensions as the base case, to isolate the effects due exclusively to the method of supplying and recovering thermal energy. The simulation model implemented in Aspen Plus® allows the alternatives to be compared under reproducible conditions, ensuring the consistency of the results obtained.

The main objectives of this phase of the study are:

- evaluate alternatives that reduce the plant's thermal and energy consumption.
- effectively manage the feed mixture to ensure the purity of the product obtained.
- maximize the plant's energy integration.

4.3.1 CASE STUDY 2 – VAPOR RECOMPRESSION (VR)

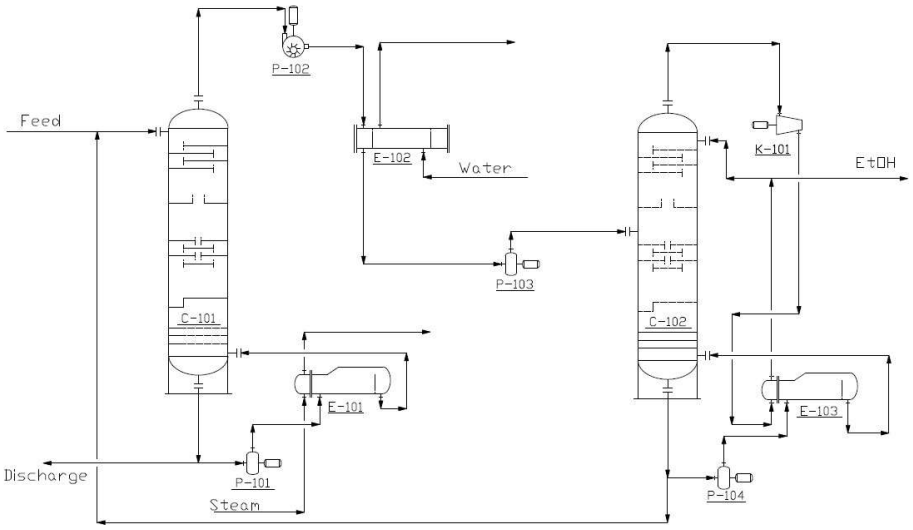

Figure 4.2: Case Study 2: Vapour Recompression Layout (VR)

The VR Case Study involves the application of vapor recompression to the C-102 column. This solution consists of recompressing the top vapors, which are brought to a higher pressure using a compressor (K-101) and then

used as a heat source to feed the E-103 reboiler of the C-102. The diagram is shown in Figure 4.2.

Technical and Thermodynamic Reasons

The decision to apply VR exclusively to C-102 stems from three main factors:

- High duty of the E-103 reboiler, which accounts for the most significant share of energy consumption in the base case.
- Head vapor temperature is already close to that required by the reboiler, making recompression particularly efficient.
- Complete reduction of industrial steam requirements for the atmospheric column (C-102).

Operation

The circuit is structured as follows:

- The top vapors from column C102, at approximately 1 bar, are extracted and sent to compressor K-101.
- Compression increases the temperature and pressure to values that enable heat transfer to the reboiler E-103.
- The recondensed vapor returns to the circuit as product and reflux stream.

Benefits

- Reduction in steam consumption of up to 53.6% compared to the base case.
- High overall Coefficient Of Performance (7.4), resulting from the favorable thermal conditions of the mixture.
- Reduced operating costs compared to heat pumps.

Limitations

- Requires a compressor sized for significant vapor flow rates.

- Requires suitable materials to handle any corrosive components or organic traces in the vapors.
- Possible distillate contamination problems in the event of damage to the bottom reboiler.

4.3.2 Case Study 3 – Closed-Cycle Heat Pump (HP)

In the second configuration, a closed-cycle heat pump (HP) is introduced, operating between the E-104 condenser of the C-102 column and the E-101 reboiler of the C-101 column. The diagram is shown in Figure 4.3.

The working fluid of the refrigeration cycle is R-1234ze, whose thermodynamic properties have been calculated using the NIST REFPROP database.

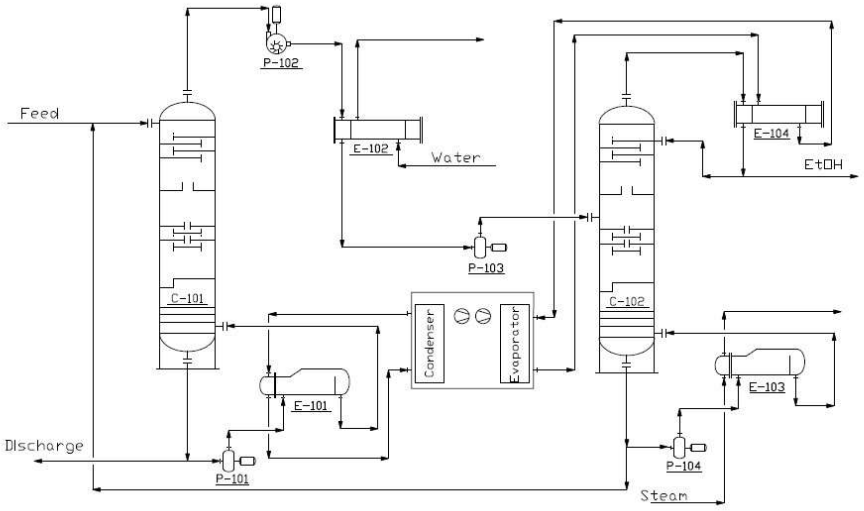

Figure 4.3: Case Study 3: Closed-circuit Heat Pump layout (HP).

Layout Architecture

The system consists of:

- an evaporator that absorbs heat from the E-104 condenser,
- a refrigerant compressor,
- a condenser that transfers heat to the E-101 reboiler,

- two intermediate heat exchange circuits to prevent direct contact between the refrigerant and the process stream.

Technical Reasons

- Minimize the risk of contamination of recovered ethanol by avoiding direct contact between the refrigerant and the water-ethanol mixture.
- Protect the internal heat exchangers of the heat pump from fouling caused by process residues.
- Recover part of the energy lost in the E-104 condenser.

Benefits

- Reduction in steam consumption for the vacuum column.
- Ability to operate without depending on variations in the vaporization load of C102.
- Greater operational flexibility than in the VR case.

Limitations

- Relatively low Coefficient Of Performance (COP=3.7), due to the high difference of temperature of the refrigeration cycle.
- High CAPEX due to the presence of a compressor, additional heat exchangers, and a refrigerant circuit.
- High sensitivity to the cost of electricity.

4.3.3 CASE STUDY 4 – HYBRID CONFIGURATION (HP + VR)

This configuration combines the advantages of the two previous strategies. As shown in Figure 4.4 of the draft, the layout includes:

- a heat pump that transfers heat from the condenser of C101 (E-102) to its reboiler (E-101),
- a compressor (K-101)that recompresses the top vapors of C102 and supplies heat to the reboiler of the same column (E-103).

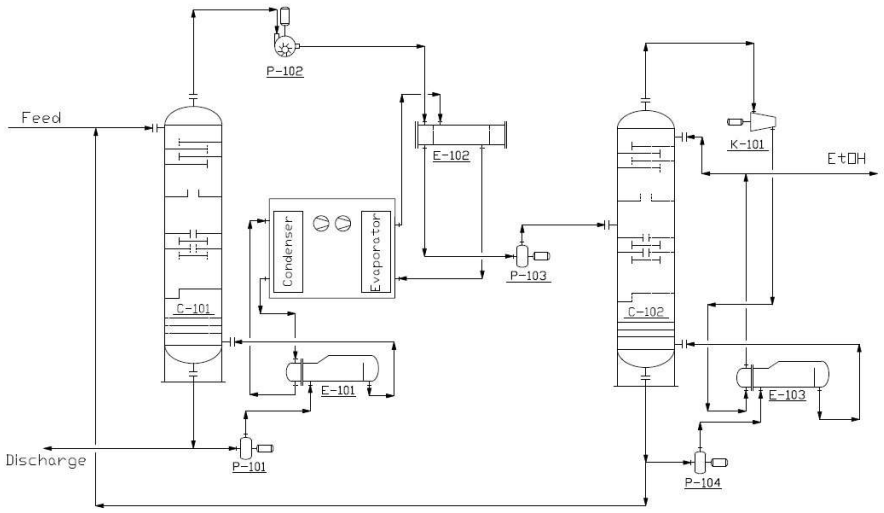

Figure 4.4: Case Study 4: Vapor Recompression and Heat Pump layout (VR + HP).

The objective of this configuration is to optimize the entire system by balancing:

- energy recovered via VR on the most energy-intensive column (C-102),
- energy recycled via HP on the column operating in vacuum (C-101).

Operating Characteristics

- Maximization of the plant's thermal self-consumption.
- Overall intermediate COP (6.0) thanks to the combination of the two technologies.
- Reduction in the use of industrial steam on both columns.

Benefits

- The highest energy savings among all configurations (≈ 83%).
- Best balance between initial investment and long-term benefits.
- Greater robustness in scenarios with high steam costs.

Limitations

- Greater plant complexity.
- Higher capital costs compared to individual configurations.

- Significant dependence on the cost of electricity, although lower than in the HP case.

4.3.4 General Considerations

All configurations were designed while keeping the following unchanged:

- column operating parameters,
- flow rates and composition of the Feed,
- flow rate and composition of the recovered Ethanol,
- main heat exchange dimensions of the base case.

This ensures that the differences observed in terms of energy and economic performance are attributable exclusively to the different energy integration methods.

4.4 Energetic Analysis

The energy analysis aims to quantify the effects of the thermal integration strategies introduced in the three alternative configurations (VR, HP, and HP+VR) compared to the base case. All assessments were conducted using data obtained from simulations in Aspen Plus®, ensuring full consistency between the operating conditions of the different configurations.

Particular attention is paid to:

- the thermal requirements of the reboilers,
- the heat removed in the condensers,
- the electrical energy required by the compressors,
- the COP of configurations using heat pumps or vapor recompression systems.

The COP was calculated according to (Equation 4.1).

$$COP = \frac{Energy\ supplied\ by\ the\ machine}{Energy\ to\ operate\ it} \qquad \textit{(Equation 4.1)}$$

An important parameter often used to characterize heat pumps is Lift, defined as the temperature difference between the hot and the cold sink.

The results allow for a direct comparison of the energy efficiency of the four alternatives and identify the benefits associated with each integration strategy.

4.4.1 Energy Analysis of Case Study 1

The traditional configuration involves the use of industrial steam to feed the E-101 and E-103 reboilers, and process water to remove heat in the E-102 and E-104 condensers. The duty values obtained from the simulation are:

- E-101 (C-101 reboiler): 360 kW
- E-103 (C-102 reboiler): 588 kW
- E-102 (C-101 condenser): 342 kW
- E-104 (C-102 condenser): 549 kW

The total thermal energy demand for the reboilers is 948 kW, which is the reference for evaluating the performance of the integrated configurations.

4.4.2 Energy Analysis of Case Study 2

The application of vapor recompression to the C102 atmospheric column allows the heat contained in the top vapors to be reused, drastically reducing the need for fresh steam. In the VR case, the K-101 compressor increases the temperature of the vapors to make it possible to supply heat to the E-103 reboiler.

Main results

- 53.6% reduction in external energy consumption compared to the base case.
- Overall COP of 7.4, a high value due to the very favorable nature of the integration: the required temperature jump is relatively low, and the recompressed vapors maintain high energy quality.
- Significant decrease in the amount of industrial steam required by column C102.

This configuration represents the most energy-efficient solution in relation to the cost of the investment, as also confirmed by the economic analysis.

4.4.3 Energy Analysis of Case Study 3

The closed-cycle heat pump transfers heat from the E-104 condenser to the E-101 reboiler via an electrically powered refrigeration cycle. The two intermediate exchangers introduced into the circuit prevent direct contact between the refrigerant and process fluids, ensuring safety and limiting fouling.

Main results

- Energy savings of 27.5% compared to the base case.
- Heat pump COP of 3.7, lower than the VR case due to the irreversibilities typical of the vapor compression cycle, the additional thermal resistances introduced by the exchangers, and the high temperature lift of the heat pump.
- Partial elimination of steam consumption for column C101.

The HP configuration allows for significant energy recovery, but has limitations related to the thermodynamic efficiency of the cycle and the high electricity demand.

4.4.4 Energy Analysis of Case Study 4

The hybrid configuration combines the two previous cases of thermal integration, using VR for column C102 and HP for column C101. This allows simultaneous heat recovery in both sections of the plant.

Main results

- Overall energy savings of approximately 83% compared to the base case, the highest value among all configurations.
- Overall COP of 6.0, the result of the synergistic interaction between the two systems.
- Substantial reduction in industrial steam requirements, to the point of almost complete elimination.

This configuration represents the most energy-efficient solution; however, as highlighted in the draft, it requires greater investment and is more complex to manage.

4.4.5 Energy Comparison

The energy requirements of the various plant configurations are summarized in Figure 5. The Base Case (reported as Base in the following) with two traditional distillation columns has the highest energy demand, with a total reboiler duty of 948.3 kWh. Implementing a Vapor Recompression (VR) system on the second column yields significant energy savings, reducing the energy required from outside by 53.6% compared to the basic configuration.

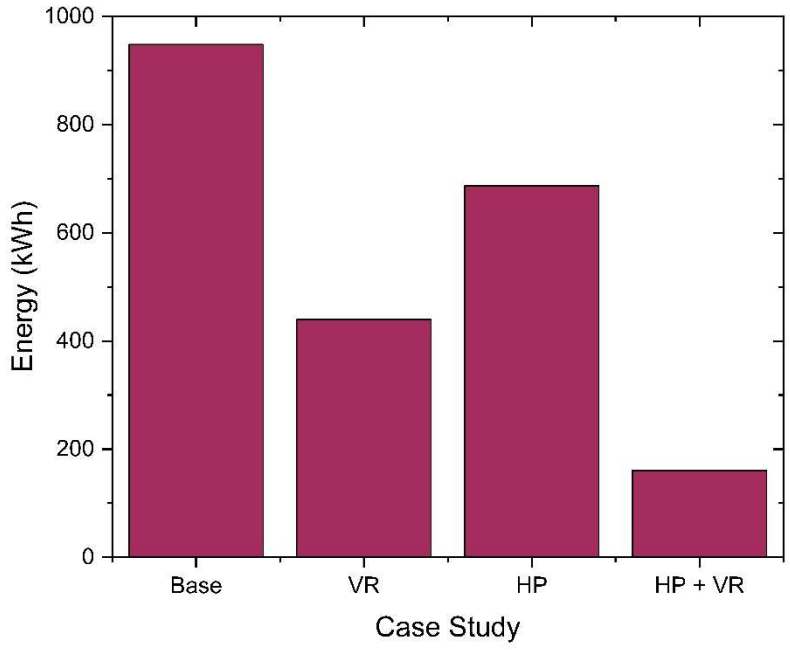

Figure 4.5: Energy requirements of the various Case Studies.

Energy consumption is lower than in the base case, even with the adoption of a closed-loop heat pump (HP) system, but performance is not the same as in the previous case (VR), and energy savings of 27.5% are achieved. This is mainly due to the lower COP of the refrigerant cycle. The combined vapor recompression and closed-loop heat pump (HP + VR) layout achieves

the best performance, resulting in approximately 83% energy savings compared to the base case.

These results confirm that integrating heat pumps into this industrial application can substantially increase the energy efficiency of a conventional distillation plant. The HP + VR combination layout offers the highest potential for improvement in the distillation plant.

To better understand and evaluate the differences in terms of energy demand, the COP was assessed for each configuration. The values obtained are shown in Table 4.4.

Table 4.4: Overall Coefficient of Performance of the various Case Studies.

Case Study	COP
VR	7.4
HP	3.7
HP + VR	6.0

The COP is a widely used indicator for evaluating the efficiency of heat pump systems. A high COP indicates a highly efficient system, providing more heat per unit of energy supplied. This makes it a crucial parameter for evaluating and optimizing energy recovery processes [139].

As shown in Table 4.4, the VR case achieves the highest COP value. This is due to the reuse of heat from superheated ethanol vapors. These maximize the ratio between the heat supplied and the energy required for recompression. The HP + VR case achieves a slightly lower overall COP than VR alone. This is due to the combination of vapor recompression with the closed-loop heat pump. Therefore, some flexibility is gained at the expense of efficiency. The HP case achieves the lowest COP due to the inherent irreversibility of the refrigerant thermodynamic cycle and the additional thermal resistances in the heat exchanges.

These differences in COP values explain the variation observed in energy savings between the different configurations. Systems with a higher COP

guarantee a greater net reduction in total energy requirements for the same compression work.

In conclusion, the energetic analysis shows that:

- VR guarantees the best balance between energy savings and thermodynamic efficiency.
- HP+VR maximizes absolute energy savings, representing the "best performance" solution.
- HP is the least energy-efficient strategy but offers operational flexibility benefits.

4.4.6 General Considerations

The energy analysis shows that the electrification of distillation operations using VR and HP can lead to significant reductions in thermal energy consumption and emissions associated with steam generation. However, performance is highly dependent on:

- the thermal conditions of the process,
- the temperature Lift required,
- the characteristics of the overhead vapors,
- the cost of electricity.

These elements, discussed in section 4.5, have a decisive influence on the economic viability of the solutions analyzed.

4.5 Economic Analysis

The economic analysis aims to assess the financial feasibility of the three integrated configurations (VR, HP, and HP+VR) in comparison with the base case, considering both the necessary investments (CAPEX) and the associated operating costs (OPEX). The approach adopted follows the logic of retrofitting: that is, only the economic impact of introducing thermal integration technologies is assessed, without including the costs of equipment already present in the original layout.

The economic factors considered include:

- Investment costs (CAPEX): compressors, additional heat exchangers, refrigerant circuits, auxiliary pumps.
- Operating costs (OPEX): electricity for compressors, residual steam, process water, and maintenance.
- Payback Period (PP): time required to recover the investment through operating savings.
- Total Annual Cost (TAC): sum of annualized investment and operating costs.
- Total Cost Distribution (TCD): percentage distribution of total costs according to energy scenarios.

The analysis was conducted assuming a plant operating 8,000 hours/year and considering a series of realistic scenarios for energy prices in the European Union.

4.5.1 Economic Assumptions

Energy costs

Based on Eurostat data [140], three scenarios were defined for the cost of electricity:

- Low Electricity costs (LE): 0.12 €/kWh
- Average Electricity costs (AE): 0.21 €/kWh
- High Electricity costs (HE): 0.39 €/kWh

Similarly, the following were considered for the cost of steam:

- Low Steam costs (LS): €35/ton
- Average Steam costs (AS): €45/ton
- High Steam costs (HS): €55/ton

These values cover the typical variability of the European market and allow the economic sensitivity of the configurations to be assessed in relation to energy price fluctuations.

Maintenance costs and CAPEX

The CAPEX estimate was made based on data found in the literature. Since this is a pharmaceutical process, AISI 316 was chosen as the material for all the equipment considered.

Maintenance is estimated at 15% of the additional CAPEX, in line with common practice in chemical-industrial retrofit analyses.

The CAPEX includes only:

- compressors (VR, HP, and HP+VR),
- energy recovery exchangers,
- heat pump intermediate exchangers,
- auxiliary refrigerant system.

Columns C101 and C102 are not counted because they are identical in all configurations.

TAC calculation

TAC is calculated by annualizing CAPEX over a useful life of 20 years, with an interest rate of 8%. This indicator is calculated according to Equation 4.2:

$$TAC = OPEX + \frac{CAPEX\ i(1+i)^n}{(1+i)^n - 1} \qquad \textit{(Equation 4.2)}$$

where i is the interest rate and n is the useful life span of the plant.

4.5.2 Results of the Economic Assessment

Comparison between CAPEX and OPEX

Figure 4.6 shows the CAPEX and OPEX for the four configurations. OPEX was calculated based on average energy and steam costs.

The results show that:

- The base case has the lowest CAPEX (no investment) but the highest OPEX.
- The VR configuration has moderate CAPEX and a significant reduction in operating costs.
- The HP configuration has the highest CAPEX, while the reduction in OPEX is not sufficient to offset the investment.
- The HP+VR hybrid case has high CAPEX but very low OPEX, making it competitive in the long term.

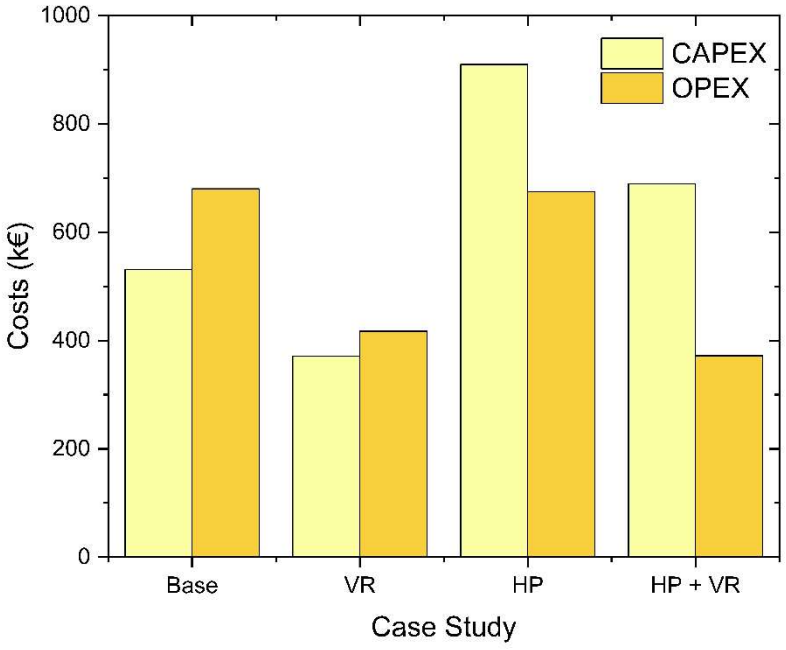

Figure 4.6: CAPEX and OPEX for the different Case Studies.

These trends are in line with energy analysis and reflect the different impact of electricity and steam consumption.

4.5.3 Payback Period Analysis

Table 4.5 shows the PP values in all nine combined scenarios (LE/AE/HE × LS/AS/HS). The main results are:

- VR is the most cost-effective configuration:
  - PP is always positive and between 1 and 2 years in most scenarios.

- PP > 2 years in the case of expensive electricity and cheap or average steam.

Table 4.5: Payback Period for the different layouts.

PP (Years)	LE		AE		HE	
	VR	1.57	VR	2.06	VR	5.67
LS	HP	35.48	HP	-19.94	HP	-4.83
	HP + VR	2.38	HP + VR	3.95	HP + VR	-12.32
	VR	1.16	VR	1.41	VR	2.51
AS	HP	11.92	HP	179.39	HP	-6.62
	HP + VR	1.63	HP + VR	2.24	HP + VR	8.90
	VR	1.92	VR	1.08	VR	1.61
HS	HP	7.16	HP	16.31	HP	-10.48
	HP + VR	1.24	HP + VR	1.56	HP + VR	3.27

- HP+VR performs well under favorable conditions:
  - PP between 1.2 and 3 years in cases with cheap electricity.
  - PP deteriorates significantly as the cost of electricity increases.
- HP is economically unfavorable:
  - Very high or even negative PP.
  - The investment is not recoverable in the AE and HE scenarios due to high electricity costs.

4.5.4 Total Annual Cost and Cumulative Cash Flow

The Cumulative Cash Flow Diagram, calculated as the sum of CAPEX and OPEX at AE and AS conditions, is shown in Figure 4.7.

The results of this indicator show that:

- The HP case has the highest Cumulative Cash Flow, due to the high costs of investment and operational costs.

- The VR and HP + VR cases have the lowest Cumulative Cash Flow, which is in line with the high COPs and reduced energy consumption of the reboilers.
- The VR case has become more cost-effective than the base case in less than a year.
- The HP + VR case has become more cost-effective within the first two years. This case becomes more cost-effective than the VR case after seven years.

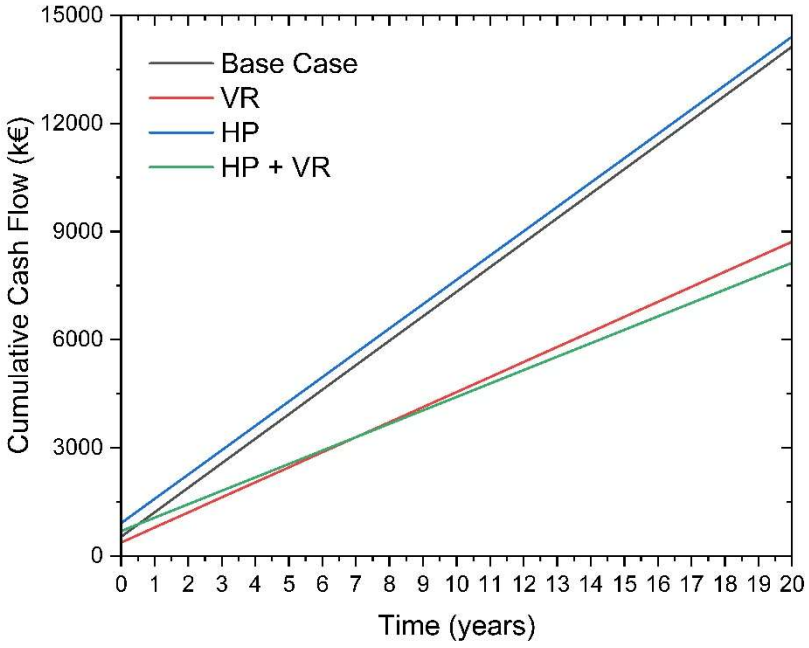

Figure 4.7: Cumulative Cash Flow Diagram.

The graph in Figure 4.8 shows the TAC of the four plant layouts calculated at AE and AS.

The results show that:

- VR case is the most economically advantageous, followed by the combined HP + VR case. Both configurations show a significant reduction in annual costs compared to the base case. This indicates a substantial improvement in economic efficiency.

- The HP case has the highest TAC due to higher investment costs that are not offset by savings in operating costs.

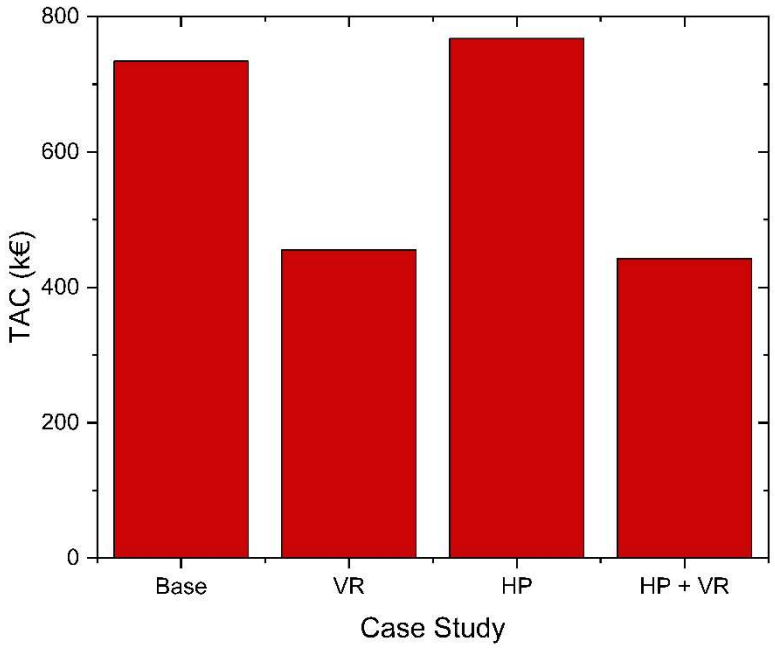

Figure 4.8: Total Annual Costs for the different Case Studies.

Overall, the graph highlights the trade-off between investment costs and operating costs. Vapor recompression involves moderate investment but guarantees significant energy savings, while the exclusive use of heat pumps does not. However, reducing steam consumption is less competitive from an overall economic point of view.

Figure 4.9 shows the cumulative TAC trend for the four Case Studies considered over time. The cumulative TAC represents the sum of the annual costs (annualized CAPEX + OPEX) incurred year by year, considering the conditions already mentioned for calculating the TAC.

The results calculated 20 years after the investment show that:

- The HP case reaches a cumulative TAC of just over €15 million.
- The Base alternative, which has a value of around €14.5 million, is mainly due to the high initial investment.

- The VR and HP + VR configurations show the lowest cumulative costs (around €9 million and €8.8 million after 20 years, respectively), confirming their economic advantage already highlighted by the analysis of annual TACs.

This temporal comparison allows us to visualize the cumulative effect of long-term economic savings. Alternatives with lower OPEX (particularly those based on vapor recompression) generate a growing gap compared to the base case, highlighting greater economic sustainability over time. Furthermore, the cumulative view enables evaluation of the balance between investment costs and operational savings over the lifespan, demonstrating how solutions with initially higher CAPEX can be more beneficial in the medium to long term.

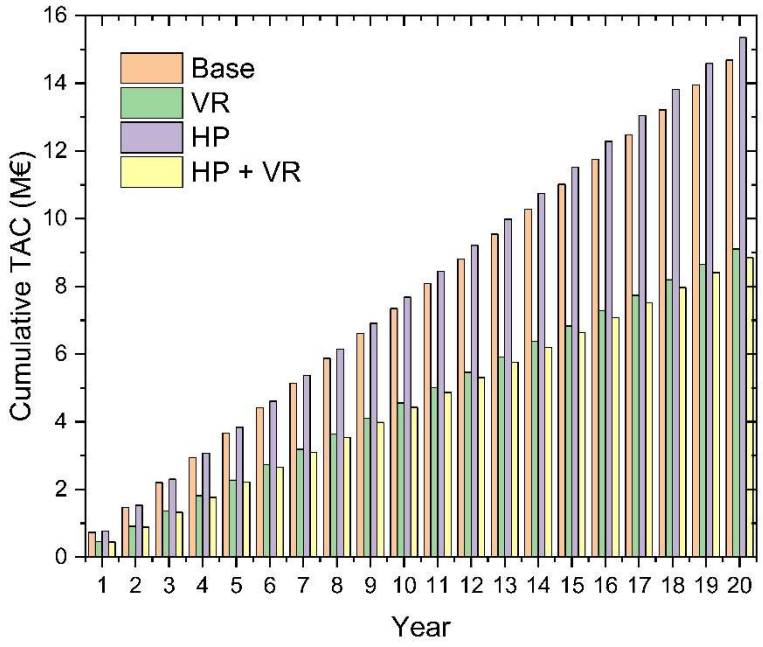

Figure 4.9: Cumulative Total Annual Costs for the different Case Studies.

4.5.5 Total Cost Distribution

Figure 4.10 illustrates the percentage breakdown of the costs for various plant configurations, plotted for each combination of electricity and steam costs.

When electricity costs are low, the total costs of electrified configurations are significantly reduced, making the integration of heat pumps economically attractive. When steam is also cheap (a), VR remains the most advantageous option thanks to lower initial investment and low operating costs.

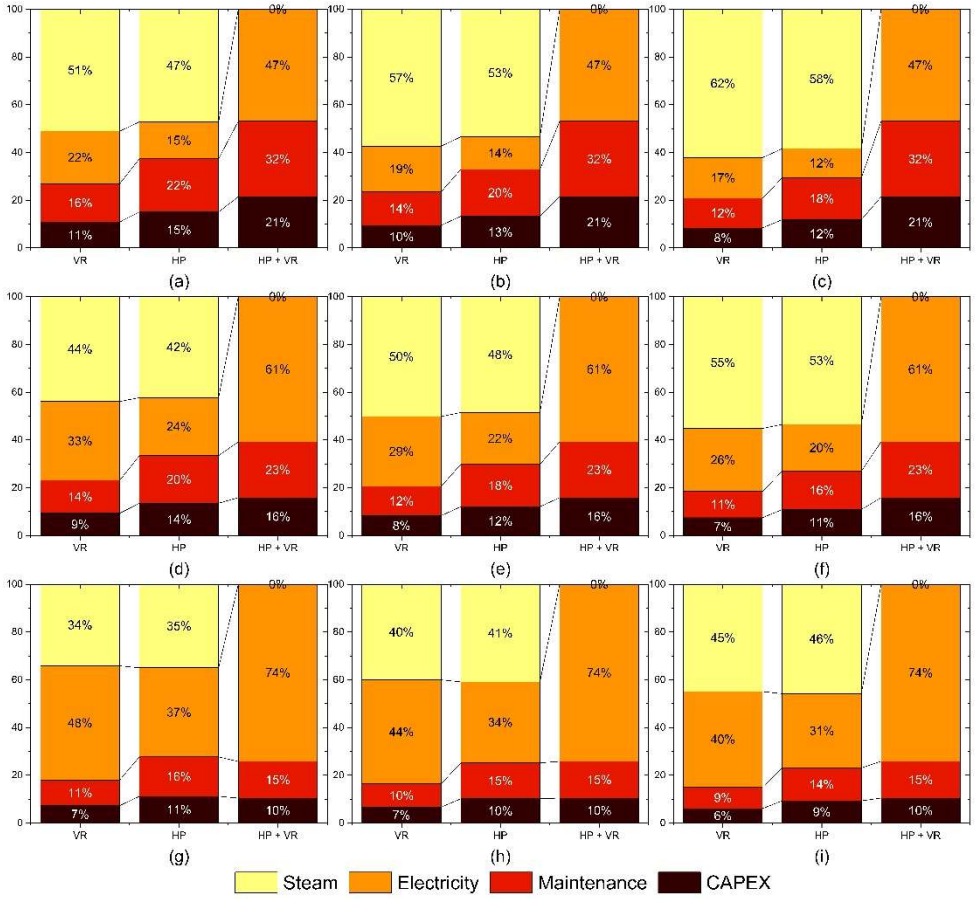

Figure 4.10: Total Cost Distribution for the three configurations in every energy cost scenario. (a): LE and LS; (b): LE and AS; (c): LE and HS; (d): AE and LS; (e): AE and AS; (f): AE and HS; (g): HE and LS; (h): HE and AS; (i): HE and HS.

As the cost of steam increases (b and c), the economic effect of reducing steam consumption becomes predominant: the relative advantage of electrified configurations grows, with a decrease in TAC and Payback Period, which fall to around 1.5 years for HP + VR and remain around one year for VR. In this scenario, the combined use of heat pumps and recompression is the most balanced solution in terms of investment, energy savings, and operational flexibility.

When the cost of electricity is average, the weight of the electrical component in operating costs becomes more significant, altering the economic balance between the different configurations. In the case of low-cost steam (d), the use of electrically powered systems is no longer advantageous: HP shows a marked increase in OPEX, and the payback period becomes negative due to the high OPEX, while HP + VR remains only marginally competitive. VR, on the other hand, strikes a good balance between CAPEX and OPEX, continuing to offer the lowest total cost. With medium or high-cost steam (e and f), the cost-effectiveness of VR is confirmed, with PPs of around one year, while HP + VR improves its position thanks to steam savings, achieving payback periods of around 2-3 years. However, HP remains penalized by the cost of electricity, making it unsustainable. Overall, in this scenario, VR represents the most robust choice from an economic perspective, while HP + VR can be considered a valid solution only when steam is particularly expensive.

When electricity costs are high, the impact of the electrical component on total costs becomes predominant and strongly penalizes all electrically powered configurations. When steam is cheap (g), VR remains the only economically sustainable option, with total costs and payback period around 6 years. HP, on the other hand, shows a sharp increase in OPEX, which far exceeds the benefits of lower steam consumption, making it uneconomical. As the cost of steam increases (h and i), HP + VR only partially compensates for the increase in electricity costs: total costs remain higher than VR, and PPs are over 3 years. HP becomes completely uneconomical in every scenario, with unrecoverable PP values.

Overall, with expensive electricity, steam recompression (VR) remains the most efficient and stable solution from an economic perspective, while configurations that include heat pumps lose competitiveness due to their high dependence on electricity.

4.5.6 General Considerations

The economic analysis shows that:

- The VR Case Study is the solution with the best cost/benefit ratio and the greatest robustness with respect to energy price variability.
- The HP+VR Case Study is an attractive option for a long-term view, especially in scenarios with high steam costs.
- Heat Pump alone is not economically competitive in the industrial case studied, unless conditions are extremely favorable (very cheap electricity and very expensive steam).

These results allow retrofit strategies to be chosen based on the energy context and plant priorities.

4.6 Conclusions

This chapter presents the results of process simulations and economic analyses for various retrofits designed to integrate energy in an industrial distillation plant. The plant is used to recover ethanol from pharmaceutical industry waste and for internal reuse of the distilled product, thus complying with the sector's stringent requirements. The analysis covered four different configurations: a Base Case, a case with vapor recompression (VR), a case with a closed-loop heat pump (HP), and a hybrid case combining the two previous technologies (HP + VR). The aim is to determine which of the proposed solutions is feasible in terms of energy consumption, operating costs, and environmental impact.

The simulation results confirm the significant potential for increasing the energy efficiency of the plant in question through VR. This case achieves a 53.6% reduction in energy demand compared to the base layout, corresponding to the shortest payback period (1.08 years in best-case conditions) and the lowest total annual costs. The HP + VR hybrid configuration has demonstrated impressive performance, achieving 83% energy savings compared to the basic configuration. This translates into a medium- to long-term economic advantage, thanks to reduced cumulative

costs over the plant's lifetime. Despite the high investment costs, this configuration offers high flexibility and greater long-term sustainability.

The economic study reveals that the stand-alone heat pump (HP) arrangement is highly susceptible to fluctuations in energy prices and is not economically viable under most scenarios. Even in the best-case scenario — low electricity and high steam costs (LE-HS) — the payback period remains somewhat lengthy (7.16 years), indicating minimal profitability. For average or high electricity prices, the payback period is exceptionally long or even negative, indicating that operational expenses outweigh potential energy savings. This trend shows the system's reliance on electricity consumption, which, combined with the high investment costs, turns the investment unprofitable. As a result, the HP design cannot be regarded as a viable retrofit solution in the present industrial case. Its implementation would only be justified in plants with access to low-cost renewable electricity or in systems where steam generation costs are exceptionally high.

Overall, the comparative study demonstrates that steam recompression, either as a solo retrofit or in conjunction with a closed-loop heat pump, is the most viable method for improving energy and economic performance of this plant. These technologies improve energy efficiency, reduce CO_2 emissions, and lower operational costs, aligning with industrial sustainability goals and energy transition policies.

In a broader sense, this study demonstrates how rigorous process simulation and technical-economic evaluation can effectively inform industrial decision-making in solvent recovery and energy integration projects. Future studies should concentrate on the experimental validation of the proposed alterations under real-world operating settings, including start-up and transient regimes, and the optimization of control techniques to ensure operational stability. Furthermore, the results should be evaluated using a Life Cycle Assessment analysis to determine the process's true environmental sustainability and obtain a more comprehensive picture.

Operational Considerations on Industrial Implementation

Although energy and economic analyses clearly show the advantages of integrated configurations, the adoption of VR, HP, and HP+VR systems in an industrial context requires some operational considerations. First, the introduction of compressors and refrigeration circuits involves changes to the plant layout, especially in terms of available space, interconnections with utilities, and integration into the existing control system. These interventions are part of normal industrial retrofitting practice but must be planned taking into account the operational continuity of the plant.

From a process management perspective, the addition of recompression systems and heat pumps requires accurate control of pressure and temperature conditions, as variations in thermal load can affect column stability. In addition, the additional exchangers introduced in HP and HP+VR configurations must be managed to minimize fouling, while compressors require predictive maintenance programs based on operating hours.

Finally, the impact on product quality must be carefully evaluated, especially in applications such as the recovery of ethanol for regulated uses. The integrated configurations do not alter the column structure or mass balances, but they do affect thermal profiles, which can influence the behavior of volatile impurities. More moderate temperatures, such as those typical of the HP configuration, could help reduce the formation of certain thermal contaminants. Although this hypothesis requires experimental verification, it represents a possible additional benefit of process electrification.

5. WASTEWATER TREATMENT AND WATER REUSE

5.1 INTRODUCTION

The pharmaceutical industry plays an indispensable role in global health and well-being by providing essential medications for the treatment and prevention of diseases. However, the manufacturing processes in this industry generate wastewater containing a variety of pollutants, including residual pharmaceuticals, solvents, heavy metals, and organic compounds. These pollutants can have significant impacts on the environment and human health if not properly treated. Treating pharmaceutical wastewater presents unique challenges due to the complexity and variability of the pollutants present. Conventional wastewater treatment methods are often inadequate for removing these pollutants, necessitating the development and optimization of advanced treatment technologies.

Water scarcity is an increasingly urgent global problem, accentuated by the growth of the world population and climate change [141]. The need for innovative strategies for water resource management has become essential to ensure a sustainable water supply for agriculture and other sectors [142]. Historically, water reuse has been practiced since ancient civilizations, with examples of the use of urban wastewater in agriculture dating back thousands of years [143]. Over time, water reuse practices have evolved

from simple irrigation systems to complex wastewater treatment plants. Today, water reuse is a widespread practice with applications ranging from agricultural irrigation to industrial use, environmental restoration, and even potable reuse. However, water reuse in agriculture requires adequate treatment to ensure food safety and environmental protection [144].

In this context, simulation is crucial in the design, evaluation, and optimization of pharmaceutical wastewater treatment plants. By employing mathematical and computer models, engineers can simulate the behavior of different treatment processes, assess their effectiveness, and identify optimal conditions for maximum pollutant removal. Simulation also allows for the exploration of various design and operational scenarios, helping to minimize costs and the environmental impact of wastewater treatment.

Pharmaceutical companies such as Takeda prioritize comprehensive wastewater management to address the variety of pollutants originating from their manufacturing processes. These include nitrogen compounds like ammonia, nitrogen, and nitrates, which can exert oxygen demand in water bodies if not properly treated, potentially violating environmental standards. Additionally, pollutants such as Chemical Oxygen Demand (COD), Biochemical Oxygen Demand (BOD), Total Organic Carbon (TOC), and Total Suspended Solids (TSS) are critical concerns due to their impacts on oxygen availability, eutrophication potential, and water clarity. By employing advanced physical, chemical, and biological treatment processes, pharmaceutical firms strive to mitigate these pollutants, minimize environmental impact, and demonstrate their commitment to sustainable wastewater management practices and environmental stewardship.

Among the emerging technologies for treating wastewater for reuse, hydrodynamic cavitation (HC) and advanced oxidation processes (AOPs) have attracted considerable attention. Hydrodynamic cavitation exploits the formation and collapse of microbubbles in a liquid to generate extreme temperature and pressure conditions, capable of degrading organic pollutants and inactivating microorganisms. AOPs, in turn, are based on the production of highly reactive free radicals, such as the hydroxyl radical

(•OH), to oxidize and mineralize pollutants. The effectiveness of hydrodynamic cavitation depends on several operational parameters, including pressure, temperature, residence time, and reactor geometry. Furthermore, it has been shown that HC can act synergistically with other treatment processes, such as ozonation and UV radiation, improving the overall efficiency of the process. Despite the promising results obtained in the laboratory, the large-scale application of hydrodynamic cavitation in wastewater treatment requires further studies to optimize operating parameters and reduce energy costs [145].

The primary objective of this study is to provide a thorough understanding of the challenges and opportunities related to pharmaceutical wastewater treatment and to demonstrate the crucial role of simulation in the design and operation of efficient and sustainable treatment systems. The simulated plant employs a combination of advanced treatment technologies to effectively remove pollutants from pharmaceutical wastewater. These technologies include:

- Advanced Oxidation: Processes such as the Fenton reaction, which uses hydrogen peroxide and iron to generate highly reactive hydroxyl radicals capable of oxidizing refractory organic pollutants.
- Membrane Filtration: Operations such as ultrafiltration and reverse osmosis, used to remove suspended solids, colloidal matter, and dissolved pollutants through semi-permeable membranes.
- Biological Treatment: Processes such as activated sludge and membrane bioreactors (MBR), which rely on microorganisms to degrade biodegradable organic matter into carbon dioxide, water, and biomass.

This chapter presents the results of a simulation of a wastewater treatment plant (WWTP) designed for water reuse in agriculture, starting from a real industrial effluent. The simulation was conducted using the commercial software SuperPro Designer and aims to evaluate the plant's performance under different operating conditions and to identify strategies to optimize

process efficiency. The simulated plant integrates a hydrodynamic cavitation and AOP system for tertiary treatment of wastewater to remove organic contaminants and inactivate pathogens, ensuring compliance with quality requirements for agricultural reuse.

Part of the results discussed in this study derive from work already published in Cecchini et al. (2025) [146], where the proposed treatment configuration was validated through a dedicated simulation and analysis of water quality and reuse potential.

5.2 Plant Description

5.2.1 Real Plant Configuration

The wastewater treatment plant (WWTP) currently operating at the industrial site is designed to treat pharmaceutical effluents characterized by high variability and significant organic and nitrogen loads.

Before detailing the process configuration, the main characteristics of the influent wastewater are summarized in Table 5.1, as they represent the key design parameters guiding both the operation of the real plant and the development of the simulation model.

Table 5.1: Properties of the effluent to be treated.

Parameter	value
Flow rate $\left(\frac{m^3}{h}\right)$	100
Chemical Oxygen Demand (COD) $\left(\frac{mg\ O}{l}\right)$	2500
Biochemical Oxygen Demand (BOD_5) $\left(\frac{mg\ O}{l}\right)$	1000
Total Kjeldahl Nitrogen (TKN) $\left(\frac{mg\ N}{l}\right)$	17
Total Protein (TP) $\left(\frac{mg\ P}{l}\right)$	3,10
Chlorine (Cl^-) $\left(\frac{mg}{l}\right)$	490
NO_3-NO_2 $\left(\frac{mg}{l}\right)$	37,3

pH	8,5

The plant relies on a biological activated sludge process implemented through a hybrid cyclical operating mode, which alternates oxidative and reductive phases to efficiently remove biodegradable organic matter, suspended solids, and nitrogen compounds.

Figure 5.1 shows a schematic representation of the wastewater treatment plant currently in use at the plant.

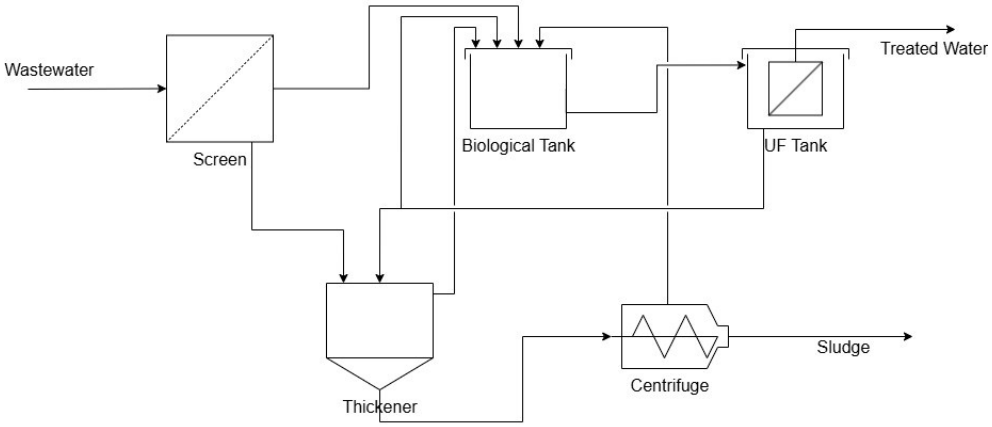

Figure 5.1: Schematic representation of the actual wastewater treatment plant.

The real WWTP consists of two large biological tanks, where the process alternates between:

- Oxidation/Nitrification phases, during which aeration supports the degradation of biodegradable carbon and the conversion of ammonium to nitrate.
- Reduction/Denitrification phases, conducted under anoxic conditions to reduce nitrates generated during the oxidative phase.

This alternating-cycle configuration is designed to optimize total nitrogen removal and to provide resilience and flexibility under fluctuating influent conditions typical of pharmaceutical wastewater. Although dynamic, this operating mode is controlled automatically, with oxygen setpoints, mixing

steps, and phase durations selected according to influent composition and regulatory discharge requirements.

Downstream of the biological section, the plant employs an extensive ultrafiltration module, which plays a key role in the clarification step and in ensuring high effluent quality.

The UF section consists of:

- 86 ultrafiltration units, each with a membrane surface area of 49.83 m^2.
- Membrane material: stainless steel SS316 casing with polymeric UF elements.

The UF unit removes suspended solids, colloidal material, and most bacteria, producing a permeate suitable for discharge and suitable as an input for tertiary or advanced oxidation treatments.

The sludge generated throughout the biological process is managed through a dedicated sludge-handling section, which includes units for thickening and dewatering, ensuring that solids are properly concentrated before final disposal. This line is supported by a series of mixers, pumps, and flow-distribution devices that maintain stable hydraulic conditions and guarantee consistent operation of the overall treatment plant.

The high degree of automation in the real plant further enhances operational stability and reduces the need for manual intervention.

5.2.2 Simplified Process Scheme Adopted for Simulation

To perform a rigorous and transparent performance analysis, the real WWTP configuration was simplified for modeling purposes using SuperPro Designer. The objective was to maintain the essential biological and physical functions of the plant while removing operational complexity linked to the cyclic mode, dynamic transitions, and control logics.

The simplified model adopts a three-stage linear configuration:

- Anoxic Reactor
- Aerobic Oxidation Basin
- Ultrafiltration Unit
- Sludge Treatment

Despite the simplification, two essential recirculation loops were maintained.

These recirculations preserve biological stability and allow the model to achieve nitrogen removal levels consistent with those of the real facility.

The simplification of the plant configuration was required for three main reasons:

- Simulation Stability: Cyclic biological processes introduce dynamic, time-dependent transitions that complicate steady-state modeling.
- Comparability with Advanced Configurations: A linear sequence enables a consistent comparison with enhanced process layouts incorporating hydrodynamic cavitation or additional oxidation steps.
- Transparency of the Mass Balance: A simplified model allows clearer isolation of the contributions of each unit operation to the overall removal performance.

Despite the simplifications, the model captures the essential biological mechanisms and separation efficiencies of the real WWTP, enabling accurate evaluation of conventional performance and assessment of technological upgrades described in later sections.

5.3 Process Modeling

Process modelling was carried out using the commercial software SuperPro Designer, with the objective of reproducing the behavior of the existing wastewater treatment plant and evaluating its performance under steady-state conditions. Simulation provides a controlled platform for investigating

pollutant removal efficiencies, testing alternative operational strategies, and establishing a transparent mass balance for each unit operation, which is particularly relevant when dealing with complex industrial effluents such as pharmaceutical wastewater.

5.3.1 SCOPE OF THE SIMULATION

The modelling effort focused exclusively on the baseline plant layout, consisting of physical pretreatment, chemical conditioning, biological treatment, and ultrafiltration. Key effluent quality parameters monitored in the simulation included COD, BOD_5, TOC, TSS, TKN, TP, and NO_3–NO_2, as these represent the main indicators of organic and nutrient removal in industrial wastewater treatment.

The purpose of the simulation was to:

- reproduce the performance of the existing process units,
- quantify pollutant removal across each stage,
- validate the model against experimental data available from the real plant and laboratory studies,
- build a consistent foundation for evaluating enhanced configurations presented in later sections.

Figure 5.2 shows the process diagram used to model the plant's wastewater treatment system.

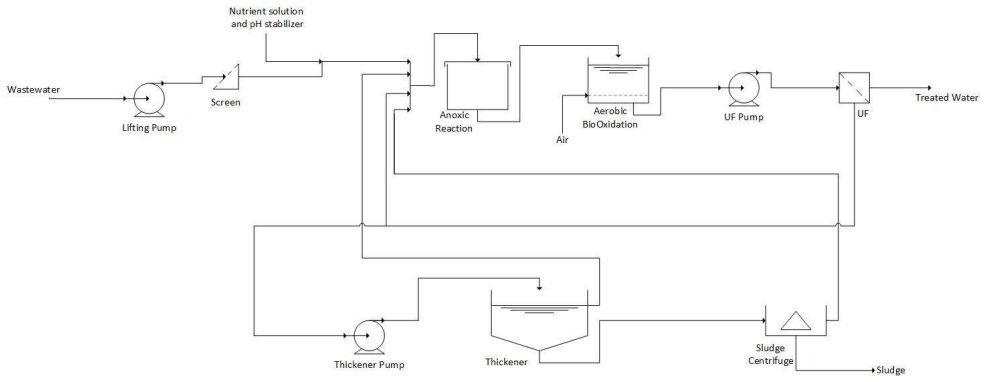

Figure 5.2: Wastewater treatment plant layout used to simulate the actual plant.

5.3.2 MODELLING OF THE BASELINE CONFIGURATION

The baseline configuration reflects the structure and operating logic of the real plant. Wastewater first undergoes fine screening to remove coarse and particulate materials. Based on influent characteristics, the screened stream is then chemically conditioned: hydrochloric acid (33%) is added until a pH of approximately 7.6 is achieved, and nitrogen and phosphorus solutions are dosed to restore nutrient balance. Average reagent consumption corresponds to 4.55 kg/h of HCl (33%) and 13.5 L/h of an N/P mixture (18%).

Following chemical conditioning, the effluent enters the biological treatment section, which consists of an anoxic denitrification tank and an aerobic oxidation/nitrification tank. These reactors were modeled as continuous stirred tank reactors in SuperPro Designer, using the stoichiometric and kinetic parameters listed below (the stoichiometry is on a mass basis).

Anoxic Reactor

Denitrification. Monod reaction. $\mathrm{K_s} = 0.4\frac{\mathrm{mg}}{\mathrm{l}}, \mathrm{k} = 0.02\mathrm{h}^{-1}$.

$$62.00NO_3 + 34.60DomWaste \rightarrow 33.40CO_2 + 13.20N_2 + 42.60H_2O + 7.40X_{vss}h$$

Biological Oxidation

Substrate degradation (DomWaste). Monod reaction. $\mathrm{K_s} = 5\frac{\mathrm{mg}}{\mathrm{l}}, \mathrm{k} = 0.066\mathrm{h}^{-1}$.

$$0.10NH_3 + 1.00DomWaste + 1.40O_2 \rightarrow 0.90CO_2 + 0.80H_2O + 0.80X_{vss}h$$

Nitrification. Monod reaction. $\mathrm{K_s} = 1.4\frac{\mathrm{mg}}{\mathrm{l}}, \mathrm{k} = 0.04\mathrm{h}^{-1}$.

$$7.50NH_3 + 1.80CO_2 + 24.60O_2 \rightarrow 25.20NO_3 + 7.70H_2O + 1.00X_{vss}h$$

Biomass decay ($X_{vss}h$). First-Order Reaction. $\mathrm{k} = 0.002\mathrm{h}^{-1}$ for $X_{vss}h$ and $X_{vss}n$.

$$1.15O_2 + 1.05X_{vss}h \rightarrow 0.10NH_3 + 1.45CO_2 + 0.45H_2O + 0.20X_{vss}i$$

$$1.15O_2 + 1.05X_{vss}n \rightarrow 0.10NH_3 + 1.45CO_2 + 0.45H_2O + 0.20X_{vss}i$$

These reactions and kinetic constants are crucial for modelling and optimizing the performance of the wastewater treatment processes in SuperPro Designer.

The baseline configuration was reconstructed in SuperPro Designer by modelling each unit operation according to the dimensions and design capacities reported in the reference study. These values, summarized in Table 5.2: Plant equipment for the simulation. represent the equipment characteristics used as input for the simulation.

Table 5.2: Plant equipment for the simulation.

Equipment	**Main Characteristic**
Lifting Pump (kW)	5
Screen Number	1
Anoxic Tank (m^3)	3450
Aerobic BioOxidation (m^3)	5200
Ultrafiltration Pump (kW)	50
UF Membrane Type	Dft Membrane
UF Membrane Number	86
Thickener Charging Pump (kW)	1
Thickener (m^3)	8.5
Sludge Sentrifuge (kW)	15
Venturi Feeding Pump (kW)	15

The effluent from the biological stage is subsequently treated through an ultrafiltration (UF) system, modelled using all 86 membrane modules present in the real plant. These membranes remove suspended solids, colloids, and residual biomass, producing a clarified permeate that represents the final effluent of the baseline configuration.

The internal recirculation flows, particularly the recycle of mixed liquor from the UF section back to the anoxic tank, were preserved in the model, maintaining recycle ratios between four and six times the influent flow rate as described in the operational data.

5.4 RESULTS

The simulation of the baseline wastewater treatment configuration enabled an evaluation of the pollutant removal performance across the anoxic, aerobic, and ultrafiltration stages. The simulated results closely reproduced the behaviour observed in the experimental analysis of the real plant, confirming the adequacy of the kinetic parameters and process assumptions adopted in the model.

The influent stream entering the treatment line is characterized by high concentrations of organic matter and suspended solids, consistent with the values previously reported for pharmaceutical effluents.

These concentrations represent a demanding load for biological treatment processes and provide a benchmark for evaluating removal efficiency.

After biological treatment and ultrafiltration, the simulated effluent shows a substantial reduction in all monitored parameters. Table 5.3 shows the composition of the Treated Water.

Table 5.3: Characteristics of Treated Water.

Parameter	Treated Water
TOC $\left(\frac{mg\ C}{l}\right)$	5,655
TP $\left(\frac{mg\ P}{l}\right)$	0,529

TKN $\left(\frac{mg\ N}{l}\right)$	1,28
NO_3-NO_2 $\left(\frac{mg\ N}{l}\right)$	25,217
COD $\left(\frac{mg\ O}{l}\right)$	15,323
BOD5 $\left(\frac{mg\ O}{l}\right)$	8,157
TSS $\left(\frac{mg}{l}\right)$	11,180

These removals confirm the high efficiency of the activated sludge process combined with ultrafiltration. The UF module plays a key role in achieving the very low concentrations of TSS observed in the permeate.

The substantial reduction in organic load indicates that the kinetic parameters adopted for substrate degradation and nitrification allowed the model to accurately represent the behaviour of the biological reactors. The simulated conversion of carbonaceous material is consistent with the Monod kinetics implemented in Section 5.3.

The anoxic stage contributed significantly to nitrogen removal, although nitrate concentrations were not the primary focus of this simulation stage. The aerobic tank achieved near-complete nitrification under the steady-state conditions tested, demonstrating adequate oxygen transfer and biological activity.

The ultrafiltration section effectively removed suspended solids and residual biomass, enabling the production of a clarified permeate with characteristics analogous to those obtained in the real plant.

The agreement between simulated and experimental values confirms that the modelling assumptions, particularly the stoichiometric coefficients, kinetic constants, and recirculation ratios, are appropriate for describing the behaviour of the Takeda wastewater treatment process. The consistency also reinforces the suitability of the biological model structure and supports its use as a reference configuration for evaluating enhanced process layouts in Section 5.5.

The baseline simulation establishes a quantitative benchmark for effluent quality that will be used to evaluate the potential benefits of introducing advanced oxidation technologies. The results presented here demonstrate that, although the current configuration achieves high removal of biodegradable organic matter and suspended solids, certain applications, such as water reuse, require further enhancement of effluent quality.

The following section (5.5) will therefore explore the integration of advanced treatment stages, including hydrodynamic cavitation and chemical oxidation, designed to further improve effluent characteristics and meet more stringent reuse standards.

5.5 Integration of Hydrodynamic Cavitation

The same plant can be equipped with an advanced oxidation section, as shown in Figure 5.3. Specifically, the advanced oxidation section includes hydrodynamic cavitation treatment, composed of a pump and a Venturi tube. HC is a process of generation, growth, and subsequent collapse of vapor-filled cavities within a liquid due to variations in local pressure. The cavities are generated in a low-pressure region, as in the throat of a Venturi tube. When these cavities travel to a region of higher pressure, they implode. The cavity collapse under certain conditions results in very high pressure and temperature near the location of collapse. These extreme local temperatures (> 2000 K) and pressures (> 100 MPa) result in the generation of highly reactive radical species (from water and dissolved air), with extreme physio-chemical effects that have been of interest to engineers and scientists due to their potential to damage equipment. On the other side, the strongly oxidizing hydroxyl radicals and local hot spots can be used for treating pollutants in water as well as for intensifying a variety of organic reactions in water [147].

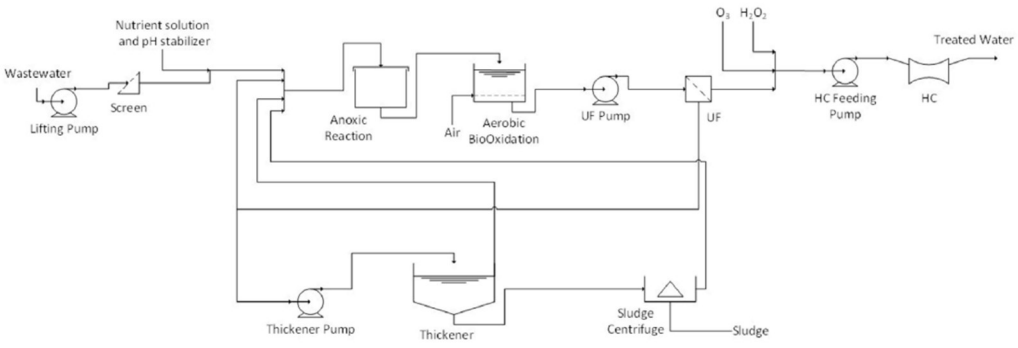

Figure 5.3: Wastewater Treatment Plant equipped with the Hydrodynamic Cavitation section.

In the context of the Takeda wastewater treatment process, the hydrodynamic cavitation stage was modelled as an additional unit operation following ultrafiltration. In the simulation, the UF permeate stream is directed to a dedicated mixing stage where oxidants are dosed before cavitation, ensuring a uniform distribution of reagents and improving reaction kinetics. As reported in the reference model, the inlet flow is subsequently pressurized by a pump capable of achieving an operating pressure of approximately 4.5 bar, which corresponds to the optimal Δp identified for maximizing cavitation intensity and pollutant degradation.

Therefore, among various AOPs, the •OH yield, removal efficiency, and energy efficiency are the main evaluation indicators. In general, less •OH is produced and higher energy consumption is required by hydrodynamic cavitation alone, but it can remarkably enhance oxidative degradation of organics by promoting the mass transfer and •OH formation in combination with other AOPs, such as Fenton oxidation [148] and ozonation [149]. Several studies also by this research group have confirmed the synergistic effect of hydrodynamic cavitation and oxidants like ozone and hydrogen peroxide, [150,151] to create a hybrid advanced oxidation process that achieves significantly greater degradation in a shorter period. In this treatment scheme, the inlet water stream of hydrodynamic cavitation is enriched with 7.5 mg/l of ozone and 0.3 M of hydrogen peroxide. These are average concentrations used in previous studies carried out on polluted water streams with different organic loads.

The permeate from ultrafiltration is thus first added with hydrogen peroxide (0.5 kg/h) and ozone (1 kg/h). It is then pumped into a Venturi tube-type hydrodynamic cavitation reactor via a pump. This pump must produce a sufficient Δp to initiate cavitation, with the ensuing synergistic effects on the previously supplied oxidants. 99% bacterial degradation was assumed for the simulation of this section, consistent with results found in the literature [152].

5.6 Comparison with Limits for Irrigation Reuse

Advanced Oxidation Processes increase the quality of treated water by mineralizing chemical species that can pass through traditional wastewater treatment without degradation [145]. In this study, a hydrodynamic cavitation system with a Venturi tube is proposed. As demonstrated in various investigations, hydrodynamic cavitation has a synergistic effect on conventional oxidants when combined with the output of earlier treatments [153].

Table 5.4 depicts the characteristics of water discharge from the two alternative system setups. The table also indicates the constraints imposed by current European guidelines on water reuse for irrigation applications [154]. As demonstrated in Table 5.4, the water leaving the ultrafiltration treatment may be appropriate for reuse as irrigation water for crops classified as Class B water applications. However, EU Regulation 741/2020 mandates that the water be disinfected before its reuse; therefore, the water exiting the Ultrafiltration section is not appropriate for irrigation reuse. The environmental parameters of this stream should be attributed to bacterial or viral remnants in the treated effluent.

Advanced oxidation methods are also covered in the guidelines for potable water reuse issued by the USEPA in 2017 as a disinfection method [155]. According to EU 741/2020, hydrodynamic cavitation treatment yields Class A water suitable for all forms of culture. It has also been demonstrated in

the literature that such a process can be efficient at removing numerous pathogens with great efficiency [152]. The reduction efficiency in environmental parameters (TOC, TP, TKN, COD, BOD_5, TSS) of the current output from the cavitation section resulted always higher than 98%. This performance can be also attributed to the degradation of residual bacterial or viral load in the output current from Ultrafiltration [156].

Table 5.4: Characteristics of the effluent from the two different plant configurations and limits for irrigation reuse in Europe.

Parameter	**UF Section**	**UE 741/2020 Class B Water**	**Hydrodynamic Cavitation Section**	**UE 741/2020 Class A Water**
TOC $\left(\frac{mg\ C}{l}\right)$	5,655		0,081	
TP $\left(\frac{mg\ P}{l}\right)$	0,529		0,005	
TKN $\left(\frac{mg\ N}{l}\right)$	1,28		0,014	
NO_3-NO_2 $\left(\frac{mg\ N}{l}\right)$	25,217		25,202	
COD $\left(\frac{mg\ O}{l}\right)$	15,323	≤125	0,234	≤10
BOD5 $\left(\frac{mg\ O}{l}\right)$	8,157	≤25	0,114	≤10
TSS $\left(\frac{mg}{l}\right)$	11,180	≤35	0,152	≤10

A quantitative assessment of the improvement achieved by the hydrodynamic cavitation process is presented in Table 5.5, which summarizes the percentage reduction of all monitored environmental parameters relative to the ultrafiltration effluent. The resulting degradation

efficiencies of 99–100% align fully with experimental observations and with the performance criteria discussed in the literature.

Table 5.5: Reduction of environmental parameters by the Hydrodynamic Cavitation section.

Parameter	Reduction %
TOC	98,57
TP	98,97
TKN	98,92
NO_3-NO_2	0,06
COD	98,47
BOD_5	98,60
TSS	98,64

This behaviour is consistent with the reaction pathways implemented in the simulation, where cavitation-induced hot spots promote water splitting, formation of hydroxyl radicals, degradation of pollutant molecules, and mineralisation into CO_2 and H_2O. Moreover, the model incorporates a 99% disinfection assumption, coherent with the pathogen inactivation yields reported by Sun et al. (2020)[152], thus explaining why no microbial indicators remain detectable after the HC stage.

From an operational perspective, the HC step acts as a polishing treatment capable of eliminating all residual contaminants that pass through biological treatment and ultrafiltration. This provides an effluent that meets the highest reuse quality standards and demonstrates the suitability of hydrodynamic cavitation as an effective tertiary process for advanced wastewater purification.

5.7 OPERATIONAL COSTS

The Operating Costs (OPEX) of the wastewater treatment plant represent the annual expenses required for its operation. These costs are crucial for the financial planning and sustainability of the facility. The main components of the OPEX are detailed below:

Electricity Costs.

Energy costs are determined by assessing the power consumption of all installed equipment, including pumps, compressors, mixers, and other machinery. The consumption is calculated by multiplying the installed power of each equipment by its average annual operating hours [157].

Key energy-consuming areas include the equalization unit, the biological compartment, the ultrafiltration unit, and the sludge line [158–160].

The compressors for oxidation and MBR are the largest consumers of energy [158,159].

The total annual energy consumption for the plant is 6360 kWh/day, with a cost approximately of 0.21 €$/kWh$ [140], leading to an annual electricity cost of approximately 463112 €$/year$ [160]. The operating costs were calculated assuming 95% of the total annual operating hours, to account for the downtime required for routine maintenance activities.

Sludge Disposal Costs.

The cost of sludge disposal depends on the nature of the sludge, with an assumption of assimilability to urban waste in this case. The daily production of wet sludge is estimated to be 4.8 m^3/day [161].

Based on a typical urban waste disposal cost is approximately 120 €$/m^3$, the annual costs for sludge disposal are approximately 180000 €.

Chemical Reagent Costs.

Chemical reagents are used for various purposes, including conditioning the influent, improving sludge dewaterability, and cleaning the ultrafiltration membranes [153]. The chemicals used include hydrochloric acid, nutrient mix, citric acid, sodium hypochlorite, and polyelectrolyte [162]. The costs for these chemicals are calculated based on their annual consumption and unit cost [153].

The total annual cost for chemical reagents is approximately 103820€.

Plant Supervision and Management Costs

The plant is designed to be highly automated and self-regulated, with most equipment having active backups. Control and remote monitoring are provided through a PLC and SCADA system.

The automated systems and remote monitoring allow for a reduction in the required personnel for operation; therefore, the plant requires only minimal daily inspections [162].

The annual cost for personnel is estimated to be 22000 € based on a daily commitment of two hours by an operator and a substitute.

Total Annual Operating Costs.

The total annual operating cost of the plant is the sum of electricity, sludge disposal, chemical reagents, and personnel costs [163]. The summarized annual OPEX is approximately 768932€. The operational costs of the treatment plant are a significant consideration, encompassing energy consumption, sludge disposal, chemical usage, and personnel costs [164,165].

In summary, the OPEX is composed of various components, with electricity and sludge disposal as the most significant costs. The chemical and personnel costs are also important contributors. The plant's design emphasizes automation and efficiency to minimize operational costs while ensuring effective wastewater treatment.

5.8 BENEFITS AND LIMITATIONS

The evaluation of the baseline configuration and the enhanced layout integrating hydrodynamic cavitation highlights several benefits as well as important limitations that influence both the technical and operational feasibility of the treatment system. This section summarises the main strengths and constraints of the two approaches, providing an overall assessment of their applicability within industrial wastewater treatment.

The combined action of the anoxic and aerobic biological stages, followed by ultrafiltration, achieves very high removal of biodegradable organic matter, suspended solids, and nitrogen species. The biological units effectively degrade most of the organic load, while the membrane barrier ensures excellent clarification. The simulation results confirm removal efficiencies exceeding 99% for key parameters, demonstrating the robustness of the baseline system for conventional discharge scenarios.

The integration of hydrodynamic cavitation provides a significant performance enhancement. As demonstrated in the simulation and supported by the literature, cavitation-induced oxidation leads to complete removal of residual organic matter, suspended solids, and biodegradable fractions. Hydroxyl radicals generated during bubble collapse enable the mineralisation of compounds that remain unaffected by biological and membrane treatment, producing an effluent of exceptionally high quality suitable for stringent reuse applications.

Hydrodynamic cavitation has been shown to achieve substantial microbial inactivation, with reported bacterial degradation yields of approximately 99% [152]. This effect complements the physical removal achieved by ultrafiltration and contributes to the overall safety of the effluent for potential reuse, especially in contexts where compliance with EU Regulation 2020/741 is required.

The HC stage operates as an add-on tertiary treatment, requiring no modification to the upstream biological or membrane units. This modularity

simplifies integration into existing plants and makes the technology suitable for retrofitting without significantly altering the hydraulic layout or operational philosophy of the treatment line.

Despite its high efficiency, the baseline configuration leaves measurable traces of TOC, COD, and TSS in the ultrafiltration permeate. These low but persistent concentrations indicate the presence of refractory compounds or soluble microbial products that cannot be fully removed by biological or membrane processes. As a result, the baseline system alone cannot meet the most stringent water quality standards associated with reuse applications, including those defined in EU 2020/741.

The introduction of hydrodynamic cavitation requires:

- pressurisation of the influent stream to achieve the pressure drop necessary for cavitation,
- continuous dosing of oxidants such as hydrogen peroxide and ozone,
- management of mechanical stress and potential wear in cavitation equipment.

These operational demands may increase maintenance needs and complicate process control compared to the baseline configuration.

The present study clearly states that electricity consumption, particularly for pumps and compressors, and chemical usage are significant contributors to OPEX. The HC stage relies on both additional energy input and chemical reagents and therefore is expected to increase operational costs relative to the baseline system. The economic trade-off between improved effluent quality and added operational complexity must be carefully evaluated.

The effectiveness of the HC process relies on precise operating conditions, including the concentration of hydrogen peroxide and ozone, the pressure drop, and the hydrodynamic behaviour within the Venturi tube. Deviations from optimal conditions may reduce radical production and consequently lower degradation efficiency. This sensitivity may limit robustness under variable influent characteristics.

5.9 CONCLUSIONS

The analysis presented in this chapter confirms the strong performance of the existing wastewater treatment configuration, where the combination of biological processes and ultrafiltration provides high removal of organic matter, suspended solids, and nitrogen species. Nonetheless, trace concentrations of refractory organics and colloidal material persist in the UF permeate, indicating that the baseline system alone is not sufficient when higher effluent quality standards or water reuse applications are required.

The integration of hydrodynamic cavitation significantly enhances treatment performance. The advanced oxidation environment generated during cavitation enables complete degradation of residual organic and particulate pollutants, while also contributing to microbial inactivation. As a modular tertiary stage, HC can be incorporated without altering upstream operations, offering a flexible polishing option for applications requiring stringent effluent quality.

Operationally, the enhanced configuration involves additional energy demand and chemical dosing, which may increase OPEX. However, these costs must be evaluated considering the substantial improvement in effluent quality and the potential benefits associated with regulatory compliance and water reuse opportunities.

Overall, the results demonstrate that hydrodynamic cavitation is a promising technology for advanced industrial wastewater treatment and aligns well with circular water management strategies.

Future work should incorporate a Life Cycle Assessment (LCA) to quantify the broader environmental implications of both the baseline and HC-enhanced configurations. LCA would allow evaluating trade-offs related to energy use, chemical consumption, and sludge production, supporting a more comprehensive assessment of sustainability and guiding the optimisation of the proposed treatment systems.

6. CONCLUSIONS

This work addressed the development of innovative and sustainable strategies for the recovery of ethanol from hydroalcoholic waste streams generated during human plasma fractionation. The research combined experimental investigations, analytical characterization, process simulation, and techno-economic and environmental evaluations to tackle both product quality and process efficiency, with the overarching goal of enabling the industrial valorisation of these complex waste streams.

The experimental activities allowed for an in-depth characterization of the volatile and semi-volatile compounds present in hydroalcoholic effluents and in the recovered ethanol. Attention was devoted to the formation of undesired contaminants under thermal conditions relevant to industrial distillation. The results demonstrated that such compounds are not significantly present in the as received streams but may form during thermal treatment depending on operating conditions and system configuration. The identification of specific precursor compounds and the assessment of their temperature- and time-dependent behaviour provided key insights into the mechanisms governing contaminant formation, highlighting critical operating windows to preserve ethanol quality.

Factorial experimental designs proved to be an effective tool for quantifying the influence of process variables and their interactions on contaminant formation. Temperature emerged as the dominant factor, while the role of

enzymatic activity and redox conditions was shown to be significant under specific operating regimes. These findings contribute to a more mechanistic understanding of quality degradation phenomena and offer practical guidelines for defining safer operating conditions in industrial applications.

From a process engineering perspective, the thesis explored alternative distillation configurations aimed at reducing energy demand and improving overall sustainability. The integration of heat pump-assisted distillation systems demonstrated a substantial potential for lowering primary energy consumption compared to conventional steam-based solutions, while maintaining separation performance. Process simulations confirmed the technical feasibility of these configurations and supported the identification of optimal operating conditions. The economic analysis showed that the proposed solutions can be competitive at industrial scale, especially when energy savings and solvent recovery are jointly considered

Considering the results obtained on contaminant formation mechanisms and the identification of specific precursor compounds, the adoption of a membrane-based treatment upstream of the distillation unit is proposed as a promising complementary strategy. Although the detailed design and experimental validation of such a system were not within the scope of this study, membrane separation could enable the selective removal of contaminant precursors from the feed, thereby reducing their thermal conversion during distillation.

The implementation of this pre-treatment step is expected to decrease the frequency of maintenance operations on the distillation unit and to significantly reduce the occurrence of off spec recovered ethanol. From an industrial perspective, membrane-based systems are characterized by relatively low capital and operating costs, which could be readily offset over time through improved process reliability, reduced downtime, and enhanced product quality. As such, this approach represents a viable and economically attractive option for further improving the robustness and sustainability of ethanol recovery from plasma fractionation waste streams.

Overall, this work demonstrates that the recovery of ethanol from plasma fractionation waste streams can be transformed from a critical operational issue into a valuable opportunity, if product quality, process design, and sustainability aspects are addressed simultaneously. The methodologies and results presented in this thesis offer a solid foundation for industrial implementation and provide transferable tools and concepts applicable to other hydroalcoholic waste streams in the pharmaceutical and chemical industries.

Future research should focus on the refinement of kinetic models for contaminant formation, the validation of proposed solutions at pilot and full industrial scale, and the further integration of solvent recovery systems within circular economy frameworks for pharmaceutical manufacturing.

BIBLIOGRAPHY

[1] S. Verma, S. Dolia, S. Makadia, N. Kumar, Insights into the Purification of C1-esterase Inhibitor from Human Plasma, Plasmatology 18 (2024) 1–13. https://doi.org/10.1177/26348535241236299.

[2] S. Pichler, K. Herbinger, A. Weber, H. Anderle, L. Gnauer, Characterization and Calibration of Cold-Alcohol Plasma Fractionation Intermediates by Kjeldahl Digestion and Digital Refractometry, Plasmatology 18 (2024). https://doi.org/10.1177/26348535241277388.

[3] J.R. Bove, Fibrinogen—Is the Benefit Worth the Risk?, Transfusion (Paris) 18 (1978) 129–136. https://doi.org/10.1046/J.1537-2995.1978.18278160573.X.

[4] W. Schneider, H. Lefevre, H. Fiedler, L.J. McCarty, An alternative method of large scale plasma fractionation for the lsolation of serum albumin, Blut Zeitschrift Für Die Gesamte Blutforschung 30 (1975) 121–134. https://doi.org/10.1007/BF01633966/METRICS.

[5] C. Huangfu, Y. Ma, M. Lv, J. Jia, X. Zhao, J. Zhang, Purification of 2-macroglobulin from Cohn Fraction IV by immobilized metal affinity chromatography: A promising method for the better utilization of plasma, Journal of Chromatography B 1025 (2016) 68–75. https://doi.org/10.1016/j.jchromb.2016.05.013.

[6] D.D. Schroeder, M.M. Mozen, Australia Antigen: Distribution during Cohn Ethanol Fractionation of Human Plasma, Science (1979) 168 (1970) 1462–1464. https://doi.org/10.1126/SCIENCE.168.3938.1462.

[7] S. YEI, M.W. Yu, Partitioning of hepatitis C virus during Cohn-Oncley fractionation of plasma, Transfusion (Paris) 32 (1992) 824–828. https://doi.org/10.1046/J.1537-2995.1992.32993110753.X.

[8] J.C. Occhino, A.H. Glasgow, S.R. Cooperband, J.A. Mannick, K. Schmid, Isolation of an Immunosuppressive Peptide Fraction from Human Plasma, The Journal of Immunology 110 (1973) 685–694. https://doi.org/10.4049/JIMMUNOL.110.3.685.

[9] R. Haider, International Trade in Pharmaceutical Products, International Journal of Applied Economics, Acounting and Management(IJAEAM) 1 (2023) 227–250. https://doi.org/10.59890/ijaeam.v1i4.913.

[10] C. Jimenez-Gonzalez, C.S. Ponder, Q.B. Broxterman, J.B. Manley, Using the Right Green Yardstick: Why Process Mass Intensity Is Used in the Pharmaceutical Industry To Drive More Sustainable Processes, Org. Process Res. Dev 15 (2011) 912–917. https://doi.org/10.1021/op200097d.

[11] Lí.M. Gaspar Ernesto, R.M. Dias Loureiro, Pharmaceutical Manufacturing in the EU and the EU–US Mutual Recognition Agreement, PDA J Pharm Sci Technol 74 (2020) 617–626. https://doi.org/10.5731/PDAJPST.2020.011437.

[12] D. Criscuolo, Pharmaceutical medicine in Italy, Pharmaceut Med 24 (2010) 15–19. https://doi.org/10.1007/BF03256794/FIGURES/TAB1.

[13] M.J. Raymond, C.S. Slater, M.J. Savelski, LCA approach to the analysis of solvent waste issues in the pharmaceutical industry, Green Chemistry 12 (2010) 1826–1834. https://doi.org/10.1039/C003666H.

[14] A.C. Bédard, A.R. Longstreet, J. Britton, Y. Wang, H. Moriguchi, R.W. Hicklin, W.H. Green, T.F. Jamison, Minimizing E-factor in the continuous-flow synthesis of diazepam and atropine, Bioorg Med Chem 25 (2017) 6233–6241. https://doi.org/10.1016/J.BMC.2017.02.002.

[15] L. Domingues, A.R.C. Duarte, A.R. Jesus, How Can Deep Eutectic Systems Promote Greener Processes in Medicinal Chemistry and Drug Discovery?, Pharmaceuticals 2024, Vol. 17, Page 221 17 (2024) 221. https://doi.org/10.3390/PH17020221.

[16] K. Yang, B. Lv, H. Shen, G. Jing, Z. Zhou, Life cycle assessment of pharmaceuticals: the ciprofloxacin hydrochloride case, International Journal of Life Cycle Assessment 26 (2021) 64–75. https://doi.org/10.1007/S11367-020-01841-6/FIGURES/4.

[17] T. Fodi, C. Didaskalou, J. Kupai, G.T. Balogh, P. Huszthy, G. Szekely, Nanofiltration-Enabled In Situ Solvent and Reagent Recycle for Sustainable Continuous-Flow Synthesis, ChemSusChem 10 (2017) 3435–3444. https://doi.org/10.1002/CSSC.201701120.

[18] R.K. Henderson, C. Jiménez-González, D.J.C. Constable, S.R. Alston, G.G.A. Inglis, G. Fisher, J. Sherwood, S.P. Binks, A.D. Curzons, Expanding GSK's solvent selection guide — embedding sustainability into solvent selection starting at medicinal chemistry, Green Chemistry 13 (2011) 854–862. https://doi.org/10.1039/C0GC00918K.

[19] L. Ciriaco, L. Izzo, G. Graziani, M.G. Ferraro, M. Piccolo, R. Ciampaglia, B. Maglione, R. Palladino, S. Albarella, E. Romano, A. Ritieni, C. Irace, P. Grieco, Chemical characterization of wheat-based waste derived from a pharmaceutical process for its potential valorization, Front Chem 12 (2024) 1437221. https://doi.org/10.3389/FCHEM.2024.1437221/BIBTEX.

[20] A.M. Hosseini, V. Bakos, A. Jobbágy, G. Tardy, P. Mizsey, M. Makó, A. Tungler, Co-treatment and utilisation of liquid pharmaceutical wastes, Periodica Polytechnica Chemical Engineering 55 (2011) 3–10. https://doi.org/10.3311/PP.CH.2011-1.01.

[21] Ç.E. Güneş, H. Şengül, Cradle-to-gate life cycle assessment of a liquid pharmaceutical product through analysis of chemical production pathways, Clean Technol Environ Policy 24 (2022) 1741–1755. https://doi.org/10.1007/S10098-022-02283-4/TABLES/6.

[22] Y. Liu, W. Wang, S. Luo, al -, Q. Han, L. ping Qiu, R. zhen Cheng, Y. Guo, P.S. Qi, Y.Z. Liu, A Review on Advanced Treatment of Pharmaceutical Wastewater, IOP Conf Ser Earth Environ Sci 63 (2017) 012025. https://doi.org/10.1088/1755-1315/63/1/012025.

[23] Q. Luo, J. Wang, J.H. Wang, Y. Shen, P. Yan, Y.P. Chen, C.C. Zhang, Fate and Occurrence of Pharmaceutically Active Organic Compounds during Typical Pharmaceutical Wastewater Treatment, J Chem 2019 (2019) 2674852. https://doi.org/10.1155/2019/2674852.

[24] J.J. Xue, D. Lei, X. Zhao, Y. Hu, S. Yao, K. Lin, Z. Wang, C. Cui, Antibiotic residue and toxicity assessment of wastewater during the pharmaceutical production processes, Chemosphere 291 (2022) 132837. https://doi.org/10.1016/J.CHEMOSPHERE.2021.132837.

[25] X. Shi, K.Y. Leong, H.Y. Ng, Anaerobic treatment of pharmaceutical wastewater: A critical review, Bioresour Technol 245 (2017) 1238–1244. https://doi.org/10.1016/J.BIORTECH.2017.08.150.

[26] Y. Jiang, X. Shi, H.Y. Ng, Aerobic granular sludge systems for treating hypersaline pharmaceutical wastewater: Start-up, long-term performances and metabolic function, J Hazard Mater 412 (2021) 125229. https://doi.org/10.1016/J.JHAZMAT.2021.125229.

[27] J. Iqbal, N.S. Shah, J. Ali Khan, M. Naushad, G. Boczkaj, F. Jamil, S. Khan, L. Li, B. Murtaza, C. Han, Pharmaceuticals wastewater treatment via different advanced oxidation processes: Reaction

mechanism, operational factors, toxicities, and cost evaluation – A review, Sep Purif Technol 347 (2024) 127458. https://doi.org/10.1016/J.SEPPUR.2024.127458.

[28] H. Ghazal, E. Koumaki, J. Hoslett, S. Malamis, E. Katsou, D. Barcelo, H. Jouhara, Insights into current physical, chemical and hybrid technologies used for the treatment of wastewater contaminated with pharmaceuticals, J Clean Prod 361 (2022) 132079. https://doi.org/10.1016/J.JCLEPRO.2022.132079.

[29] R. Guedes-Alonso, S. Montesdeoca-Esponda, J. Pacheco-Juárez, Z. Sosa-Ferrera, J.J. Santana-Rodríguez, A Survey of the Presence of Pharmaceutical Residues in Wastewaters. Evaluation of Their Removal using Conventional and Natural Treatment Procedures, Molecules 2020, Vol. 25, Page 1639 25 (2020) 1639. https://doi.org/10.3390/MOLECULES25071639.

[30] A.M. Enright, S. McHugh, G. Collins, V. O'Flaherty, Low-temperature anaerobic biological treatment of solvent-containing pharmaceutical wastewater, Water Res 39 (2005) 4587–4596. https://doi.org/10.1016/J.WATRES.2005.08.037.

[31] A.M. Deegan, B. Shaik, K. Nolan, K. Urell, M. Oelgemöller, J. Tobin, A. Morrissey, Treatment options for wastewater effluents from pharmaceutical companies, International Journal of Environmental Science & Technology 2011 8:3 8 (2011) 649–666. https://doi.org/10.1007/BF03326250.

[32] J.O. Eniola, R. Kumar, M.A. Barakat, J. Rashid, A review on conventional and advanced hybrid technologies for pharmaceutical wastewater treatment, J Clean Prod 356 (2022) 131826. https://doi.org/10.1016/J.JCLEPRO.2022.131826.

[33] M.J. Savelski, C.S. Slater, P. V. Tozzi, C.M. Wisniewski, On the simulation, economic analysis, and life cycle assessment of batch-mode organic solvent recovery alternatives for the pharmaceutical

industry, Clean Technol Environ Policy 19 (2017) 2467–2477. https://doi.org/10.1007/S10098-017-1444-8/FIGURES/6.

[34] H.T. Do Thi, P. Mizsey, A.J. Toth, Separation of Alcohol-Water Mixtures by a Combination of Distillation, Hydrophilic and Organophilic Pervaporation Processes, Membranes 2020, Vol. 10, Page 345 10 (2020) 345. https://doi.org/10.3390/MEMBRANES10110345.

[35] H. Xiao, Y. Feng, W.R.F. Goundry, S. Karlsson, Organic Solvent Nanofiltration in Pharmaceutical Applications, Org Process Res Dev 28 (2024) 891–923. https://doi.org/10.1021/ACS.OPRD.3C00470/ASSET/IMAGES/LARGE/OP3C00470_0026.JPEG.

[36] E.A. Aboagye, J.D. Chea, K.M. Yenkie, Systems level roadmap for solvent recovery and reuse in industries, IScience 24 (2021) 103114. https://doi.org/10.1016/J.ISCI.2021.103114.

[37] E.C. Tarango Brito, C.E. Barrera Díaz, L.I. Ávila Córdoba, B.A. Frontana Uribe, D.A. Solís Casados, Recovery and Reuse of Acetone from Pharmaceutical Industry Waste by Solar Distillation, Processes 2025, Vol. 13, Page 361 13 (2025) 361. https://doi.org/10.3390/PR13020361.

[38] C. Guo, Energy-economic analysis of ionic liquids extractive-heat pump distillation process for recovery of ethanol and isopropyl alcohol from wastewater, Sep Purif Technol 276 (2021) 119338. https://doi.org/10.1016/J.SEPPUR.2021.119338.

[39] J.H.X. Lim, K. Goh, D.Y.F. Ng, J. Chew, R. Wang, Layer-by-layer hierarchically structured nanofibrous membrane scaffolds incorporating metal-organic framework and carbon nanotube adsorbents for high-performance versatile organic solvent recovery, J Clean Prod 404 (2023) 136925. https://doi.org/10.1016/J.JCLEPRO.2023.136925.

[40] H. Nekkanti, A.K. Galam, A.K. Vadaga, A Comprehensive Review of Distillation in the Pharmaceutical Industry : Review Article, Journal of Pharma Insights and Research 2 (2024) 138–145. https://doi.org/10.69613/0YHX1W60.

[41] G. Lewandowicz, W. Białas, B. Marczewski, D. Szymanowska, Application of membrane distillation for ethanol recovery during fuel ethanol production, J Memb Sci 375 (2011) 212–219. https://doi.org/10.1016/J.MEMSCI.2011.03.045.

[42] H. Doğan, A. Genç, İ. Telci, Comparison of conventional steam distillation and industrial-type microwave-assisted distillation systems for lavandin (Lavandula × intermedia Emeric Ex Loisel): Energy consumption, essential oil yield, and quality, Journal of Essential Oil Bearing Plants 28 (2025) 126–139. https://doi.org/10.1080/0972060X.2025.2451392.

[43] T. Pahua-Angel, M. Estarrón-Espinosa, E. Castaño-Tostado, E.M. Mercado-Silva, S.L. Amaya-Llano, J.D. Padilla-de la Rosa, Innovative Technology of Continuous-Steam Distillation with Packed Column to Obtain Essential Oil-Differentiated Fractions from Mexican Lime (Citrus aurantifolia), ChemEngineering 2024, Vol. 8, Page 88 8 (2024) 88. https://doi.org/10.3390/CHEMENGINEERING8050088.

[44] V.H. Grisales Díaz, G. Olivar Tost, Techno-economic analysis of extraction-based separation systems for acetone, butanol, and ethanol recovery and purification, Bioresour Bioprocess 4 (2017) 1–13. https://doi.org/10.1186/S40643-017-0142-Z/FIGURES/5.

[45] Q. Li, N. Hu, S. Zhang, Q. Wu, J. Qi, Energy-saving heat integrated extraction-azeotropic distillation for separating isobutanol-ethanol-water, Sep Purif Technol 255 (2021) 117695. https://doi.org/10.1016/J.SEPPUR.2020.117695.

[46] L. Petrescu, C.M. Cormos, Classical and Process Intensification Methods for Acetic Acid Concentration: Technical and Environmental Assessment, Energies (Basel) 15 (2022) 8119. https://doi.org/10.3390/EN15218119/S1.

[47] S. Niazi, J.A. Díaz-López, A. Nieto-Márquez, Process design and simulation of methyl isobutyl ketone (MIBK) dehydration by batch distillation: A study on unit configuration and operational policies, Sep Purif Technol 350 (2024) 127942. https://doi.org/10.1016/J.SEPPUR.2024.127942.

[48] E. de J. Hernández-Hernández, J. Cabrera-Ruiz, H. Hernández-Escoto, C. Gutiérrez-Antonio, S. Hernández, Simulation study of the production of high purity ethanol using extractive distillation: Revisiting the use of inorganic salts, Chemical Engineering and Processing - Process Intensification 170 (2022) 108670. https://doi.org/10.1016/J.CEP.2021.108670.

[49] J.A. Shamim, G. Auti, H. Kimura, S. Fei, W.L. Hsu, H. Daiguji, A. Majumdar, Concept of a hybrid compression-adsorption heat pump cycle, Cell Rep Phys Sci 3 (2022) 101131. https://doi.org/10.1016/J.XCRP.2022.101131.

[50] D.B. Boman, A.W. Raymond, S. Garimella, Adsorption Heat Pump Cycles, (2021) 7–27. https://doi.org/10.1007/978-3-030-72180-0_2.

[51] J. Sun, Y. Wang, K. Wu, Z. Ge, Y. Yang, Analysis of a New Super High Temperature Hybrid Absorption-Compression Heat Pump Cycle, Energies 2022, Vol. 15, Page 7515 15 (2022) 7515. https://doi.org/10.3390/EN15207515.

[52] G.B. Wang, X.R. Zhang, Thermoeconomic analysis of optimization potential for CO2 vapor compression cycle: From transcritical to supercritical operation for waste heat recovery from the steam condenser, Int J Energy Res 43 (2019) 297–312. https://doi.org/10.1002/ER.4263.

[53] G. Villa, J.L. Corrales Ciganda, G. Abrami, T. Toppi, Absorption Heat Transformer and Vapor Compression Heat Pump as Alternative Options for Waste Heat Upgrade in the Industry, Energies 2025, Vol. 18, Page 3454 18 (2025) 3454. https://doi.org/10.3390/EN18133454.

[54] K. Hamid, S. Ren, I. Tolstorebrov, A. Hafner, C.C. Wang, U. Sajjad, T.M. Eikevik, Development and experimental assessment of oil free combine absorption-compression heat pump with NH3/H2O mixture working fluid, Appl Energy 383 (2025) 125352. https://doi.org/10.1016/J.APENERGY.2025.125352.

[55] M.P. Andersen, B. Zühlsdorf, W.B. Markussen, J.K. Jensen, B. Elmegaard, Heat pumps for combined heating and cooling in industrial applications: A generalised approach, Appl Therm Eng 264 (2025) 125454. https://doi.org/10.1016/J.APPLTHERMALENG.2025.125454.

[56] D. Flórez-Orrego, M.E.R. Domingos, F. Maréchal, Techno-economic and environmental analysis of high temperature heat pumps integration into industrial processes: the ammonia plant and pulp mill cases, Sustainable Energy Technologies and Assessments 60 (2023) 103560. https://doi.org/10.1016/J.SETA.2023.103560.

[57] S. Trevisan, B. Buchbjerg, A. Höeg, R. Guedez, Techno-Economic Comparative Assessment of High Temperature Heat Pump Architectures for Industrial Pumped Thermal Energy Storage, Proceedings of the ASME Turbo Expo 6 (2024). https://doi.org/10.1115/GT2024-128910.

[58] W. Wu, Y. Du, H. Qian, H. Fan, Z. Jiang, S. Huang, X. Zhang, Industrial Park low-carbon energy system planning framework: Heat pump based energy conjugation between industry and buildings, Appl Energy 369 (2024) 123594. https://doi.org/10.1016/J.APENERGY.2024.123594.

[59] F. Schlosser, M. Jesper, J. Vogelsang, T.G. Walmsley, C. Arpagaus, J. Hesselbach, Large-scale heat pumps: Applications, performance, economic feasibility and industrial integration, Renewable and Sustainable Energy Reviews 133 (2020) 110219. https://doi.org/10.1016/J.RSER.2020.110219.

[60] J. Zhai, X. Chen, X. Sun, H. Xie, Economically and thermodynamically efficient pressure-swing distillation with heat integration and heat pump techniques, Appl Therm Eng 218 (2023) 119389. https://doi.org/10.1016/J.APPLTHERMALENG.2022.119389.

[61] J. Zhu, B. Zhang, H. Zhang, L. Hao, Heat Pump-Assisted Extractive Pressure-Swing Distillation with Integrated Feed Preconcentration/Solvent Recovery for Isopropanol-Benzene-Water Separation, Sep Purif Technol 358 (2025) 130295. https://doi.org/10.1016/J.SEPPUR.2024.130295.

[62] X. You, I. Rodriguez-Donis, V. Gerbaud, Reducing process cost and CO2 emissions for extractive distillation by double-effect heat integration and mechanical heat pump, Appl Energy 166 (2016) 128–140. https://doi.org/10.1016/J.APENERGY.2016.01.028.

[63] E. Díez, P. Langston, G. Ovejero, M.D. Romero, Economic feasibility of heat pumps in distillation to reduce energy use, Appl Therm Eng 29 (2009) 1216–1223. https://doi.org/10.1016/J.APPLTHERMALENG.2008.06.013.

[64] Y. Xu, J. Li, Q. Ye, Y. Li, Energy efficient extractive distillation process assisted with heat pump and heat integration to separate acetonitrile/1,4-dioxane/water, Process Safety and Environmental Protection 156 (2021) 144–159. https://doi.org/10.1016/J.PSEP.2021.09.042.

[65] S. Boldyryev, M. Ilchenko, G. Krajačić, Improving the Economic Efficiency of Heat Pump Integration into Distillation Columns of

Process Plants Applying Different Pressures of Evaporators and Condensers, Energies 2024, Vol. 17, Page 951 17 (2024) 951. https://doi.org/10.3390/EN17040951.

[66] Z. Mekidiche, J.A. Labarta, J. Javaloyes-Anton, J.A. Caballero, From power to heat: Strategies for electrifying distillation for sustainable chemical processes, Appl Therm Eng 257 (2024) 124316. https://doi.org/10.1016/J.APPLTHERMALENG.2024.124316.

[67] W.L. Luyben, Optimum vacuum distillation pressure, Chemical Engineering and Processing - Process Intensification 171 (2022) 108630. https://doi.org/10.1016/J.CEP.2021.108630.

[68] M.S. Atta, H. Khan, M. Ali, R. Tariq, A.U. Yasir, M.M. Iqbal, S.U. Din, J. Krzywanski, Simulation of Vacuum Distillation Unit in Oil Refinery: Operational Strategies for Optimal Yield Efficiency, Energies 2024, Vol. 17, Page 3806 17 (2024) 3806. https://doi.org/10.3390/EN17153806.

[69] Z. Si, D. Han, Y. Song, J. Chen, L. Luo, R. Li, Experimental investigation on a combined system of vacuum membrane distillation and mechanical vapor recompression, Chemical Engineering and Processing - Process Intensification 139 (2019) 172–182. https://doi.org/10.1016/J.CEP.2019.04.007.

[70] F. Han, S. Liu, K. Wang, X. Zhang, Enhanced Performance of Membrane Distillation Using Surface Heating Process, Membranes 2021, Vol. 11, Page 866 11 (2021) 866. https://doi.org/10.3390/MEMBRANES11110866.

[71] Q. Chen, B. Muhammad, F.H. Akhtar, D. Ybyraiymkul, W.S. Muhammad, Y. Li, K.C. Ng, Thermo-economic analysis and optimization of a vacuum multi-effect membrane distillation system, Desalination 483 (2020) 114413. https://doi.org/10.1016/J.DESAL.2020.114413.

[72] D.S. Sholl, R.P. Lively, Seven chemical separations to change the world, Nature 2016 532:7600 532 (2016) 435–437. https://doi.org/10.1038/532435a.

[73] W. Zeb, M. Roosen, P. Knockaert, S. Janssens, D. Withoeck, M. Kusenberg, J. Hogie, P. Billen, S. Tavernier, K.M. Van Geem, S. De Meester, Purification and characterisation of post-consumer plastic pyrolysis oil fractionated by vacuum distillation, J Clean Prod 416 (2023) 137881. https://doi.org/10.1016/J.JCLEPRO.2023.137881.

[74] G. Zha, C. Yang, Y. Wang, X. Guo, W. Jiang, B. Yang, New vacuum distillation technology for separating and recovering valuable metals from a high value-added waste, Sep Purif Technol 209 (2019) 863–869. https://doi.org/10.1016/J.SEPPUR.2018.09.038.

[75] S. Ma, G. Zhang, C. Shi, Q. Dong, T. Ji, Achieving Practical Venue Recycle of Waste Oil-Based Drilling Fluids with Vacuum Distillation Technology, ACS Omega 8 (2023) 16306–16314. https://doi.org/10.1021/ACSOMEGA.3C00967/ASSET/IMAGES/LARGE/AO3C00967_0011.JPEG.

[76] E.A. Mahrous, M.A. Farag, Trends and Applications of Molecular Distillation in Pharmaceutical and Food Industries, Separation & Purification Reviews 51 (2022) 300–317. https://doi.org/10.1080/15422119.2021.1924205.

[77] Z. peng XU, L. li JIA, Z. qiang HE, X. yi GUO, Q. hua TIAN, A review of preparing high-purity metals by vacuum distillation, Transactions of Nonferrous Metals Society of China 34 (2024) 1634–1654. https://doi.org/10.1016/S1003-6326(24)66496-4.

[78] Council of Europe, The European Pharmacopoeia, 10th ed., 2019.

[79] M.A. Gantumur, N. Sukhbaatar, A. Qayum, A. Bilawal, B. Tsembeltsogt, K.C. Oh, Z. Jiang, J. Hou, Characterization of major volatile compounds in whey spirits produced by different distillation

stages of fermented lactose-supplemented whey, J Dairy Sci 105 (2022) 83–96. https://doi.org/10.3168/JDS.2021-20748.

[80] M.J. Claus, K.A. Berglund, L.J. Claus, K.A. Berglund, M.J. Claus, FRUIT BRANDY PRODUCTION BY BATCH COLUMN DISTILLATION WITH REFLUX, J Food Process Eng 28 (2005) 53–67. https://doi.org/10.1111/J.1745-4530.2005.00377.X.

[81] M. Yagishita, O. Reber, D. Alter, R. Kölling, D. Einfalt, Optimizing Aroma Compound Fractionation in Pear Brandy Distillation by Controlling Their Relative Volatility, Food Bioproc Tech 18 (2025) 7095–7111. https://doi.org/10.1007/S11947-025-03815-8/FIGURES/12.

[82] N. Jamaković, N. Spaho, Influence of Initial Alcohol Content in Distillate on Distribution of Methanol and Higher Alcohols During Redistillations, Lecture Notes in Networks and Systems 128 LNNS (2020) 786–794. https://doi.org/10.1007/978-3-030-46817-0_89.

[83] M. Esteban-Decloux, N.C.R. Tano, H. Grangeon, Simulation of the behaviour of volatile compounds during batch multi-stage distillation of whisky, Journal of the Institute of Brewing 128 (2022) 171–187. https://doi.org/10.1002/JIB.704.

[84] Y. Lin, N. Zhang, Y. Lin, Y. Gao, H. Li, C. Zhou, W. Meng, W. Qin, Transcriptomic and metabolomic correlation analysis: effect of initial SO2 addition on higher alcohol synthesis in Saccharomyces cerevisiae and identification of key regulatory genes, Front Microbiol 15 (2024) 1394880. https://doi.org/10.3389/FMICB.2024.1394880/BIBTEX.

[85] L.A. Hazelwood, J.M. Daran, A.J.A. Van Maris, J.T. Pronk, J.R. Dickinson, The Ehrlich pathway for fusel alcohol production: A century of research on Saccharomyces cerevisiae metabolism, Appl Environ Microbiol 74 (2008) 2259–2266. https://doi.org/10.1128/AEM.02625-07/ASSET/505C4E0C-01FE-

46E8-B651-
82FF952313E9/ASSETS/GRAPHIC/ZAM0080887450003.JPEG.

[86] E.J. Pires, J.A. Teixeira, T. Brányik, A.A. Vicente, Yeast: The soul of beer's aroma - A review of flavour-active esters and higher alcohols produced by the brewing yeast, Appl Microbiol Biotechnol 98 (2014) 1937–1949. https://doi.org/10.1007/S00253-013-5470-0/FIGURES/3.

[87] Y. Jiang, T. Zhang, P. Kusumanchi, S. Han, Z. Yang, S. Liangpunsakul, Alcohol Metabolizing Enzymes, Microsomal Ethanol Oxidizing System, Cytochrome P450 2E1, Catalase, and Aldehyde Dehydrogenase in Alcohol-Associated Liver Disease, Biomedicines 2020, Vol. 8, Page 50 8 (2020) 50. https://doi.org/10.3390/BIOMEDICINES8030050.

[88] R. Teschke, Alcoholic Liver Disease: Alcohol Metabolism, Cascade of Molecular Mechanisms, Cellular Targets, and Clinical Aspects, Biomedicines 2018, Vol. 6, Page 106 6 (2018) 106. https://doi.org/10.3390/BIOMEDICINES6040106.

[89] S. Mostrou, A. Nagl, M. Ranocchiari, K. Föttinger, J.A. Van Bokhoven, The catalytic and radical mechanism for ethanol oxidation to acetic acid, Chemical Communications 55 (2019) 11833–11836. https://doi.org/10.1039/C9CC05813C.

[90] A.A. Kiss, R. Smith, Rethinking energy use in distillation processes for a more sustainable chemical industry, Energy 203 (2020) 117788. https://doi.org/10.1016/J.ENERGY.2020.117788.

[91] V.H. Grisales Díaz, G. Olivar Tost, Techno-economic analysis of extraction-based separation systems for acetone, butanol, and ethanol recovery and purification, Bioresour Bioprocess 4 (2017) 12-. https://doi.org/10.1186/S40643-017-0142-Z/FIGURES/5.

[92] M.A. Gadalla, Z. Olujic, P.J. Jansens, M. Jobson, R. Smith, Reducing CO2 Emissions and Energy Consumption of Heat-Integrated

Distillation Systems, Environ Sci Technol 39 (2005) 6860–6870. https://doi.org/10.1021/ES049795Q.

[93] X. Tian, R. Wang, H. Wang, C. Li, J. Liu, Energy-saving extractive distillation processes design and optimization for the separation of ethyl acetate and n-heptane azeotrope, Fuel 379 (2025) 132974. https://doi.org/10.1016/J.FUEL.2024.132974.

[94] E.V. Silva, J.L.F. Alves, G.D. Mumbach, G.F. Reus, R.A.F. Machado, A. Bolzan, C. Marangoni, Performance comparison of falling film distillation process configurations for energy-saving ethanol-water separation, Journal of Industrial and Engineering Chemistry 135 (2024) 480–492. https://doi.org/10.1016/J.JIEC.2024.01.059.

[95] N. Hu, J. Guo, Q. Wu, H. Yue, Q. Li, Design and evaluation of energy-saving total distillation separation of N,N-Dimethylacetamide/acetic acid/water, Sep Purif Technol 282 (2022) 120154. https://doi.org/10.1016/J.SEPPUR.2021.120154.

[96] H.T. Do Thi, A.J. Toth, Life cycle assessment of the manufacturing and operation of distillation column for eliminating volatile and organic halogen compounds from process wastewater, SN Appl Sci 5 (2023) 305-. https://doi.org/10.1007/S42452-023-05540-3/FIGURES/5.

[97] A. Amelio, G. Genduso, S. Vreysen, P. Luis, B. Van Der Bruggen, Guidelines based on life cycle assessment for solvent selection during the process design and evaluation of treatment alternatives, Green Chemistry 16 (2014) 3045–3063. https://doi.org/10.1039/C3GC42513D.

[98] H.T. Do Thi, A.J. Toth, Environmental evaluation and comparison of hybrid separation methods based on distillation and pervaporation for dehydration of binary alcohol mixtures with life cycle, PESTLE, and

multi-criteria decision analyses, Sep Purif Technol 348 (2024) 127684. https://doi.org/10.1016/J.SEPPUR.2024.127684.

[99] J. Zhu, B. Zhang, H. Zhang, L. Hao, Heat Pump-Assisted Extractive Pressure-Swing Distillation with Integrated Feed Preconcentration/Solvent Recovery for Isopropanol-Benzene-Water Separation, Sep Purif Technol 358 (2025) 130295. https://doi.org/10.1016/J.SEPPUR.2024.130295.

[100] Y. Xu, J. Li, Q. Ye, Y. Li, Energy efficient extractive distillation process assisted with heat pump and heat integration to separate acetonitrile/1,4-dioxane/water, Process Safety and Environmental Protection 156 (2021) 144–159. https://doi.org/10.1016/J.PSEP.2021.09.042.

[101] Z. Mekidiche, J.A. Labarta, J. Javaloyes-Anton, J.A. Caballero, From power to heat: Strategies for electrifying distillation for sustainable chemical processes, Appl Therm Eng 257 (2024) 124316. https://doi.org/10.1016/J.APPLTHERMALENG.2024.124316.

[102] Q. Wu, Z. Wang, W. Xu, L. Xin, R. Hu, Z. Zhu, Y. Wang, P. Cui, Innovative extractive distillation process combining preconcentration and solvent recovery functions for efficiently separating diisopropyl ether/isopropanol/water, Sep Purif Technol 360 (2025) 131021. https://doi.org/10.1016/J.SEPPUR.2024.131021.

[103] T. Wu, C. Wang, J. Liu, Y. Zhuang, J. Du, Design and 4E analysis of heat pump-assisted extractive distillation processes with preconcentration for recovering ethyl-acetate and ethanol from wastewater, Chemical Engineering Research and Design 201 (2024) 510–522. https://doi.org/10.1016/J.CHERD.2023.12.011.

[104] J. Zhai, X. Chen, X. Sun, H. Xie, Economically and thermodynamically efficient pressure-swing distillation with heat integration and heat pump techniques, Appl Therm Eng 218 (2023)

119389. https://doi.org/10.1016/J.APPLTHERMALENG.2022.119389.

[105] M.J. Raymond, C.S. Slater, M.J. Savelski, LCA approach to the analysis of solvent waste issues in the pharmaceutical industry, Green Chemistry 12 (2010) 1826–1834. https://doi.org/10.1039/C003666H.

[106] A.J. Tóth, D. Fózer, P. Mizsey, P.S. Varbanov, J.J. Klemeš, Physicochemical methods for process wastewater treatment: powerful tools for circular economy in the chemical industry, Reviews in Chemical Engineering 39 (2023) 1123–1151. https://doi.org/10.1515/REVCE-2021-0094/ASSET/GRAPHIC/J_REVCE-2021-0094_FIG_007.JPG.

[107] M.J. Savelski, C.S. Slater, P. V. Tozzi, C.M. Wisniewski, On the simulation, economic analysis, and life cycle assessment of batch-mode organic solvent recovery alternatives for the pharmaceutical industry, Clean Technol Environ Policy 19 (2017) 2467–2477. https://doi.org/10.1007/S10098-017-1444-8/FIGURES/6.

[108] C.T.A. Moermond, N. Puhlmann, L. Pieters, A. Matharu, L. Boone, M. Dobbelaere, H. Proquin, K. Kümmerer, A.M.J. Ragas, R. Vidaurre, B. Venhuis, D. De Smedt, Eco-pharma dilemma: Navigating environmental sustainability trade-offs within the lifecycle of pharmaceuticals – A comment, Sustain Chem Pharm 43 (2025) 101893. https://doi.org/10.1016/J.SCP.2024.101893.

[109] E.A. Aboagye, J.D. Chea, K.M. Yenkie, Systems level roadmap for solvent recovery and reuse in industries, IScience 24 (2021) 103114. https://doi.org/10.1016/J.ISCI.2021.103114.

[110] T. Burnouf, Plasma fractionation, ISBT Sci Ser 7 (2012) 62–67. https://doi.org/10.1111/j.1751-2824.2012.01557.x.

[111] T. Burnouf, An overview of plasma fractionation, Ann Blood 3 (2018) 33–33. https://doi.org/10.21037/aob.2018.05.03.

[112] J.J. La Scala, C.A. Ulven, J.A. Orlicki, R. Jain, G.R. Palmese, U.K. Vaidya, J.M. Sands, Emission modeling of styrene from vinyl ester resins, Clean Technol Environ Policy 9 (2007) 265–279. https://doi.org/10.1007/S10098-006-0076-1/METRICS.

[113] J.J. La Scala, J.A. Orlicki, R. Jain, C.A. Ulven, G.R. Palmese, U.K. Vaidya, J.M. Sands, Emission modeling of styrene from vinyl ester resins with low hazardous air pollutant contents, Clean Technol Environ Policy 11 (2009) 283–292. https://doi.org/10.1007/S10098-008-0181-4/METRICS.

[114] X. Yin, Y. Liu, Y. Miao, G. Xian, X. Yin, Y. Liu, Y. Miao, G. Xian, Water Absorption, Hydrothermal Expansion, and Thermomechanical Properties of a Vinylester Resin for Fiber-Reinforced Polymer Composites Subjected to Water or Alkaline Solution Immersion, Polymers 2019, Vol. 11, 11 (2019). https://doi.org/10.3390/POLYM11030505.

[115] J. Sajapin, M. Hellwig, Studies on the synthesis and stability of α-ketoacyl peptides, Amino Acids 52 (2020) 1425–1438. https://doi.org/10.1007/s00726-020-02902-8.

[116] Y. Wang, Y. Tang, Y. Shao, Theoretical investigation of the selective dehydration and dehydrogenation of ethanol catalyzed by small molecules, J Mol Graph Model 76 (2017) 521–534. https://doi.org/10.1016/j.jmgm.2017.05.009.

[117] V. Mas, R. Kipreos, N. Amadeo, M. Laborde, Thermodynamic analysis of ethanol/water system with the stoichiometric method, Int J Hydrogen Energy 31 (2006) 21–28. https://doi.org/10.1016/j.ijhydene.2005.04.004.

[118] A. Schünberg, R. Moubacher, THE STRECKER DEGRADATION OF-AMINO ACIDS, 1951. https://pubs.acs.org/sharingguidelines.

[119] C.-K. Shu, M.L. Hagedorn, B.D. Mookherjee, C.-T. Ho, pH Effect on the Volatile Components in the Thermal Degradation of Cysteine, Chichester, 1985. https://pubs.acs.org/sharingguidelines.

[120] W.J. de Bruyn, C.D. Clark, M. Senstad, Production of acetaldehyde from ethanol in coastal waters, Environmental Science and Pollution Research 27 (2020) 12673–12682. https://doi.org/10.1007/s11356-020-07880-8.

[121] J.S. Deetz, C.A. Luehr, B.L. Vallee, Human Liver Alcohol Dehydrogenase Isozymes: Reduction of Aldehydes and Ketones1, 1984. https://pubs.acs.org/sharingguidelines.

[122] S. Das, S. Mozumdar, A. Maitra, Activity and conformation of yeast alcohol dehydrogenase (YADH) entrapped in reverse micelles, J Colloid Interface Sci 230 (2000) 328–333. https://doi.org/10.1006/jcis.2000.7079.

[123] F. Lei, M. Rotbøll, S.B. Jørgensen, A biochemically structured model for Saccharomyces cere6isiae, 2001. www.elsevier.com/locate/jbiotec.

[124] R. Lortie, A. Fassouane, J.-M. Laval, C. Bourdillon', Displacement of Equilibrium in Electroenzymatic Reactor for Acetaldehyde Production Using Yeast Alcohol Dehydrogenase, 1991.

[125] Y.C. Chi, S.L. Lee, Y.P. Lee, C.L. Lai, S.J. Yin, Modeling of Human Hepatic and Gastrointestinal Ethanol Metabolism with Kinetic-Mechanism-Based Full-Rate Equations of the Component Alcohol Dehydrogenase Isozymes and Allozymes, Chem Res Toxicol 31 (2018) 556–569. https://doi.org/10.1021/acs.chemrestox.8b00003.

[126] L. Di, A. Balesano, S. Jordan, S.M. Shi, The Role of Alcohol Dehydrogenase in Drug Metabolism: Beyond Ethanol Oxidation, AAPS Journal 23 (2021). https://doi.org/10.1208/s12248-020-00536-y.

[127] H.J. Edenberg, J.N. McClintick, Alcohol Dehydrogenases, Aldehyde Dehydrogenases, and Alcohol Use Disorders: A Critical Review, Alcohol Clin Exp Res 42 (2018) 2281–2297. https://doi.org/10.1111/acer.13904.

[128] D. Meier-Tackmann, D.P. Agarwal, H.W. Goeddef, PLASMA ALCOHOL DEHYDROGENASE IN NORMAL AND ALCOHOLIC INDIVIDUALS*, 1984.

[129] L. Schwarzmann, R.U. Pliquett, A. Simm, B. Bartling, Sex-related differences in human plasma NAD+/NADH levels depend on age, Biosci Rep 41 (2021). https://doi.org/10.1042/BSR20200340.

[130] S. Aquino Neto, J.C. Forti, V. Zucolotto, P. Ciancaglini, A.R. De Andrade, The kinetic behavior of dehydrogenase enzymes in solution and immobilized onto nanostructured carbon platforms, Process Biochemistry 46 (2011) 2347–2352. https://doi.org/10.1016/j.procbio.2011.09.019.

[131] K. Dalziel, Kinetic Studies of Liver Alcohol Dehydrogenase and pH with Coenzyme Preparations of High Purity Effects, 1963.

[132] F.W. Wagner, A.R. Burger, B.L. Vallee, Kinetic Properties of Human Liver Alcohol Dehydrogenase: Oxidation of Alcohols by Class I Isoenzymes+, 1983.

[133] W.F. Bosron, D.W. Crabb, T.-K. Li, Relationship Between Kinetics of Liver Alcohol Dehydrogenase and Alcohol Metabolism, 1983.

[134] C.J. Dickenson, F.M. Dickinson, A Study of the pH-and Temperature-Dependence of the Reactions of Yeast Alcohol Dehydrogenase with Ethanol, Acetaldehyde and Butyraldehyde as Substrates, 1975.

[135] C.T. Yao, C.L. Lai, H.S. Hsieh, C.W. Chi, S.J. Yin, Establishment of steady-state metabolism of ethanol in perfused rat liver: The quantitative analysis using kinetic mechanism-based rate equations of

alcohol dehydrogenase, Alcohol 44 (2010) 541–551. https://doi.org/10.1016/j.alcohol.2010.07.002.

[136] T.H. Yang, S. Jessie Lue, UNIQUAC and UNIQUAC-HB models for the sorption behavior of ethanol/water mixtures in a cross-linked polydimethylsiloxane membrane, J Memb Sci 415–416 (2012) 534–545. https://doi.org/10.1016/J.MEMSCI.2012.05.041.

[137] N.M. Farhan, S.S. Ibrahim, Q.F. Alsalhy, Modeling and simulation of pervaporation (PV) separation for alcohol dehydration, Heliyon 9 (2023). https://www.cell.com/heliyon/fulltext/S2405-8440(23)00920-9 (accessed October 2, 2025).

[138] M.J. O McLinden, M. Thol, E.W. Lemmon, M.O. McLinden, International Refrigeration and Air Conditioning Conference. Paper 1041. International Refrigeration and Air Conditioning Conference at Purdue, Thermodynamic Properties of Trans-1 3 (2010) 3. http://docs.lib.purdue.edu/iracc/1041 (accessed October 2, 2025).

[139] M. Ma, O. Pektezel, V. Ballerini, P. Valdiserri, E. Rossi di Schio, Performance Predictions of Solar-Assisted Heat Pumps: Methodological Approach and Comparison Between Various Artificial Intelligence Methods, Energies 2024, Vol. 17, Page 5607 17 (2024) 5607. https://doi.org/10.3390/EN17225607.

[140] Eurostat, Electricity price statistics - Statistics Explained - Eurostat, (2025). https://ec.europa.eu/eurostat/statistics-explained/index.php?title=Electricity_price_statistics (accessed October 30, 2025).

[141] E.W. Tow, A.L. Hartman, A. Jaworowski, I. Zucker, S. Kum, M. AzadiAghdam, E.R. Blatchley, A. Achilli, H. Gu, G.M. Urper, D.M. Warsinger, Modeling the energy consumption of potable water reuse schemes, Water Res X 13 (2021). https://doi.org/10.1016/j.wroa.2021.100126.

[142] V.K. Gupta, I. Ali, T.A. Saleh, A. Nayak, S. Agarwal, Chemical treatment technologies for waste-water recycling - An overview, RSC Adv 2 (2012) 6380–6388. https://doi.org/10.1039/c2ra20340e.

[143] K. Goyal, A. Kumar, Development of water reuse: A global review with the focus on India, Water Science and Technology 84 (2021) 3172–3190. https://doi.org/10.2166/wst.2021.359.

[144] V. Lazarova, Milestones in water reuse : the best success stories, International Water Association, 2020.

[145] M. Prisciandaro, V. Innocenzi, Advanced wastewater oxidation processes and their role in water reuse for a circular economy, Water Management and Circular Economy (2023) 81–102. https://doi.org/10.1016/B978-0-323-95280-4.00015-1.

[146] F. Cecchini, K. Ayedi, V. Innocenzi, M. Dassatti, G.M. di Celso, M. Prisciandaro, ADVANCING WATER CIRCULARITY: A SIMULATION OF HYDRODYNAMIC CAVITATION AND MEMBRANE PROCESSES FOR SUSTAINABLE INDUSTRIAL WASTEWATER REUSE, Detritus 2025 - Volume (2025) 104. https://doi.org/10.31025/2611-4135/2025.19525.

[147] M. Prisciandaro, M. Capocelli, V. Piemonte, D. Barba, Process analysis applied to water reuse for a “closed water cycle” approach, Chemical Engineering Journal 304 (2016) 602–608. https://doi.org/10.1016/j.cej.2016.06.134.

[148] V. Innocenzi, M. Prisciandaro, M. Centofanti, F. Vegliò, Comparison of performances of hydrodynamic cavitation in combined treatments based on hybrid induced advanced Fenton process for degradation of azo-dyes, J Environ Chem Eng 7 (2019) 103171. https://doi.org/10.1016/J.JECE.2019.103171.

[149] Z. Wu, H. Shen, B. Ondruschka, Y. Zhang, W. Wang, D.H. Bremner, Removal of blue-green algae using the hybrid method of

hydrodynamic cavitation and ozonation, J Hazard Mater 235–236 (2012) 152–158. https://doi.org/10.1016/J.JHAZMAT.2012.07.034.

[150] K. Ayedi, V. Innocenzi, M. Prisciandaro, Application of hybrid oxidative processes based on cavitation for the treatment of methyl blue solutions, Sustain Water Resour Manag 10 (2024) 1–13. https://doi.org/10.1007/S40899-024-01060-Z/TABLES/4.

[151] V. Innocenzi, A. Colangeli, M. Prisciandaro, Methyl orange decolourization through hydrodynamic cavitation in high salinity solutions, Chemical Engineering and Processing - Process Intensification 179 (2022) 109050. https://doi.org/10.1016/J.CEP.2022.109050.

[152] X. Sun, J. Liu, L. Ji, G. Wang, S. Zhao, J.Y. Yoon, S. Chen, A review on hydrodynamic cavitation disinfection: The current state of knowledge, Science of the Total Environment 737 (2020). https://doi.org/10.1016/j.scitotenv.2020.139606.

[153] B. Wang, H. Su, B. Zhang, Hydrodynamic cavitation as a promising route for wastewater treatment – A review, Chemical Engineering Journal 412 (2021). https://doi.org/10.1016/j.cej.2021.128685.

[154] EUROPEAN PARLIAMENT, REGULATION (EU) 2020/741 OF THE EUROPEAN PARLIAMENT AND OF THE COUNCIL of 25 May 2020 on minimum requirements for water reuse, 2020.

[155] USEPA, Potable Reuse Compendium, 2017.

[156] G. Mazziotti di Celso, M. Prisciandaro, Wastewater reuse by means of UF membrane process: a comparison with Italian provisions, Desalination Water Treat 51 (2013) 1615–1622. https://doi.org/10.1080/19443994.2012.705053.

[157] S. Dutta, B. Gupta, S.K. Srivastava, A.K. Gupta, Recent advances on the removal of dyes from wastewater using various adsorbents: A

critical review, Mater Adv 2 (2021) 4497–4531. https://doi.org/10.1039/d1ma00354b.

[158] C.G. Lopresto, S. Naccarato, L. Albo, M.G. De Paola, S. Chakraborty, S. Curcio, V. Calabrò, Enzymatic transesterification of waste vegetable oil to produce biodiesel, Ecotoxicol Environ Saf 121 (2015) 229–235. https://doi.org/10.1016/j.ecoenv.2015.03.028.

[159] E.H. Ezechi, M.H. Isa, K. Muda, S.R.M. Kutty, A comparative evaluation of two electrode systems on continuous electrocoagulation of boron from produced water and mass transfer resistance, Journal of Water Process Engineering 34 (2020). https://doi.org/10.1016/j.jwpe.2020.101133.

[160] C. Agarkoti, P.D. Thanekar, P.R. Gogate, Cavitation based treatment of industrial wastewater: A critical review focusing on mechanisms, design aspects, operating conditions and application to real effluents, J Environ Manage 300 (2021). https://doi.org/10.1016/j.jenvman.2021.113786.

[161] A. Mukherjee, A. Mullick, R. Teja, P. Vadthya, A. Roy, S. Moulik, Performance and energetic analysis of hydrodynamic cavitation and potential integration with existing advanced oxidation processes: A case study for real life greywater treatment, Ultrason Sonochem 66 (2020). https://doi.org/10.1016/j.ultsonch.2020.105116.

[162] G. Mancuso, M. Langone, G. Andreottola, A critical review of the current technologies in wastewater treatment plants by using hydrodynamic cavitation process: principles and applications, J Environ Health Sci Eng 18 (2020) 311–333. https://doi.org/10.1007/s40201-020-00444-5.

[163] R. Hamidi, M. Damizia, P. De Filippis, D. Patrizi, N. Verdone, G. Vilardi, B. de Caprariis, Recent developments and future outlooks of hydrodynamic cavitation as an intensification technology for

renewable biofuels production, J Environ Chem Eng 11 (2023). https://doi.org/10.1016/j.jece.2023.110819.

[164] S.J. Judd, Membrane technology costs and me, Water Res 122 (2017) 1–9. https://doi.org/10.1016/j.watres.2017.05.027.

[165] K. Ayedi, V. Innocenzi, G.M. Di Celso, M. Prisciandaro, Water reuse in the textile industry with integrated treatments: membranes and advanced oxidation processes, Desalination Water Treat 309 (2023) 158–164. https://doi.org/10.5004/dwt.2023.29875.

ACKNOWLEDGEMENTS

I would like to dedicate a few lines to thank all those who accompanied me throughout this period of study.

I would like to thank the University of L'Aquila and the Department of Industrial and Information Engineering and Economics for providing me with the opportunity to pursue the education and training I have received over these years.

I wish to express my deepest gratitude to my supervisors, Professor Marina Prisciandaro and Professor Valentina Innocenzi. You will always represent for me an example of professionalism and personal integrity. You have demonstrated, time and again, that with solid preparation and dedication it is possible to achieve great results. This work would not exist without you.

I would also like to thank Professor Aurora Santos López from the Universidad Complutense de Madrid and the entire INPROQUIMA research group for helping me address challenges that initially seemed impossible. I carry with me a very fond memory of my time in Madrid, above all thanks to the wonderful people I met during that period.

I thank Takeda Manufacturing Italia for giving me the opportunity to challenge myself with this project and for allowing me to grow professionally through this experience.

I am deeply grateful to my family for their constant support, patience, and understanding throughout this journey. Their encouragement, especially during the most demanding moments of this path, gave me the strength to persevere and continue moving forward. This work belongs to you as well.

If I have reached this point, it is also thanks to all the people I have met along my path. To those who are here, to those who have been, and to those who will remain, I am truly grateful.

Tesi redatta con il cofinanziamento dell'Unione europea-*NextGeneration EU*
Piano Nazionale di Ripresa e Resilienza Missione 4, Componente 2 –
Investimento 3.3. del PNRR – "Dottorati innovativi che rispondono ai fabbisogni di innovazione delle imprese" – CUP E11I22000210001